Characterization of radiotolerance in potato and development of a gamma radiation phytosensor.

A Dissertation Presented for the
Doctor of Philosophy
Degree
The University of Tennessee, Knoxville

Robert Graham Sears
December 2023

DEDICATION

I dedicate this dissertation to my mother and father, Amy and Randy Sears. None of this work would be possible without their love, guidance, and support.

ACKNOWLEDGMENTS

The author would like to acknowledge all mentors whose guidance, both formal and informal, was essential to the creation of this dissertation. This includes committee members C. Neal Stewart, Scott C. Lenaghan, Feng Chen, and Tessa Burch-Smith. In addition, the guidance of Stephen Rigoulot, Alessandro Occhialini, Britany Morgan, Reginald Millwood, Yongil Yang, Alex Pfotenhauer, Li Li and Holly Brabazon played a large role in my success as a student.

In addition, the help of many of the postdocs, graduate students and technicians at the Center for Agricultural Synthetic Biology were necessary for success. This includes but is not limited to Caitlin Barnes, Chandler Brown, Brianna Jacobs, Timothy Chaffin, Tayebeh Kakeshpour, Mariah Seaberry, Jessica Stockdale, Bryce Trull, and C. Tyler Newton.

The love and friendship of my friends and family were also essential in the completion of my degree. Most importantly my partner, Cassandra, and our dog, Slim. Additionally, my friends Parker, Chelsey, Rob, Kelsey, Elijah, and Grace. All of my extended friends and family deserve plenty of thanks for politely listening and asking questions about the work within this manuscript during holidays. Much of the credit for my curiosity about plants can be attributed to these people and their excellent questions. Of these, Laura Danes and her steady supply of tomato seedlings and gardening tips played a large part in my pursuance of plant science as a child and young adult.

Special thanks to Max Cichon, Tamara Isaacs-Smith, and the staff at Auburn University whose assistance was essential to all gamma radiation treatments.

The author acknowledges funding by the Defense Advanced Research Projects Agency (Award No. HR0011-18-2-0049) and USDA Hatch grants to C. Neal Stewart and Scott C. Lenaghan. The views, opinions, and/or findings expressed are those of the authors and should not be interpreted as representing the official views of policies of the Department of Defense or the United States Government (Approved for Public Release, Distribution Unlimited).

ABSTRACT

As humans pursue space travel and nuclear energy, the risk of harm from ionizing radiation increases. On Earth or in space, plants are essential to our personal and environmental health. Plants serve as sentinels, bioremediators and food sources in areas of high ionizing radiation, therefore it is essential to understand how ionizing radiation affects plant biology. This work aimed to understand plant responses to ionizing radiation in the potato chassis and apply that knowledge to generate novel phenotypes for nuclear energy and space applications. The first gamma radiation phytosensor was developed for monitoring at standoff distances greater than three meters. The expression of *Ramazzottius varieornatus* (tardigrade) 'Damage suppressor' protein was found to be ineffective at increasing plant radiotolerance. Lastly, ionizing radiation response was characterized at low doses, revealing a threshold of response in plants between 2 and 4 Gy. This information can be used to create more sensitive radiation phytosensors and additional radioprotection strategies. All of the work here relied on tissue-specific expression patterns, resulting in a final research chapter on the application of artificial intelligence to understanding cell type differences, so that improved engineering strategies can be generated. This work developed the first field-deployable radiation phytosensor and laid the groundwork for many future phytosensors and radiotolerant plant cultivars. Through this work, humanity can pursue a safer relationship with ionizing radiation.

TABLE OF CONTENTS

LIST OF TABLES

LIST OF FIGURES

CHAPTER I: PLANTS, HUMANS, AND IONIZING RADIATION.

Plants are essential to humanity's continued relationship with ionizing radiation.

As humanity pursues carbon-neutral energy production and long-term spaceflight, the risk of ionizing radiation harming human and environmental health grows. Increased risk of ionizing radiation necessitates improvements in radiation sensing technologies and a better understanding of how ionizing radiation impacts biology. Pursuing improved radiation detection technologies and understanding biological radiotolerance will ensure that ionizing radiation pollution is quickly identified with low risk to human health and the environment around a pollutant can be engineered to be more radiation resilient. These benefits extend to long term space flight, where the impact of space radiation on human health is poorly understood and food production systems will be experiencing constant ionizing radiation stress. Plants are the essential basis of the health of ecosystems and food systems on Earth and in space. Understanding the impact of radiation on plants and developing plant-centric sensing and mitigation strategies is therefore the most straightforward way to ensure human health as the nuclear energy and spaceflight industries grow.

In space and on Earth, the sensing and reporting of ionizing radiation is currently done using mechanical sensors such as Geiger counters, but these devices have major drawbacks including the limited availability of such equipment, the reliance on batteries or a power grid for their function, their weight, and the requirement of physically carrying these devices into potentially dangerous areas to acquire measurements[1-3]. The limitations of these dosimeters compounded by the mismanagement of meltdown situations led to unnecessary illness and death during nuclear power plant catastrophes in the past[1, 3]. At Fukushima, damage to the power grid led to mechanical sensors failing and citizens being moved to areas of higher radiation rather than away from danger[3]. Just one in twenty-four mechanical sensor sites were functional following the earthquake and the subsequent tsunami that hit the area[3]. At Chernobyl, all available sensors at the time of the incident were either mechanically damaged or were not capable of measuring the high levels of radiation present[1]. Though no emergencies have arisen yet in space, it has been demonstrated that there are many types of ionizing radiation that fall outside of the calibration of standard mechanical dosimeter[4]. This means that a mechanical sensor in space could underestimate the impact of rare forms of radiation that are only present in space. A plant-based dosimeter could address all drawbacks of mechanical sensors in each of these scenarios by being cheaply scalable across a landscape, detectable at a standoff distance, fully self-sufficient and self-replicating, and delivering a biologically-relevant output that does not need to be calibrated.

In addition to sensing, plants are often present in radioactive areas and have been shown to sequester radioactive material. Plants uptake radionuclides such as Cesium-137 through direct contact and through soil water using the same ion channels as those for elements like potassium[5]. Though there is concern that plant-sequestered radionuclides could threaten human health if introduced into the food system[6], plant sequestration is preferable to adsorption of radionuclides to the soil, where they remain tightly bound and effectively mean the area will be contaminated for many years[7]. There is an upper limit for radiotolerance in all plant species, exemplified by the 'red forest' of dead Scots Pine trees near the Chernobyl power plant[8]. Ecosystems surviving a nuclear emergency would allow for sequestration of radionuclides over time without the need for human presence. If plants could be engineered to have increased radiotolerance, the intensive replanting efforts like those required around Chernobyl[8] could be avoided, saving money and lowering risks to human health.

Increasing plant radiotolerance may be essential to long term spaceflight, where food will need to be grown for the entire duration of a long trip to other celestial bodies. Multigenerational studies have been conducted on pea plants[9], wheat[9], and rapeseed[10] in space, with pea plants undergoing the longest successional growth on the International Space Station (ISS). After the four generations and 368 days of growth time, no impacts on reproduction, seed viability, or DNA damage markers were observed[9], though these experiments were inherently small due to the resource limitations of the ISS. This has led researchers to focus more on the space constraints on sustainable food production during space flight, rather than the impacts of ionizing radiation[11]. However, a journey to Mars is expected to last 900 days[12], just under three times as long as the duration of the pea plant experiment. Observations in areas around Chernobyl with lower ionizing radiation emittance rates than the ISS have demonstrated impacts of radiation on reproduction and germination time in the span of one generation[13]. The length of future space flights combined with on-ground studies suggest that there may be impacts in space that were not observable given the logistical barriers on board the ISS. Though the logistical problems of food production in space are clear, increased radiotolerance of crop species will likely be needed once large-scale food production is achieved on space-faring vessels.

Whether as sensors, remediators, or simply as food, plants have been and will continue to be essential to humanity's relationship with ionizing radiation. In order to safely develop nuclear technologies and explore space, radiation tolerance and sensor strategies should be developed.

Review of ionizing radiation and its impact on biology

Ionizing radiation must be understood at a fundamental level in order to understand its interactions with an organism. Radiation refers to any subatomic particle that is emitted from a source and travels through space at the speed of light (or nearly the speed of light). This definition represents a wide variety of observable phenomena in our universe, from the heat-inducing waves in a home microwave to the heavy nuclei that make up galactic cosmic rays. Generally, types of radiation are grouped by their mass, energy, and potential to induce chemical or physical reactions when they strike other matter. Much of the electromagnetic radiation spectrum includes photons which have a wavelength greater than 400 nanometers, frequencies less than 7.50 terahertz, and energies less than 3.10 electron volts, which are considered non-ionizing radiation. These types of radiation are generally low energy photons that have little detrimental effect on biology in comparison to higher energy types of radiation. Indeed, photons in the 400 – 1000 nm frequency drive photosynthesis on Earth, creating the driving force of carbon assimilation into biological systems and creating the basis of nearly all ecosystems[14]. Cells have been able to develop precise photosystems which capture the energy of 400 – 1000 nm photons, translating physical energy into chemical energy at a very high efficiency[14, 15]. Land plants generally conduct photosynthesis with a narrower range of photon wavelengths (400 – 700 nm) because these wavelengths carry much more energy and are plentiful in terrestrial environements[14]. Although high flux of radiation in this range can damage photosynthetic organisms through the overloading of photosystems and reactive oxygen species (ROS) production[16], heterotrophs generally experience few deleterious effects from exposure to 400+ nm photons, making these types of radiation relatively biologically inert.

Going up in energy within electromagnetic mass-less forms of radiation, photons in the ultraviolet, X-ray, and gamma ray spectra make up a group of indirectly ionizing types of radiation. Ultraviolet (UV) wavelengths are the lowest energy photons in this range, having wavelengths between 100 and 400 nm with delineations within this range that vary depending on

field of study[17]. Photons in this range are emitted by the Sun and largely absorbed by Earth's atmosphere, with greater flux of higher energy photons in this range found as an organism goes up in altitude[18]. UV radiation is dangerous for all biology because it can induce DNA lesions[19], as well as stimulate peroxidation of essential proteins[20, 21] and lipids[22] through generation of ROS. In animal cells, UV-induced DNA damage is known to drive cell cycle arrest and apoptosis[23]. Plant cells appear more resilient to UV-induced damage than animal cells, with apoptotic symptoms appearing only at very high UV treatments that are not relevant to life on Earth[24, 25]. This makes sense given their dependence on sunlight and sessile growth habit, which would require them to either avoid high UV irradiance through lifecycle adaptations or through development of UV screens and ROS scavengers.

X-ray and gamma photons have even shorter wavelengths, and therefore higher energy, than UV photons. These photons are naturally rare on Earth, being emitted only from soil-borne isotopes of elements such as potassium, uranium, and thorium[26]. The delineation between these two classes is historically vague, with one definition claiming X-rays are produced by electrons while gamma rays are produced by a nucleus, and a second definition arbitrarily saying photons with less than 0.01 nm wavelengths are gamma rays and above that threshold are X-rays[27]. Outside of those definitions, gamma photons are higher energy and more penetrative than X-rays, with both gamma and X-rays having higher energy and penetration than UV photons. Much like UV, gamma and X-rays indirectly ionize a substrate through interactions with a wide variety of cellular molecules (usually water) to generate ROS, which then go on to interact with other cellular molecules and disrupt their function. While gamma and X-rays can disrupt proteins, lipids, and secondary metabolite synthesis[28, 29], the lasting effects of these photons generally arise from mutations caused by DNA lesions stimulated by ROS in the nucleus[30]. In Arabidopsis, 29% of all genes upregulated after gamma treatment are related to DNA damage and repair[31], indicating that a third of the plant's response to ionizing radiation is solely for maintenance of the genome, while every other part of the cell's response split's the remaining two thirds. The highly penetrative nature of X-ray and gamma photons paired with their ability to impart a large amount of energy along their path makes them arguably the most dangerous types of radiation to biology. A single photon can generate many ROS across the entire thickness of a biological sample, quickly generating long-lasting DNA mutations that can forever alter the health of a cell.

The last class of radiation are the directly ionizing particles. This class of radiation includes alpha particles, beta particles, and a full spectrum of charged nuclei which can be ejected during various extreme atomic decay scenarios. All of these types of radiation have atomic mass (unlike photons) and have a constant charge state which allows them to directly ionize the molecules they collide with. A common form of directly ionizing radiation is the alpha particle, which is essentially a helium nucleus that has been ejected from a much larger/unstable atom. Alpha particles consist of a two proton and two neutron nucleus with a +2 charge that can actively accept electrons from its environment, and therefore carries a lot of energy per particle (4 – 10 megaelectron volts)[32]. In studies which use an ion beam, alpha particles generate many more chromosomal aberrations than gamma rays at consistent absorbed doses[33, 34]. Due to their mass, alpha particles have poor penetration into biological tissue, meaning that damage to biology in real-world settings is mostly achieved through the uptake of alpha emitters (Americium – 241, for example) rather than external exposure to alpha particles[32]. In fact, penetrance is so poor that many regulatory agencies estimate that alpha particles do not penetrate the layer of dead skin on humans. From existing literature, it appears that uptake of ^{214}Am and uranium does upregulate DNA repair and ROS scavenging machinery similarly to ionizing

photons[32, 35], but ^{214}Am and other alpha emitters are inefficiently extracted from soil and have little transference to aboveground tissues[35, 36]. The high energy and low penetration of alpha radiation makes the danger of short-term exposures relatively low for cells but long-term uptake of environmental alpha emitters is a concern in contaminated areas.

A class of directly ionizing radiation that splits the difference between the properties of alpha and gamma radiation is beta particles. Beta particles are electrons or positrons that have been ejected from a nucleus, carrying less energy (~0.5 megaelectron volts) than alpha particles but having much greater penetration due to their lower atomic mass. The process of beta decay occurs in an unstable nucleus with too many neutrons, such as Cesium – 137, and converts a neutron into a proton and an ejected electron which becomes the beta radiation particle[37]. When beta particles collide with some forms of matter, they can produce X-rays which can increase the ionization which occurs in a medium[38]. Generally, beta radiation is underrepresented in the literature compared to other types of ionizing radiation. However, it should be noted that a large portion of the ecosystem damage around Chernobyl was caused by beta-emitting isotopes, though gamma-emitters did also play a large role[39]. In experiments directly comparing the effects of beta and gamma radiation on soybean, the effects of either radiation type were equal if total absorbed dose was held constant[40]. This suggests that in certain circumstances where a beta source is close to biological tissue, beta particles penetrate well enough to induce ROS production and DNA damage similarly to gamma radiation. It must be noted, though, that it would take many more beta particles than gamma photons to deliver the same amount of energy through biological tissue.

The last class of ionizing radiation are the more specialty particles, such as heavy ions. Heavy nuclei radiation are the nuclei of many different types of matter without their electrons, which can include any ion heavier than alpha particles from lithium to nickel[41]. These particles often are the product of phenomena such as stars undergoing supernova, where enough energy is present to separate these large nuclei from their electron clouds. Although rare, these particles can deliver an incredible amount of energy to a biological medium and some are more penetrative than any current space shielding can absorb[42]. The effects of heavy ions on biological tissue appear to be much more potent than gamma radiation, though mutagenesis phenotypes are similar to most other types of radiation treatments[43]. Due to their rarity and high energy states, it is unclear how detrimental these particles will be to life space on a practical level, but the amount of energy they can impart to biological tissues does warrant caution and further study.

Of the types of radiation discussed, gamma radiation presents the greatest danger to humans and the environment due to its commonality among nuclear power sources and highly penetrative properties. Therefore, scenarios for sensor and radiotolerance strategies will account for these factors rather than the high energy transfer properties of alpha and heavy ion particles.

Impacts of gamma radiation in plants and their responses

As discussed above, gamma photons are highly energetic and have no mass, meaning they pass completely through a biological medium and shed a very small amount of their energy as they proceed. As a gamma photon passes through the electron clouds of atoms in a cell, it imparts some amount of energy. If the energy is greater than the ionization energy of the atom it interacted with, an electron will leave its orbit and a reactive species will be produced[44.] Since cells are mostly water (ionization energy = 12.6 eV[45]), gamma rays emitted from Cobalt-60 (1.17 and 1.33 MeV) easily ionize water and create highly reactive hydroxyls, which quickly interact with surrounding molecules, causing cellular damage[44]. Oxidative stress leads to the

peroxidation of unsaturated fats in lipid membranes[46], proteins at cysteine and methionine residues[47,48], and DNA damage through the generation of single-stranded and double-stranded breaks[49]. Repair mechanisms for proteins are relatively simple, with proteins such as glutaredoxins and thioredoxins reversing oxidative damage to protein thiols[50]. In contrast, membrane and genome repair mechanisms are highly complex, requiring the coordinated expression and activity of many different proteins[51,52]. Reactive oxygen species are produced as a normal part of homeostasis maintenance in plants as well as a stressor[53], meaning localized protein and lipid oxidation are commonplace during the course of a day. Additionally, ROS production and signaling in organelles is a large part of plant responses to biotic[54] and abiotic stress[55]. ROS signaling is typically delivered from organelles to the nucleus through protein intermediates[56] to avoid mutagenic DNA damage. This makes DNA damage one of the most unique and dangerous consequences of gamma radiation treatment. In order to design phytosensor and radioprotection strategies, the impact of ionizing radiation on DNA and the subsequent cellular response should be the focus of engineering efforts. By understanding and engineering the plant DNA damage response, plants can serve as improved sentinels and food sources as humanity pursues long-term spaceflight and carbon-free energy.

Scope of this dissertation

This dissertation is composed of five chapters, each focused on learning about ionizing radiation's impact on plants following the design-build-test-learn strategy most commonly found in engineering. Chapter II describes the creation of the first field-deployable gamma radiation phytosensor. Chapter III details the impact of constitutive expression of tardigrade damage suppressor protein on radiotolerance in potato. Chapter IV builds on the previous chapters through RNAseq analysis of potato irradiated at low doses of gamma radiation in order to design new phytosensor and radiotolerance strategies. Chapter V diverges from the previous four, proposing the application of existing cell typing AI to address the needs of plant metabolic engineering. Chapter V was inspired by the tissue-specific expression of the phytosensor construct and was featured as a Forum article in Trends in Plant Sciences.

References

1. Medvedev, Z. A. *The legacy of Chernobyl* (eds. Medvedev, Z and Norton, W.) W.W. Norton: New York (1990).
2. Knoll, G. F. *Radiation detection and measurement*. John Wiley & Sons: 2010.
3. Povinec, P. et al. "3 - Fukushima Accident." In *Fukushima Accident* (eds. Povinec, P., Hirose, K., and Aoyama, M.) pages 55-102 (Elsevier: Boston, 2013).
4. Chancellor, J. et al. Limitations in predicting the space radiation health risk for exploration astronauts. *NPJ Microgravity* **4**, 8 (2018).
5. Rai, H. and Kawabata, M. The dynamics of radio-cesium in soils and mechanism of cesium uptake into higher plants: newly elucidated mechanism of cesium uptake into rice plants. *Frontiers in Plant Science* **11**, 528 (2020).
6. Fesenko, S. et al. An extended critical review of twenty years of countermeasures used in agriculture after the Chernobyl accident. *Science of The Total Environment* **383**, 1-24 (2007).
7. Hashimoto, S. et al. "Behavior of Radiocesium in the Forest." In *Forest Radioecology in Fukushima: Radiocesium Dynamics, Impact, and Future.* (eds. Hashimoto, S. Komatsu, M. and Miura, S.) pages 21-46 (Springer Nature: Singapore, 2022)
8. Yoschenko, V. et al. Radioactive contaminated forests in Fukushima and Chernobyl. *Journal of Forest Research* **23**, 3-14 (2018).
9. Sychev, V. N. et al. Spaceflight effects on consecutive generations of peas grown onboard the Russian segment of the International Space Station. *Acta Astronautica* **60**, 426-432 (2007).
10. Musgrave, M. et al. Gravity independence of seed-to-seed cycling in *Brassica rapa*. *Planta* **210**, 400-406 (2000).
11. Carillo, P. et al. Challenges for a sustainable food production system on board of the International Space Station: a technical review. *Agronomy* **10**, 687 (2020).
12. Galts, C. A journey to Mars: The medical challenges associated with deep space travel and possible solutions. *University of British Columbia Medical Journal* **8**, 38-39 (2017).
13. Boratyński, Z. et al. Ionizing radiation from Chernobyl affects development of wild carrot plants. *Scientific Reports* **6**, 39282 (2016).
14. Blankenship, R. *Molecular Mechanisms of Photosynthesis*, Third Edition. (John Wiley & Sons, 2021).
15. Wolf, B. & Blankenship, R. Far-red light acclimation in diverse oxygenic photosynthetic organisms. *Photosynthesis Research* **142**, 349-359 (2019).
16. Proctor, M. & Smirnoff, N. Ecophysiology of photosynthesis in bryophytes: major roles for oxygen photoreduction and non-photochemical quenching? *Physiologia Plantarum* **141**, 130-140 (2011).
17. Diffey, B. Sources and measurement of ultraviolet radiation. *Methods* **28**, 4-13 (2002).
18. Blumthaler, M. et al. Increase in solar UV radiation with altitude. *Journal of Photochemistry and Photobiology B: Biology* **39**, 130-134 (1997).
19. Britt, A. et al. UV-sensitive mutant of Arabidopsis defective in the repair of pyrimidine-pyrimidinone(6-4) dimers. *Science* **261**, 1571-1574 (1993).
20. Campbell, D. et al. The cyanobacterium *Synechococcus* resists UV-B by exchanging photosystem II reaction-center D1 proteins. *Proceedings of the National Academy of Sciences* **95**, 364-369 (1998).

21. Bischof, K. et al. Effects of ultraviolet radiation on photosynthesis and related enzyme reactions of marine macroalgae. *Planta* **211**, 555-562 (2000).
22. Murphy, T. Membranes as targets of ultraviolet radiation. *Physiologia Plantarum* **58**, 381-388 (1983).
23. Smith, M. et al. Involvement of the p53 tumor suppressor in repair of u.v.-type DNA damage. *Oncogene* **10**, 1053-1059 (1995).
24. Danon, A. & Gallois, P. UV-C radiation induces apoptotic-like changes in *Arabidopsis thaliana*. *FEBS Letters* **437**, 131-136 (1998).
25. Nawkar, G. et al. UV-induced cell death in plants. *International Journal of Molecular Sciences*, **14,** 1608-1628 (2013).
26. Minty, B. Fundamentals of airborne gamma-ray spectrometry. *AGSO Journal of Australian Geology and Geophysics* **17**, 39-50 (1997).
27. Tafti, A. & Byerly, D. "X-ray image acquisition" in StatPearls [Internet] (StatPearls Publishing, 2022).
28. Kiong, L. et al. Physiological responses of *Orthosiphon stamineus* plantles to gamma irradiation. *American-Eurasian Journal of Sustainable Agriculture* **2**, 135-149 (2008).
29. Petruzzellis, F. et al. The pitfalls of in vivo imaging techniques: evidence for cellular damage caused by synchrotron X-ray computed micro-tomography. *New Phytologist* **220**, 104-110 (2018).
30. Sachs, R. et al. Radiation-produced chromosome aberrations: colourful clues. *Trends in Genetics* **16**, 143-146 (2000).
31. Kim, J. et al. Differentially expressed genes in response to gamma-irradiation during the vegetative stage in *Arabidopsis thaliana*. *Molecular Biology Reports* **41**, 2229-2241 (2014).
32. Biermans, G. et al. Biological effects of α-radiation exposure by ^{241}Am in *Arabidopsis thaliana* seedlings are determined both by dose rate and ^{241}Am distribution. *Journal of Environmental Radioactivity* **149**, 51-63 (2015).
33. Hase, Y. et al. Biological effects of ion beams in *Nicotiana tabacum* L. *Radiation and Environmental Biophysics* **38**, 111-115 (1999).
34. Yamaguchi, H. et al. Effects of ion beam irradiation on mutation induction and nuclear DNA content in chrysanthemum. *Breeding Science* **60**, 398-404 (2010).
35. Vandenhove, H. et al. Oxidative stress reactions induced in beans (*Phaseolus vulgaris*) following exposure to uranium. *Plant Physiology and Biochemistry* **44**, 795-805 (2006).
36. Sokolik, G. et al. Soil–plant transfer of plutonium and americium in contaminated regions of Belarus after the Chernobyl catastrophe. *Environment International* **30**, 939-947 (2004).
37. Kónya, J. & Nagy, N. "Chapter 4 - Radioactive Decay" in *Nuclear and Radiochemistry*, Second Edition. (eds. J. Kónya & N. Nagy) pages 49-84 (Elsevier, 2018).
38. Choppin, G. et al. *Radiochemistry and Nuclear Chemistry*, Fourth Edition. (eds. G. Choppin G., Liljenzin, J., Rydberg, J. and Ekberg, C.) pages 163-208 (Academic Press, Oxford; 2013).
39. Hinton, T. et al. Radiation-induced effects on plants and animals: Findings of the United Nations Chernobyl Forum. *Health Physics* **93**, 427-440 (2007).
40. Killion, D. & Constantin, M. Effects of separate and combined beta and gamma irradiation on the soybean plant. *Radiation Botany* **14**, 91-99 (1974).

41. Badhwar, G. & O'Neill, P. Long-term modulation of galactic cosmic radiation and its model for space exploration. *Advances in Space Research* **14**, 749-757 (1994).
42. Chancellor, J. et al. Space radiation: The number one risk to astronaut health beyond low Earth orbit. *Life* **4**, 491-510 (2014).
43. Mei, M. et al. Mutagenic effects of heavy ion radiation in plants. *Advances in Space Research* **14**, 363-372 (1994).
44. Gudkov, S. et al. Effect of ionizing radiation on physiological and molecular processes in plants. *Journal of Environmental Radioactivity* **202**, 8-24 (2019).
45. Ward, J. "DNA damage produced by ionizing radiation in mammalian cells: identities, mechanisms of formation, and reparability." In *Progress in Nucleic Acid Research and Molecular Biology*. (eds. Cohn, W., Moldave, K.) Volume 35, pages 95-125 (Academic Press, 1988)
46. Shah, K. et al. Effect of cadmium on lipid peroxidation, superoxide anion generation and activities of antioxidant enzymes in growing rice seedlings. *Plant Science* **161**, 1135-1144 (2001).
47. Foyer, C. & Noctor, G. Oxidant and antioxidant signalling in plants: a re-evaluation of the concept of oxidative stress in a physiological context. *Plant, Cell & Environment* **28**, 1056-1071 (2005).
48. Mittler, R. et al. Reactive oxygen species signalling in plant stress responses. *Nature Reviews Molecular Cell Biology* **23**, 663-679 (2022).
49. Manian, V. et al. Detection of genes in *Arabidopsis thaliana* L. responding to DNA damage from radiation and other stressors in spaceflight. *Genes (Basel)* **12** (2021).
50. Tarrago, L. et al. Regeneration mechanisms of *Arabidopsis thaliana* methionine sulfoxide reductases B by glutaredoxins and thioredoxins. *The Journal of Biological Chemistry* **284**, 18963-18971 (2009).
51. Schapire, A. et al. Plasma membrane repair in plants. *Trends in Plant Science* **14**, 645-652 (2009).
52. Spampinato, C. Protecting DNA from errors and damage: an overview of DNA repair mechanisms in plants compared to mammals. *Cellular and Molecular Life Sciences* **74**, 1693-1709 (2017).
53. Mittler, R. ROS are good. *Trends in Plant Science* **22**, 11-19 (2017).
54. Torres, M. ROS in biotic interactions. *Physiologia Plantarum* **138**, 414-429 (2010).
55. Choudhury, F. et al. Reactive oxygen species, abiotic stress and stress combination. *The Plant Journal* **90**, 856-867 (2017).
56. Tripathy, B. & Oelmüller, R. Reactive oxygen species generation and signaling in plants. *Plant Signaling & Behavior* **7**, 1621-1633 (2012).

CHAPTER II: ENGINEERED GAMMA RADIATION PHYTOSENSORS FOR ENVIRONMENTAL MONITORING

A version of this chapter was published in the Plant Biotechnology Journal:
Sears, R.G., Rigoulot, S.B., Occhialini, A., Morgan, B., Kakeshpour, T., Brabazon, H., Barnes, C.N., Seaberry, E.M., Jacobs, B., Brown, C., Yang, Y., Schimel, T.M., Lenaghan, S.C. and Neal Stewart, C., Jr. (2023) Engineered gamma radiation phytosensors for environmental monitoring. *Plant Biotechnology Journal* **21**(9), 1745-1756. https://doi.org/10.1111/pbi.14072

RGS, SBR, SCL, CNS designed the phytosensor strategy; RGS, HB, EMS, and CNB generated transgenic phytosensors in potato; RGS, AO, BM, TK, HB, CNB, EMS, BJ, CB, YY, and TMS collected data; RS, AO, BM, and YY analyzed data; RS, SBR, AO, BM, CNS, and SCL wrote the article.

Abstract

Nuclear energy, already a practical solution for supplying energy on a scale similar to fossil fuels, will likely increase its footprint over the next several decades to meet current climate goals. Gamma radiation is produced during fission in existing nuclear reactors and thus the need to detect leakage from nuclear plants, and effects of such leakage on ecosystems will likely also increase. At present, gamma radiation is detected using mechanical sensors that have several drawbacks, including: (i) limited availability; (ii) reliance on power supply; and (iii) requirement of human presence in dangerous areas. To overcome these limitations, we have developed a plant biosensor (phytosensor) to detect low-dose ionizing radiation. The system utilizes synthetic biology to engineer a dosimetric switch into potato utilizing the plant's native DNA damage response (DDR) machinery to produce a fluorescent output. In this work, the radiation phytosensor was shown to respond to a wide range of gamma radiation exposure (10–80 Gray) producing a reporter signal that was detectable at >3 m. Further, a pressure test of the top radiation phytosensor in a complex mesocosm demonstrated full function of the system in a 'real world' scenario.

Introduction

Globally there is renewed interest in adopting nuclear power as a cleaner alternative to coal power plants to meet increasingly aggressive climate goals. Despite the success of many nuclear reactors, the public still remains wary of failures, such as Chernobyl in 1986 and Fukushima Daiichi in 2011, and the environmental impact of these incidents[1, 2]. To assuage public concerns and increase safety, there is a need for new technologies to monitor for radiation contamination. For highly penetrative ionizing radiation such as gamma radiation, clear risk to human health appears above doses of 0.1 Gy (acute) or 0.3 Gy (chronic), with the $LD_{50/30}$ for humans at approximately 4 Gy and certain death at ≥ 10 Gy acute exposures[3]. Current mechanical sensors are not feasible for long-term environmental monitoring of ionizing radiation due to costs associated with maintenance and operation. Further, mechanical sensors do not provide an accurate measure of the biological impact of low doses of exposure over an extended period of time. With the advent of synthetic biology, plant biosensors (phytosensors) are emerging as a feasible option to detect and report the presence of environmental disturbances[4]. Phytosensors are uniquely tuned to their environment (soil, water, and air), and the reporters produced by these biosensors directly reflect a biological impact on the surrounding ecosystem.

Plants have a history of use as radiation phytosensors. After Chernobyl, pine tree forests were used as a visual indicator of radioactivity with the phenotypes observed correlating

dosimetrically to both radiation dose received and the radiation emittance rate[5]. Compared to mammals, plants have a much higher radiotolerance, allowing them to persist and monitor exposures much higher than their animal counterparts[6]. A key component of plants' radiotolerance is their native DNA damage response (DDR) pathway. When organisms are exposed to gamma radiation there is a rapid increase in the reactive oxygen species (ROS), which produce numerous single- and double-strand breaks. These DNA breaks are repaired through a complex network of genes that coordinate the repair and maintain the genome integrity. As with nearly all eukaryotes, in Arabidopsis DNA breaks are sensed primarily by ataxia telangiectasia-mutated (ATM) and ataxia telangiectasia-mutated and Rad3-related (ATR) protein kinases as part of protein complexes at the lesion site[7, 8]. ATM and ATR then catalyze the phosphorylation of many protein targets to induce cell cycle arrest and initiate DNA repair[9]. Subsequent phosphorylation of a key plant transcription factor, Suppressor of Gamma Response 1 (SOG1), activates the protein enabling binding to a specific DNA motif [CTT(N)7AAG][10, 11] and activation of many downstream DNA repair genes, such as *RAD51*[11-12]. *RAD51* encodes a recombinase that is essential for homologous recombination and repair of DNA strand breaks. In other eukaryotes, RAD51 forms a homodimer and upon activation binds to double-strand breaks and facilitates strand exchange[14]. In previous work, a promoter consisting of a tetrameric repeat of the SOG1 binding site was used to express a reporter gene in response to a genotoxic stress[11], demonstrating the feasibility of such an approach to sense-and-report gamma radiation.

The overall objective of this work was to develop a fully functional phytosensor for sensing and reporting the presence of gamma radiation in the environment. Potato (*Solanum tuberosum*) was chosen as the chassis organism due to its tetraploid genome and its role as a true crop plant. Additionally, potato's nuclear genome can be effectively engineered. The *mEmerald* green fluorescent protein was chosen as the reporter molecule due to the ability to easily detect the signal at a standoff distance of ≥ 3-meters with a low-cost imaging system. The radiation-responsive promoters of the genes *PCNA*, *UVH1*, *RAD51*, and a synthetic *4xRAD51* promoter were selected for initial testing. Utilizing a design-build-test strategy employed in the development of other phytosensors[15, 16], these components were engineered to meet the requirement of a fully functional gamma radiation phytosensor.

Results

Design and assembly of gamma radiation sensing systems

In order to determine the radiotolerance of potato as a potential phytosensor, an initial dosing experiment was conducted to determine the phenotypic response of four-week-old plants across a range of doses from 0 to 250 Gy (Figure 2.1A). All figures and tables are located in an appendix at the end of the chapter. All dosing distances and times are indicated in Table 2.3. After irradiation, the phenotypes of the treated plants were assessed, first at anthesis and then at senescence (Figure 2.2,3). At anthesis, plants treated with ≥ 20 Gy had impaired apical growth and showed a significant growth delay (Figure 2.2). Plants treated with 80 Gy had severely reduced plant height which corresponded with an increase in leaf fresh and dry weight per unit area, and chlorophyll content (Figures 2.2B-E). At the end of the plants' life cycle, potato treated with 20-40 Gy recovered to a similar height and dry biomass production to that of untreated plants by producing lateral stems, with 40 Gy treated plants having the greatest overall stem length and stem biomass (Figure 2.3C-F). This translated to a significantly lower stem density compared to 0-20 Gy treated plants (Figure 2.3G). Starting at ≥ 20 Gy a progressive reduction of tuber yield was also observed (Figure 2.3H-J). Plants treated with 80 Gy showed a severe

phenotype throughout their entire life cycle and did not reach maturity, though they did produce small tubers (Figure 2.3). Above 80 Gy the phenotype was so severe that no growth was observed, and thus doses above this range were excluded from further analysis.

After identifying an effective range of doses for which potato could sense-and-report gamma radiation, genes that were strongly upregulated across the selected dose range (0-80 Gy) were identified and mined their promoter sequences. The initial gene targets were the native potato genes *StPCNA*, *StUVH1* and *StUVR7*. qRT-PCR was performed using leaf samples collected before treatment, along with 1.5, 9 and 24 hours after treatment to determine if the genes were upregulated, and the time course of expression. Among the native potato DDR genes analyzed, *StPCNA* expression was the most responsive to gamma radiation, showing a significant induction at ≥ 5 Gy, while *StUVH1* only had a significant increase at 80 Gy. *StUVR7* showed no response at any of the doses tested, and thus was excluded from further testing (Figure 2.1B). In addition to being the most sensitive, *StPCNA* was rapidly induced (1.5 h) up to 26.9-fold above basal levels at > 40 Gy, and 10-fold at 10 Gy. *StUVH1* expression achieved only a 2.2-fold increase above baseline at doses > 40 Gy, and no significant induction below 40 Gy at any timepoint tested. While the magnitude of *StPCNA* expression was high during the first 9 hours tested, the expression level fell significantly after 24 hours, indicating a burst response to the single dosing scheme. Based on this data, it was hypothesized that the promoters of *StPCNA* and *StUVH1* could be used to develop sensors for gamma radiation.

Promoters for *StPCNA* and *StUVH1* were mined as potential candidates to use as sensors for gamma radiation. Plant promoters are notorious for their variability in length, with many plant promoters being in excess of 1000 bp[17]. Since these genes' promoters have not been characterized, the approximate regions of -1800 to +18 for *StPCNA* and *StUVH1* were extracted from the potato genome and domesticated for use in GoldenGate cloning. This length was selected in order to encompass cis elements within the promoter regions of these genes while not adding additional cloning difficulties due to very long, repetitive sequences. The *StPCNA* and *StUVH1* native promoters along with previously characterized *AtSOG1* DNA binding motif [CTT$(N)_7$AAG] from the At*RAD51* promoter[10,11] were used to design promoter switches for gamma radiation sensing. Transgene expression cassettes containing the promoter-5'UTR region of either *StPCNA*, *StUVH1* or *AtRAD51* (Table 2.4) were fused to the *mEmerald* fluorescent reporter gene along with a viral Cowpea Mosaic Virus 3'UTR (3CPMV-nos), producing the pPCNA, pUVH1 and pRAD51 plant transformation vectors (Figure 2.1C), respectively. Additionally, a synthetic promoter including four repeats (4x) of the AtSOG1 binding motif [5' – CGAGACTTGTTGAAGAAGGCCTTT – 3'] from *AtRAD51*'s promoter fused to a minimal 35S promoter-Tobacco Mosaic Virus Ω leader was also designed (Table 2.4). A *mEmerald* transgene cassette including this *4xRAD51* promoter and the 3CPMV-nos 3'UTR was used to assemble the p4xRAD51 transformation vector (Figure 2.1C). Both native and synthetic promoter constructs included a screenable and selectable marker for selection of transgenic events (Figure 2.4). Once transformed into potato, these phytosensor constructs can be evaluated for radiation inducibility as well as fluorescence at a three-meter standoff.

Testing of gamma radiation sense-and-report

Transgenic potato events were created using each of the sense-and-report cassettes described above (*$StPCNA_{pro}$*, *$StUVH1_{pro}$*, *$AtRAD51_{pro}$* and *$4xRAD51_{pro}$*). Three independent transgenic events (events 1-3) were selected for each construct, and events were genotyped using Southern blot to select representatives with both single and multiple copies of the transgene (Table 2.1,

Figure 2.5). In addition to determining the number of inserts, the baseline expression of the reporter gene, *mEmerald*, was measured relative to the housekeeping gene *StEF1α* (Table 2.1, Figure 2.5). Not surprisingly, *4xRAD51$_{pro}$* event 1 had the highest baseline expression of > 2.6-fold relative to the housekeeping gene, since this event contained four copies of the *4xRAD51$_{pro}$::mEmerald* transgene. For initial testing, the downselected events were challenged as four-week-old plantlets in tissue culture at the highest dose, 80 Gy, to determine if the phytosensor architecture functionally expressed *mEmerald* after insult by gamma radiation. Based on qRT-PCR analysis, all events for *4xRAD51$_{pro}$* and *StPCNA$_{pro}$* showed significant induction of *mEmerald* in response to 80 Gy of gamma radiation (Figure 2.6A). The largest fold induction was observed for the *4xRAD51$_{pro}$* events 1-3 with significant ($p < 0.05$) induction of 11.80-fold, 5.35-fold, and 9.89-fold, respectively. To a lesser degree, *StPCNA$_{pro}$* events 1- 3, were significantly ($p < 0.05$) upregulated from 1.74-2.09-fold. Only two of the three *AtRAD51$_{pro}$* events (2 & 3) showed significant fold induction, while the *StUVH1$_{pro}$* events showed both increased and decreased expression depending on the event (Figure 2.6A). As the goal was to develop a fully functional phytosensor capable of reporting at standoff, it was necessary to determine if the *mEmerald* signal produced in response to the radiation treatment was detectable at > 3 m. All *4xRAD51$_{pro}$* events were able to be detected by the fluorescence-inducing laser projector (FILP)[18] system, demonstrating the potential of these events as functional radiation phytosensors (Figure 2.6B). *AtRAD51$_{pro}$*, *StUVH1$_{pro}$*, and *StPCNA$_{pro}$* events did not show a clear increase in fluorescence after treatment, and thus were excluded from further testing (Figure 2.6B). Based on the initial testing at the maximum dose of 80 Gy, the *4xRAD51$_{pro}$* events met the criteria for a radiation phytosensor. However, an 80 Gy dose is a relatively high dose for monitoring scenarios, therefore these *4xRAD51$_{pro}$* phytosensor events were selected for further testing at a variety of doses and as whole plants in pots.

For in-depth characterization of the *4xRAD51$_{pro}$* phytosensing events, four-week-old plants in soilless media were treated with 0, 5, 10, and 40 Gy of gamma radiation. Both spectrofluorometer and FILP image data confirmed high fluorescent reporter accumulation after radiation treatments in all transgenic events (Figure 2.7A, B). Based on measurement of the *mEmerald* reporter, peak induction of events 1 (6.3-fold) and 2 (4.9-fold) were reached at 48 hours, while the peak of event 3 (3.6-fold) was observed at 72 hours. Not surprisingly the 40 Gy dose had the highest reporter signal in all events, with all events able to report 40 Gy at standoff within 24 hours of treatment ($p < 0.05$). The lowest detectable dose at standoff was 10 Gy for all events within 48 hours of treatment. *4xRAD51$_{pro}$* event 3 was the only event that demonstrated the potential to detect signals at 5 Gy; however, this trend was variable between the FILP and fluorometry analysis (Figure 2.7C). Among the three events, *4xRAD51$_{pro}$* event 1 had the strongest reporter signal in both the FILP and fluorometry assays (Figure 2.7B, C) and therefore was downselected for further testing.

In order to determine the sensitivity to radiation and the time course for functional reporting from a single exposure, data from the *4xRAD51$_{pro}$* event 1 phytosensor was collected at 8-72 hours at a range of exposures (Figure 2.8A-C). The spectrofluorometer data showed significant fluorescent induction at 7.5 Gy at 8 hours post-treatment (1.6-fold increase compared to 0 Gy plants) and a maximum fluorescence of 5.6-fold above untreated plants when treated with 80 Gy after 72 hours. Based on the doses tested, the limit for detection of the *4xRAD51$_{pro}$* event 1 phytosensor was 7.5 Gy (Figure 2.8A). FILP image data collected at 72 hours demonstrated a similar trend as spectrofluorometer data, although the FILP signal of plants treated with 7.5 Gy was not significantly different from untreated plants (Figure 2.8B).

Interestingly, the *4xRAD51$_{pro}$* event 1 phytosensor produces a strong fluorescent response even when damage is significant enough to cause loss of gravitropic growth (Figure 2.8C).

Pressure test of radiation phytosensor in mesocosms

To evaluate the performance of the top radiation phytosensor in a simulated natural environment, *4xRAD51$_{pro}$* event 1 plants were grown in mesocosms with and without weedy competitors (Figure 2.9). *4xRAD51$_{pro}$* event 1 phytosensors and wild-type controls were analyzed in time-course by both spectrofluorometer and FILP starting at 8 hours until complete decay to background fluorescent level (0 Gy). Spectrofluorometer data showed significant reporting of 40 Gy at 8 hours post-treatment but not 10 Gy. Significant reporting of 10 Gy via spectrofluorometer and FILP occurred at 24 hours post-treatment and persisted at 48 hours post-treatment in both mesocosm conditions (Figure 2.10A-C). Plants treated with 10 Gy returned to background fluorescence levels after 7 days when observed by spectrofluorometer and 10 days via FILP, while 40 Gy treated-plants took one month to return to pre-radiation levels (Figure 2.10A,B). In the FILP images, as shown in previous figures, the stems and leaf veins are visibly brighter than the leaf portions without vasculature (Figure 2.10C). No significant effect of competitors on fluorescent response was detected in either the spectrofluorometer or the FILP data sets (ANOVA, $p < 0.05$).

To test whether phytosensors were able to persist in the environment, plant phenotypic analysis was performed over the plants' lifecycle in mesocosms. Both wild-type and *4xRAD51$_{pro}$* plants were significantly affected by competition or exposure to radiation, but there was no significant interaction between competition and radiation dose for either genotype (Figure 2.11, Table 2.2). Wild type and phytosensor plants grown in competitive mesocosms demonstrated significant reductions in fresh total aboveground biomass, fresh tuber mass, and number of tubers compared to those grown alone (Table 2.2). Both genotypes exhibited a significant decrease in number of tubers when exposed to both 10 and 40 Gy radiation in mesocosms without competition (Figure 2.11, Table 2.2). Fresh total aboveground biomass was affected by exposure to radiation in a dose-specific manner in both wildtype and *4xRAD51$_{pro}$* plants and while there was no significant change in biomass at 10 Gy, there was a significant increase in the aboveground biomass at 40 Gy (Figure 2.11, Table 2.2). Both genotypes exhibited a significant reduction in tuber number and mass after exposure to 40 Gy radiation when grown alone (Figure 2.11, Table 2.2). Leaf number was not affected by competition or radiation in either genotype (Figure 2.11, Table 2.2). No significant interaction between genotype and community or dose was observed, indicating that there is no difference in how the phenotype of the genetically engineered phytosensor responds to dose and/or community compared to wildtype controls (Table 2.2).

Discussion

Initial irradiation of the *S. tuberosum* chassis indicated that potato is viable for radiation phytosensing. Our results suggest that gamma radiation treatments below 40 Gy stimulates vegetative growth at the cost of tuber mass, a desirable trait for an ionizing radiation phytosensor. This is in contrast to work done in tomato, showing nearly half the vegetative biomass accumulation in plants treated with 25 Gy from a Calcium heavy ion source[19]. The difference in radiotolerance between potato and tomato could be due to a myriad of factors, including the difference between ionizing radiation from a Cobalt-60 source versus a Calcium heavy ion source, as well as the increase in ploidy from potato to tomato diluting the effect of

mutations[20]. The sunken meristem phenotype observed in this study aligns well with the phenotypes observed in pine species around Chernobyl[21] and Fukushima[22, 23]. Based on biomass data and the sunken meristem phenotype, it is likely that ≥ 20 Gy disorganizes the balance of gene expression which maintains the meristematic tissues[24], with 80 Gy and above destroying meristematic growth. These field studies do not report the stimulatory "hormesis" effect of ionizing radiation on vegetative growth seen here and widely in the literature[25-28], though these pine species were receiving a constant low dose while this study used quick, relatively intense doses. The intention of this sensor was to produce maximum aboveground vegetation to be visible to detectors, therefore phenotypes such as increased stem biomass after ≤ 40 Gy irradiation aid in sensor performance rather than harm the sensor. The potato chassis is therefore an adequate short-term sensor at 80 Gy and below, while long term-establishment of the sensor can experience a maximum of 40 Gy. Both radiation levels are well above what humans can survive.

Performance of the synthetic promoter construct was superior to the native potato promoter constructs tested in this study. Induction of native gene expression was greatest at 1.5-hours post-treatment and continues for *StPCNA* through 24 hours, which is consistent with similar experiments in *Arabidopsis*[10, 29]. The *StPCNA* promoter was expected to perform well based on the genes' essential role as a protein clamp holding DNA polymerases[30, 31] onto lesion sites to coordinate repair of nearly all types of DNA lesions[32]. Native *StPCNA* appeared to be highly inducible (26.9-fold at 40 Gy) but this inducibility did not transfer to the $StPCNA_{pro}$ phytosensor construct (~2-fold at 80 Gy across 3 transgenic events). When comparing basal expression (Figure 2.5A) to FILP images of the $4xRAD51_{pro}$, $StPCNA_{pro}$, and $AtRAD51_{pro}$ events (Figure 2.6B), 0.5-1-fold expression compared to the *StEF1α* reference gene results in fluorescence that can be plainly observed via FILP. If the $StPCNA_{pro}$ was behaving as it did in its native context, these sensors should show no visible fluorescence when uninduced and very light fluorescence when induced. In all three events, there was much more uninduced *mEmerald* transcript present compared to *StPCNA* transcript but much lower relative induction from the higher basal level. It is possible that the 3'UTR from cowpea mosaic virus included in the phytosensor construct is raising the basal level of transcript by preventing degradation of the mRNA[33]. Additionally, plant *PCNA* promoters are known to be regulated by a number of cell cycle factors such as E2F transcription factors[34, 35]. These sites are typically within - 600 bp of the transcription start site[36], though lower induction after gamma radiation treatment could be due to unidentified cis elements that were not included in the *StPCNA* promoter region used for the phytosensor construct.

Surprisingly, native *StUVH1* was only induced at 40 and 80 Gy, *StUVR7* was uninduced at all treatments, and the $StUVH1_{pro}$ construct was downregulated in two of the three transgenic events. Studies in *Arabidopsis* indicate that the UVH1/UVR7 endonuclease is essential for nucleotide excision repair of pyrimidine dimers and that these proteins play a role in genome stability and gamma radiation tolerance[37, 38]. Poor induction of *StUVH1* paired with the fact that its endonuclease partner, *StUVR7*, was not induced at all by gamma radiation indicates that either: 1) these genes in potato do not have the same role in homologous recombination and nucleotide excision repair as they do in *Arabidopsis*[39]; 2) these genes' role in DNA repair can be carried out without induction of transcript when irradiated with 40 Gy or less; or 3) the genomic context of potato and polyploidy results in other unidentified homologs of the loci tested being upregulated. The possibility of *UVH1* and *UVR7* having reduced roles in homologous recombination should be investigated, as most plant DNA repair research is conducted in

Arabidopsis and rice[40]. If the process of homologous recombination in *Solanum* species differs from these model species, this could have major impacts on our understanding of plant DNA repair. Additionally, this gap in DNA repair knowledge could hinder applications such as CRISPR-Cas mediated insertion of foreign DNA into commercially important *Solanum* species, a process which relies on homologous recombination or non-homologous end joining[41, 42].

The *AtRAD51* promoter did not behave as expected in the context of its phytosensor construct. Previous characterizations of the *AtRAD51* promoter report over 40-fold induction in *Arabidopsis* seedlings when treated with the radiomimetic Zeocin[11]. Qualitatively similar results were seen when the promoter was used in the context of a transgene driving GUS expression in that same paper. Additionally, the induction of *AtRAD51* in response to gamma radiation in its native context is consistent enough to be considered a dosimeter for gamma radiation[43]. Like the performance of the $StPCNA_{pro}$, the difference between the previous reports on native *AtRAD51* and the $AtRAD51_{pro}$ phytosensor construct could be due to the 3'UTR added to stabilize the *mEmerald* transcript. This data could also suggest that other motifs in the *AtRAD51* promoter may assist in activation of the gene and that these motifs are not bound by trans-activators in potato. Plant promoters exhibit an incredible amount of variation even among close relatives; furthermore, the *AtRAD51* and putative *StRAD51* promoter regions exhibit only 44.9% homology and there are no $CTT(N)_7AAG$ motifs within 2000 bp of the *StRAD51* start codon in the published potato genome. This lack of homology suggests that the *AtRAD51* promoter would not be regulated similarly to the native *Arabidopsis* context, even though the overall DDR machinery appear to remain consistent between *Arabidopsis* and potato.

Despite the poor performance of the *AtRAD51* promoter in the context of a potato radiation phytosensor, four repeats of the *AtRAD51* SOG1 binding site provided an adequate promoter for a radiation phytosensor. At 10 Gy, this sensor produced a maximum 2.17-fold above basal during the 24h-72h peak reporting window when detected by FILP. This is consistent with other published phytosensors, with reporting beginning at 24 hours post-treatment and fluorescence fold-changes in the single digits appear to be the limit regardless of stimuli[44-46]. The performance of the sensor is not hindered by field conditions and the sensor construct was not a metabolic burden on the potato chassis. Based on the performance of the $4xRAD51_{pro}$ phytosensor, plants deployed in field conditions can report ≥ 10 Gy of ionizing radiation to a drone-mounted FILP apparatus with a relatively low-powered laser and camera system flying three meters away as soon as 24 hours after its release into the environment. This sensing threshold and timescale would be highly useful during a meltdown similar to Chernobyl or Fukushima where radioactive solids were released into the environment and continued to irradiate their surroundings for weeks. In these scenarios, widely dispersed plants could pinpoint presence of an ionizing radiation source based on nearby sensor's peak fluorescence intensity and the duration in which the sensor remains turned on. Based on the sensor's performance in mesocosms and relatively high sensing threshold (LD_{99} for humans is 8 Gy), it is unlikely that the $4xRAD51_{pro}$ sensor would report DNA damage from stimuli other than ionizing radiation.

Additionally, the 4xRAD51 construct appeared to have 'leaky' expression when uninduced, leading to a relatively high basal fluorescence compared to wild type potato. Uninduced fluorescence for 4xRAD51 event 1 was 100,000-200,000 cps while wild type *S. tuberosum* cv. 'Desiree' was 20,000-60,000 cps, meaning basal fluorescence of the sensor was typically 5-fold higher than the background fluorescence of a potato leaf. This is consistent with the increased rate of the cell cycle occurring in young tissue which will inherently experience more DNA lesions due to double-stranded breaks, stalled replication forks, and repairing

incorrectly inserted bases[47, 48]. These expression patterns seen in the potato phytosensor suggest that previous characterization of SOG1-induced DDR in *Arabidopsis*[11] and rice[49] remains consistent in *Solanaceae*. Though basal stem fluorescence does allow sensor plants to stick out from a surrounding plant canopy, new iterations of the sensor will need to improve upon the established SOG1 transcriptional switch to either lower basal fluorescence associated with growing tissue and/or increase SOG1 presence in leaf tissue types to increase fluorescence in the sensor plant's canopy. This sensor represents an indirect biosensor[50] which relies on many molecular interactions which leads to SOG1 binding the *4xRAD51* promoter. Indirect biosensors are inherently prone to more error than the direct biosensors reviewed by Liu et al., 2022 where the reporter is directly activated by the stimulus, which is clear given the high level of basal fluorescence in all $4xRAD51_{pro}$ events. If a direct biosensor could be devised for ionizing radiation, this could offer improvements on the current sensor design.

Analytically, leaf spectroscopy was more sensitive in detecting differences between untreated and treated plants compared to standoff detection using FILP. A large factor in each of these measurements was the proportion of vascular tissue in the reading, whether it be leaf veins in the area read by the spectrofluorometer or all vascular tissue visible when imaged with the FILP. Fluorescence was much higher in vascular tissue compared to 'leaf' tissue types (mesophyll, palisade, epidermis, etc.) in all 4xRAD51 events across all experiments. This expression pattern is consistent with reported higher expression of SOG1 in actively growing and vascular tissue[51, 52] and that NAC family transcription factors are broadly associated with meristem and vascular tissue types[53-55]. The spectrofluorometer used in this work is designed to read flat leaf tissue and attempts to read the stem directly allowed ambient light into the detector. Efficient extraction of FILP pixel data relies on the thresholding function of ImageJ[56] being done on chlorophyll a fluorescence images of the phytosensor plants, meaning that all green tissue of the plant is averaged into the mean pixel value for a sensor. To optimize sensor performance, the observation equipment used should be tailored to detect stem and vascular fluorescence while disregarding tissue types such as mesophyll which do not fluoresce as brightly in the $4xRAD51_{pro}$ sensors.

This sensor currently uses a green fluorescent protein as the reporter which can only be observed with specialized equipment such as a FILP. This reporter was chosen due to low native fluorescence in potato's leaves in the GFP emission spectrum, resulting in a very specific reporter in the context of plant tissue. The requirement of specialized mechanical equipment does not address the problem associated to current radiation sensors, which is that the mechanical parts can either be damaged or unavailable in the event of an emergency. Future iterations of the sensor using a specific, plainly visible reporter would be ideal so that the general public can be warned of danger without the need for equipment. To this end, reporter phenotypes such as high purple anthocyanin accumulation[57], bright pink tissue[58], or bleaching[59] can be achieved by using different genetic circuits to change cytosolic and plastid metabolism. The key to these reporting strategies is making sure various stressors and life stage transitions do not produce a similar phenotype, thus making the sensor non-specific. The first iteration of the gamma radiation phytosensor is deployable when using the green fluorescent reporter, though future iterations should incorporate a reporter that functions without extra equipment.

Conclusion

In this work we developed a usable gamma radiation phytosensor able to sense and report ≥10 Gy of gamma radiation in the environment at a standoff distance of 3 meters. The Gray unit is a measure of absorbed dose (joules/kg) but this is in contrast to radiation conditions during radiation emergencies. During these emergencies, radioactive material has contaminated the environment and is constantly releasing ionizing radiation at a certain intensity. For example, just after the Chernobyl disaster ambient levels of radiation were estimated to range from 300 Sieverts/hour near the reactor core to 0.1 sieverts/hour at the nearby concrete mixing unit[60]. Considering the sievert-to-Gray conversion for gamma radiation, the radiation phytosensor here developed would reach its 10 Gy sensing threshold after 2 minutes and 100 hours, respectively. Treatment times during this experimentation ranged from 2 to 16 hours with transcript abundance peaking 1.5 hours after treatment and fluorescence peaking 48-72 hours after treatment. In this gamma radiation range, 40 Gray was reported as early as 8 hours while 10 Gray required 24 hours to produce a significant response, meaning this sensor would have been useful for those responding to the Chernobyl disaster and catastrophes like it. More investigation is needed to understand the sensor's performance under longer, low-intensity irradiation. At what radiation intensity will the plant's DNA repair machinery overtake the time the sensor requires to accumulate enough reporter protein? This and other specification questions need to be answered before the sensor can be deployed.

Though improvements and further testing should be carried out, *4xRAD51$_{pro}$* event 1 is the first ionizing radiation phytosensor which can report at a 3-meter standoff, and is the first self-propagating, self-repairing dosimeter. This sensor, and phytosensors generally, are important tools as humanity seeks out a more sustainable existence. Through this academic work and future phytosensor research, electricity-independent environmental sensing will become a viable tool for humans to understand our impact on the environment.

Materials and methods

Plant material and growth conditions

Wild type *Solanum tuberosum* cv. 'Desiree' was procured from the Wisconsin Seed Potato Certification Program at the University of Wisconsin - Madison and kept in sterile culture on modified Murashige and Skoog media for transformation[61]. After transformation and genotyping qPCR, events were maintained in tissue culture.

For experiments where plants were in pots, plants were removed from tissue culture and placed into a 4-inch plastic pot filled with a soilless media and allowed to adjust to ambient humidity for one week under a closed lid inside of a growth chamber. After this the lid was removed, plants were grown within the growth chamber an additional three weeks until the beginning of the experiment. Growth chambers were set to a 16-hour light / 8-hour dark daylight regime, with daytime temperature set to 20 ºC and nighttime temperature set to 18 ºC. Plants were fertilized with Peter's 20-20-20 fertilizer after hardening and after 3 weeks in soil.

Gamma radiation treatment

Gamma radiation treatment was done by adjusting plants' distance and dosage time from a Cobalt-60 source to reach a total dose (reported in this paper in Gray). Treatment times and distances can be found for each of the experiments in Table 2.3.

Construct design and cloning

The promoter region of genes involved in DNA repair were mined from available sequence databases and domesticated for Golden-Gate cloning as described before[62, 63]. These sequences include: 734 bp upstream/18 bp downstream the start codon of *AtRAD51* (TAIR id: AT5G20850); 1818 bp upstream/18 bp downstream the start codon of *StUVH1* (Phytozome id: PGSC0003DMT400067435); and 1898 bp upstream/18 bp downstream the start codon of *StPCNA* (Phytozome id: PGSC0003DMT400078207). The Golden-Gate compatible synthetic promoter *4xRAD51* was chemically synthesized by GeneArt (Invitrogen, Thermo Fisher Scientific). This promoter includes the AtSOG1 DNA binding motif ($CTT(N)_7AAG$) repeated in tandem 4 times[64] fused to the *CaMV 35S* minimal promoter region (+1; -47) along with the *TMV Ω* leader. Promoter regions used in this work are indicated in Table 2.4. Putative gamma radiation inducible promoters together with the *3CPMV-nos* 3'UTR[65] used to assemble *mEmerald* (FPbase ID: AD4BK) expression cassettes into the level-2 acceptor plasmid pAGM4723 using Golden-Gate cloning as described before[62, 63]. The *AtRAD51*, *StUVH1*, *StPCNA* and *4xRAD51* inducible cassettes were used to assemble the pRAD51, pUVH1, pPCNA, and p4xRAD51 phytosensor constructs, respectively.

Plant transformation

Transformation of *Solanum tuberosum* cv. 'Desiree' was performed using an established method[61]. At least ten shoots from separate calli were recovered and propagated separately per construct, with ten being kept after successful genotyping via PCR. Three of those events were then selected for further testing based on vigorous growth phenotype and a range of basal fluorescence.

Genotyping via Southern Blot

Southern blots were performed to determine transgene copy number for the transgenic radiation phytosensor events by established methods[66]. Briefly, 5 µg of genomic DNA from three biological replicates of each phytosensor construct and line were extracted using the CTAB method. After extraction, DNA was cut using AflII, BspHI, and KasI enzymes and fragments were separated on a 1% agarose gel for 5.5 hours. DIG hybridization probes for a 500 bp sequence of mEmerald coding sequence were generated using primers Fw 10 and Rv 18 and the Roche PCR DIG Probe Synthesis Kit. The probe membrane was then placed onto the gel, crosslinked, hybridized, and detected according to the above protocol.

qRT-PCR

RNA was extracted from tissue samples stored in RNAlater solution (Sigma-Aldrich) after dosing and extracted using a TRI Reagent extraction protocol (Molecular Research Center) and RNA Clean and Concentrator kit (Zymo) with a DNase I treatment. Two thousand nanograms of RNA from each sample was used to generate cDNA with the Applied Biosystems™ High-Capacity cDNA Reverse Transcription Kit (Fisher). The cDNA was generated, then 1.08 ng cDNA was used for qPCR a single 5 µl qPCR reaction using the PowerUp™ SYBR™ Green Master Mix (Fisher) and its associated protocol. An Applied Biosystems QuantStudio 6 Flex qPCR instrument and its associated software were used. The primers used for native genes, mEmerald, and *StEF1α* can be found in Table 2.5. For all primer sets, qPCR settings include 2 minutes at 50ºC, 10 minutes at 95ºC, then 40 cycles where temperature begins at 95ºC for fifteen seconds, descends 1.6ºC per second to 60ºC where it holds for one minute, then ascends to 95ºC

at the same rate. Results were analyzed using the $2^{(-\Delta\Delta C_T)}$ method with mEmerald C_T values first being set relative to *EF1α* expression, then relative to the appropriate average 0 Gy ΔC_T value to calculate fold change induced by gamma radiation treatment[67]. Primer efficiencies were equal and therefore not included in $2^{(-\Delta\Delta C_T)}$ calculations.

Spectrofluorometer measurements and data analysis

Measurements were taken with a Fluorolog®-3 spectrofluorometer (Horiba / Jobin Yvon, Excitation for mEmerald measurements was 465 nm and emission was observed from 500-515 nm, with 509-511 representing peak emission[68]. The second, third, and fourth leaves from the meristem were measured twice on each plant. The counts per second (CPS) for 509-511 nm of each read were then averaged to create a mean CPS for a biological replicate. The mean CPS values for each biological replicate for a construct x event x treatment combination were then averaged to calculate the mean and standard error. Statistics were calculated using the JMP Pro 15 software (SAS, Cary, NC) ANOVA function ($p < 0.05$) and mean separation with a Tukey's HSD ($p < 0.05$).

Fluorescence-inducing laser projector photographs

The fluorescence-inducing laser projector designed by Rigoulot et al., 2021 was used to observe plant fluorescence at a distance of three meters[69]. Images of mEmerald fluorescence were taken with the 465 nm laser and 525 nm emission filter with an exposure of 300 milliseconds with 200 watts of laser power. Chlorophyll images were taken with the 465 nm laser and 625 nm emission filter with an exposure of 300 milliseconds and a laser power of 1-2 watts. All images were processed and analyzed for pixel intensity using the ImageJ program[70]. Pixel data was analyzed in ImageJ by identifying plant tissue in the chlorophyll a image using the Image > Adjust > Thresholding function. Then, Analyze > Analyze particles was used to generate ROIs for the plants in the image. Once generated, the ROIs were measured on the mEmerald fluorescence images and mean pixel values for each plant were averaged to generate a treatment / event average.

Mesocosm experiments

Each mesocosm was contained within a 34.6 cm x 21 cm x 12.4cm plastic bin filled with a 2:1 mix by volume of potting and field soil, collected at the East Tennessee AgResearch and Education Center (Knoxville, TN, USA), respectively. Previous studies have shown a combination of field and potting soil to yield the highest biomass of *S. tuberosum*. Furthermore, while this soil composition is not solely derived from the field, it is likely to resemble natural conditions around agricultural fields where regular tilling and fertilizing prevent field soil from compacting. Plants were watered as needed.

To assess the effect of competitors on the top performing transgenic *S. tuberosum* sense and report genotype (p4xRAD51) in response to radiation, communities were constructed with and without weedy neighbors. We chose the following heterospecifics: Cyperus esculentus (yellow nutsedge) and Portulaca oleracea (common purslane). These species were chosen to represent a variety of growth habits (prostrate, erect), life histories (annuals and perennials), status (native and invasive), and reproductive strategies (outcrossing, self-fertilizing, and asexual propagation), as these factors have been shown to influence competition among plants[71]. In addition, all species are known to commonly occur across the globe and are considered invasive species outside of their native ranges. These competitors were germinated on potting soil in the

greenhouse and grown for four weeks before being transplanted into communities with focal individuals. Each mesocosm containing neighbors had two replicates per transgenic event and wild type *S. tuberosum*, two replicates *C. esculentus*, and four replicates *P. oleracea* totaling 8 plants in each competitive mesocosm. For mesocosms without competition, two replicate individuals of each *S. tuberosum* genotype were planted at each end of the mesocosm, totaling 4 individuals. Each community mesocosm was replicated three times, totaling 6 biological replicates per community per radiation dosage (72 *S. tuberosum* total).

Mesocosms were grown in the University of Tennessee: Knoxville North Greenhouse. To supplement the available light, LED growth lights (Fluence SPYDR 2x LED Grow Light, Fluence, Austin, TX, USA) were installed and set to a photoperiod of 16hr light/8hr dark. Mesocosms were watered as needed. One week after transplanting, to allow for plant establishment and limit stress, mesocosms were transported to the cobalt-60 facility for radiation treatments. During transportation, all mesocosm bins were placed in sealed 14 Qt (13.25 L) plastic bins.

Mesocosm measurements

RNA was extracted from tissue samples of the newest three fully expanded leaves of focal *S. tuberosum* individuals at 1.5 hours post-treatment to measure gene expression of mEmerald. Fluorescence was measured using the Fluorolog and FILP, as described above, at 24, 48, 72, 168, 240, 360, and 672 hours.

To quantify the effect of competitors on *S. tuberosum*, traits were measured eight weeks after planting, when plants naturally senesced. Fresh and dry total aboveground biomass and tuber mass, and number of tubers, leaves, and primary and secondary branches were measured for each focal *S. tuberosum*. Fresh biomass and tuber mass and number of tubers, leaves, and primary and secondary branches were collected at harvest. For measurements of dry total aboveground biomass and tuber mass, tissues were dried for two weeks at 55ºC prior to measurement.

Mesocosm statistical analysis

FILP images and trait measurements from mesocosms were analyzed using R v. 4.1.3 (R Core Team 2022). Fluorescence, measured as pixel intensity per unit area, was quantified from FILP generated images using NIH ImageJ software. To test whether transgenic *S. tuberosum* fluorescence was affected by competition and radiation dose, pixel intensity per unit area was the dependent variable and radiation dosage ("treat"), community, and their interaction were treated as fixed effects in generalized linear models using the "glm" function in the stats package. Since wildtype *S. tuberosum* does not naturally produce GFP, p4XRAD51 event 1 plants at 0 Gy in mesocosms without competition were set as the reference for fluorescence; wildtype was not included in the analysis. Analysis of Variance (ANOVA) and Covariance (ANCOVA) were performed using the stats package and car package[72], respectively. Since there was no significant interaction between dosage and community, the effect of dosage was analyzed using the Dunnett's Test to compare multiple treatments to the control using the "DunnettTest" function in the DescTools package within each community type[73].

For trait measurements from mesocosms, traits were treated as the dependent variable and genotype, dosage, community and their interactions were treated as fixed effects using generalized linear models as described above; total aboveground biomass and tuber mass measurements were analyzed using a guassian distribution, while number of tubers, leaves, and

primary and secondary branches were analyzed using the poisson distribution. Wildtype plants in mesocosms without competition at 0 Gy were set as the reference. ANOVA, ANCOVA, and Dunnett's Test for each trait were performed as described above. In addition, to test for effect of community type on traits, pairwise differences for each trait were calculated between community types for each genotype within each radiation dosage. We used the function "pairwise" in the emmeans package[74]. We estimated the effect of competition for each estimated marginal means using Tukey's method to adjust significance thresholds for multiple comparisons.

References

1. Medvedev, Z. The legacy of Chernobyl / Zhores A. Medvedev. (W.W. Norton, New York; 1990).
2. Povinec, P., Hirose, K. & Aoyama, M. in Fukushima Accident. (eds. P.P. Povinec, K. Hirose & M. Aoyama) 55-102 (Elsevier, Boston; 2013).
3. Metting, N. The DOE Ionizing Radiation Dose Ranges Chart. *Office of Environment, Health, Safety, and Security, United States Department of Energy* (Washington, DC; 2017). Article number AU-22 001-2018.
4. Volkov, A. & Markin, V. in Plant Electrophysiology: Signaling and Responses. (ed. A.G. Volkov) 173-206 (Springer Berlin Heidelberg, Berlin, Heidelberg; 2012).
5. Yoschenko, V. et al. Radioactive contaminated forests in Fukushima and Chernobyl. *Journal of Forest Research* **23**, 3-14 (2018).
6. Real, A. et al. Effects of ionising radiation exposure on plants, fish and mammals: relevant data for environmental radiation protection. *Journal of Radiological Protection: Official Journal of the Society for Radiological Protection* **24**, A123-A137 (2004).
7. Kimura, S. & Sakaguchi, K. DNA repair in plants. *Chemical Reviews* **106**, 753-766 (2006).
8. Nisa, M. et al. The Plant DNA Damage Response: Signaling Pathways Leading to Growth Inhibition and Putative Role in Response to Stress Conditions. *Frontiers in Plant Science* **10**, 653 (2019).
9. Roitinger, E. et al. Quantitative phosphoproteomics of the ataxia telangiectasia-mutated (ATM) and ataxia telangiectasia-mutated and rad3-related (ATR) dependent DNA damage response in *Arabidopsis thaliana*. *Molecular & Cellular Proteomics: MCP* **14**, 556-571 (2015).
10. Yoshiyama, K. et al. Suppressor of gamma response 1 (SOG1) encodes a putative transcription factor governing multiple responses to DNA damage. *Proceedings of the National Academy of Sciences of the United States of America* **106**, 12843-12848 (2009).
11. Ogita, N. et al. Identifying the target genes of SUPPRESSOR OF GAMMA RESPONSE 1, a master transcription factor controlling DNA damage response in Arabidopsis. *The Plant Journal: for Cell and Molecular Biology* **94**, 439-453 (2018).
12. Yoshiyama, K. et al. Increased phosphorylation of Ser-Gln sites on SUPPRESSOR OF GAMMA RESPONSE1 strengthens the DNA damage response in *Arabidopsis thaliana*. *The Plant Cell* **29**, 3255-3268 (2017).
13. Doutriaux, M. et al. Isolation and characterisation of the RAD51 and DMC1 homologs from *Arabidopsis thaliana*. *Molecular & General Genetics: MGG* **257**, 283-291 (1998).
14. Sung, P. & Robberson, D. DNA strand exchange mediated by a RAD51-ssDNA nucleoprotein filament with polarity opposite to that of RecA. *Cell* **82**, 453-461 (1995).
15. Persad, R. et al. The Q-System as a synthetic transcriptional regulator in plants. *Frontiers in Plant Science* **11**, 245 (2020).
16. Liu, W. et al. Bacterial pathogen phytosensing in transgenic tobacco and Arabidopsis plants. *Plant Biotechnology Journal* **11**, 43-52 (2013).
17. Ali, S. & Kim, W. A fruitful decade using synthetic promoters in the improvement of transgenic plants. *Frontiers in Plant Science* **10**, 1433 (2019).
18. Rigoulot, S. et al. Imaging of multiple fluorescent proteins in canopies enables synthetic biology in plants. *Plant Biotechnology Journal* **19**, 830-843 (2021).

19. Arena, C. et al. Suitability of *Solanum lycopersicum* L. 'Microtom' for growth in Bioregenerative Life Support Systems: exploring the effect of high-LET ionising radiation on photosynthesis, leaf structure and fruit traits. *Plant Biology (Stuttgart, Germany)* **21**, 615-626 (2019).
20. Sparrow, A. et al. Some factors affecting the responses of plants to acute and chronic radiation exposures. *Radiation Botany* **1**, 10-34 (1961).
21. Kozubov, G. & Taskaev, A. Radiobiologicheskiye issledovaniya khvoinikh v raione Chernobyl'skoi katastrofy (Radiobiological studies of coniferous species in the area of the ChNPP accident). *Moscow, Design Information. Cartography* (2002).
22. Yoschenko, V. et al. Morphological abnormalities in Japanese red pine (*Pinus densiflora*) at the territories contaminated as a result of the accident at Fukushima Dai-Ichi Nuclear Power Plant. *Journal of Environmental Radioactivity* **165**, 60-67 (2016).
23. Watanabe, Y. et al. Morphological defects in native Japanese fir trees around the Fukushima Daiichi Nuclear Power Plant. *Scientific Reports* **5**, 13232 (2015).
24. Carles, C. & Fletcher, J. Shoot apical meristem maintenance: the art of a dynamic balance. *Trends in Plant Science* **8**, 394-401 (2003).
25. Maity, J. et al. Modulation of some quantitative and qualitative characteristics in rice (*Oryza sativa* L.) and mung (*Phaseolus mungo* L.) by ionizing radiation. *Radiation Physics and Chemistry* **74**, 391-394 (2005).
26. Sax, K. The effect of ionizing radiation on plant growth. *American Journal of Botany* **42**, 360-364 (1955).
27. Kuzin, A. et al. Stimulation of plant growth by exposure to low level γ-radiation and magnetic field, and their possible mechanism of action. *Environmental and Experimental Botany* **26**, 163-167 (1986).
28. Volkova, P. et al. Radiation hormesis in plants. *Current Opinion in Toxicology* **30**, 100334 (2022).
29. Culligan, K. et al. ATR and ATM play both distinct and additive roles in response to ionizing radiation. *The Plant Journal: for Cell and Molecular Biology* **48**, 947-961 (2006).
30. Strzalka, W. et al. Crystal structures of the *Arabidopsis thaliana* proliferating cell nuclear antigen 1 and 2 proteins complexed with the human p21 C-terminal segment. *Protein Science: a Publication of the Protein Society* **18**, 1072-1080 (2009).
31. Bravo, R. et al. Cyclin/PCNA is the auxiliary protein of DNA polymerase-delta. *Nature* **326**, 515-517 (1987).
32. Strzalka, W. & Ziemienowicz, A. Proliferating cell nuclear antigen (PCNA): a key factor in DNA replication and cell cycle regulation. *Annals of Botany* **107**, 1127-1140 (2011).
33. Meshcheriakova, Y. et al. Fine-tuning levels of heterologous gene expression in plants by orthogonal variation of the untranslated regions of a nonreplicating transient expression system. *Plant Biotechnology Journal* **12**, 718-727 (2014).
34. Egelkrout, E. et al. Two E2F elements regulate the proliferating cell nuclear antigen promoter differently during leaf development. *The Plant Cell* **14**, 3225-3236 (2002).
35. Uemukai, K. et al. Transcriptional activation of tobacco E2F is repressed by co-transfection with the retinoblastoma-related protein: cyclin D expression overcomes this repressor activity. *Plant Molecular Biology* **57**, 83-100 (2005).

36. Kosugi, S. et al. Two of three promoter elements identified in a rice gene for proliferating cell nuclear antigen are essential for meristematic tissue-specific expression. *The Plant journal: for Cell and Molecular Biology* **7**, 877-886 (1995).
37. Hefner, E. et al. Arabidopsis mutants sensitive to gamma radiation include the homologue of the human repair gene ERCC1. *Journal of Experimental Botany* **54**, 669-680 (2003).
38. Vannier, J. et al. ERCC1/XPF protects short telomeres from homologous recombination in *Arabidopsis thaliana*. *PLoS Genetics* **5**, e1000380 (2009).
39. Dubest, S. et al. Roles of the AtErcc1 protein in recombination. *The Plant journal: for Cell and Molecular Biology* **39**, 334-342 (2004).
40. Gimenez, E. & Manzano-Agugliaro, F. DNA damage repair system in plants: A worldwide research update. *Genes* **8**, 299 (2017).
41. Lee, K. et al. CRISPR/Cas9-mediated targeted T-DNA integration in rice. *Plant Molecular Biology* **99**, 317-328 (2019).
42. Collonnier, C. et al. Towards mastering CRISPR-induced gene knock-in in plants: Survey of key features and focus on the model *Physcomitrella patens*. *Methods* **121-122**, 103-117 (2017).
43. Ryu, T. et al. Transcriptome-based biological dosimetry of gamma radiation in Arabidopsis using DNA damage response genes. *Journal of Environmental Radioactivity* **181**, 94-101 (2018).
44. Persad-Russell, R. et al. Specific bacterial pathogen phytosensing is enabled by a synthetic promoter-transcription factor system in potato. *Frontiers in Plant Science* **13**, 873480 (2022).
45. Fethe, M. et al. The performance of pathogenic bacterial phytosensing transgenic tobacco in the field. *Plant Biotechnology Journal* **12**, 755-764 (2014).
46. Abd El-Halim, H. et al. Evaluation of two promoters for generating transgenic potato plants as salicylic acid biosensors. *Biologia Plantarum* **64**, 535-540 (2020).
47. Schärer, O. Chemistry and biology of DNA repair. *Angewandte Chemie (International ed. in English)* **42**, 2946-2974 (2003).
48. Hu, Z. et al. Mechanisms used by plants to cope with DNA damage. *Annual Review of Plant Biology* **67**, 439-462 (2016).
49. Nishizawa-Yokoi, A. et al. The role of rice SOG1 and SOG1-like in DNA damage response. *bioRxiv*, 2022.2001.2021.477278 (2022).
50. Liu, Y. et al. Biological and molecular components for genetically engineering biosensors in plants. *BioDesign Research* **2022**, 9863496 (2022).
51. Klepikova, A. et al. A high resolution map of the *Arabidopsis thaliana* developmental transcriptome based on RNA-seq profiling. *The Plant journal: for Cell and Molecular Biology* **88**, 1058-1070 (2016).
52. Pagano, A. et al. Identification and characterization of SOG1 (Suppressor of Gamma Response 1) homologues in plants using data mining resources and gene expression profiling. *Genes* **13**, 667 (2022).
53. Yamaguchi, M. et al. Vascular-related NAC-DOMAIN7 is involved in the differentiation of all types of xylem vessels in Arabidopsis roots and shoots. *The Plant journal: for Cell and Molecular Biology* **55**, 652-664 (2008).

54. Ohtani, M. et al. A NAC domain protein family contributing to the regulation of wood formation in poplar. *The Plant Journal: for Cell and Molecular Biology* **67**, 499-512 (2011).
55. Takada, S. et al. The CUP-SHAPED COTYLEDON1 gene of Arabidopsis regulates shoot apical meristem formation. *Development (Cambridge, England)* **128**, 1127-1135 (2001).
56. Schindelin, J. et al. Fiji: an open-source platform for biological-image analysis. *Nature Methods* **9**, 676-682 (2012).
57. Zuluaga, D. et al. *Arabidopsis thaliana* MYB75/PAP1 transcription factor induces anthocyanin production in transgenic tomato plants. *Functional Plant Biology: FPB* **35**, 606-618 (2008).
58. He, Y. et al. A reporter for noninvasively monitoring gene expression and plant transformation. *Horticulture Research* **7**, 152 (2020).
59. Mochizuki, N. et al. Arabidopsis genomes uncoupled 5 (GUN5) mutant reveals the involvement of Mg-chelatase H subunit in plastid-to-nucleus signal transduction. *Proceedings of the National Academy of Sciences of the United States of America* **98**, 2053-2058 (2001).
60. Medvedev, G. Chernobyl Notebook. *Joint Publications Research Service* (1989).
61. Chronis, D. et al. Potato transformation. *Bio-Protocol* **4**, e1017-e1017 (2014).
62. Engler, C. et al. A Golden Gate modular cloning toolbox for plants. *ACS Synthetic Biology* **3**, 839-843 (2014).
63. Occhialini, A. et al. MoChlo: A versatile, modular cloning toolbox for chloroplast biotechnology. *Plant Physiology* **179**, 943-957 (2019).
64. Ogita, N. et al. Identifying the target genes of SUPPRESSOR OF GAMMA RESPONSE 1, a master transcription factor controlling DNA damage response in Arabidopsis. *The Plant Journal* **94**, 439-453 (2018).
65. Meshcheriakova, Y. et al. Fine-tuning levels of heterologous gene expression in plants by orthogonal variation of the untranslated regions of a nonreplicating transient expression system. *Plant Biotechnology Journal* **12**, 718-727 (2014).
66. Mellars, G. & Gomez, K. Mutation detection by Southern blotting. *Methods in Molecular Biology (Clifton, N.J.)* **688**, 281-291 (2011).
67. Livak, K. & Schmittgen, T. Analysis of relative gene expression data using real-time quantitative PCR and the 2−ΔΔCT Method. *Methods* **25**, 402-408 (2001).
68. Cubitt, A., Woollenweber, L. & Heim, R. in Methods in Cell Biology, Vol. 58. (eds. K.F. Sullivan & S.A. Kay) 19-30 (Academic Press, 1998).
69. Rigoulot, S. et al. Imaging of multiple fluorescent proteins in canopies enables synthetic biology in plants. *Plant Biotechnology Journal* **19**, 830-843 (2021).
70. Schneider, C. et al. NIH Image to ImageJ: 25 years of image analysis. *Nature Methods* **9**, 671-675 (2012).
71. Fazlioglu, F. et al. Reproductive efficiency and shade avoidance plasticity under simulated competition. *Ecology and Evolution* **6**, 4947-4957 (2016).
72. Fox, J. & Weisberg, S. An [R] Companion to Applied Regression, Third Edition. (Thousand Oaks CA: Sage., 2019).
73. Signorell, A. et al. DescTools: Tools for Descriptive Statistics. R package version 0.99.40 (2021).

74. Lenth, R. emmeans: estimated marginal means, aka least-squares means. R package version 1.4.7. (2022).

Appendix

Table 2.1: Basal expression and transgene copy number of the phytosensor events examined in this study.

Results of the qRT-PCR and southern blots shown in Figure 2.5 combined into a table. Data shown includes the expression of *mEmerald* CDS compared to the expression of the reference gene *Elongation Factor 1α* (*StEF1α)* and the copy number as determined by Southern Blot with a probe designed for the mEmerald CDS. Superscript lettering reflects the results of statistical comparison of lines within a construct by ANOVA ($p < 0.05$) and a post hoc mean separation with Tukey's adjustment ($p < 0.05$).

Phytosensor Construct	Event	Basal expression relative to *StEF1*α	Transgene copy number
p4×RAD51	1	2.60x[a]	4
	2	0.38x[b]	1
	3	0.48x[b]	2
pRAD51	1	0.64x[a]	2
	2	0.54x[a]	1
	3	1.10x[b]	1
pUVH1	1	0.94x[a]	1
	2	1.45x[ab]	1
	3	2.42x[b]	4
pPCNA	1	0.50x[a]	2
	2	0.57x[a]	1
	3	1.86x[b]	1

Table 2.2: The effect of field conditions and weedy competitors on p4xRAD51 event 1 phenotype.

Results of an ANOVA based on GLM to test for effect of genotype ("geno"), radiation dose ("dose"), community type, and their interactions on potato traits at harvest. Measurements of fresh total aboveground biomass, number of tubers, and fresh total tuber mass were taken after plants naturally senesced.

Factor	Df	Number of leaves		Aboveground biomass		Number of tubers		Tuber mass	
		LR Chisq	p	LR Chisq	p	LR Chisq	p	LR Chisq	p
Geno	1	1.10	0.29	3.93	0.05	0.23	0.64	0.40	0.53
Dose	2	4.52	0.1	15.73	0	12.41	0	26.07	0
Community	1	0.31	0.58	40.2	0	5.14	0.02	31.54	0
Geno:Dose	2	1.10	0.41	1.79	0.41	0.58	0.75	2.10	0.35
Geno:Community	1	0.96	0.56	0.33	0.56	0.12	0.73	0.07	0.79
Dose:Community	2	1.64	0.15	3.77	0.15	2.62	0.27	4.12	0.13
Geno:Dose:Community	2	0.75	0.69	0.74	0.69	0.46	0.79	2.76	0.25

Table 2.3: Gamma radiation treatment calculations for all experiments.

These tables list the intended absorbed dose treatments in Gray and the calculations done to determine the correct distance from the source for a given time of treatment. Due to space constraints, some treatments had do be done at a distance range which centered on the intended dose but spread beyond this distance. For these, the distance range and absorbed dose range are provided. The dose tables correspond to the experiments in this article as follows: (A) – Figures 2.1, 2.2, and 2.3; (B) – Figure 2.7; (C) – Figure 2.8A-C; (D) – Figure 2.9-11.

A

Designed Treatment (Gray)	Total rad	Treatment rate (rad / sec)	Distance from source (meters)	Distance range (meters)	Treatment Range (Gray)
0	0	0	-	-	-
5	500	0.0694	1.569	-	-
10	1000	0.1389	1.165	-	-
20	2000	0.2778	0.865	-	-
40	4000	0.5556	0.642	-	-
80	8000	1.1111	0.476	-	-

B

Designed Treatment (Gray)	Total rad	Treatment rate (rad / sec)	Distance from source (meters)	Distance range (meters)	Treatment Range (Gray)
0	0	0	-	-	-
5	500	0.0347	2.114	1.96 - 2.27	4.25 - 5.95
10	1000	0.0694	1.569	1.42 - 1.72	8.06 - 12.68
40	4000	0.2778	0.865	0.71 - 1.02	27.42 - 62.80

C

Designed Treatment (Gray)	Total rad	Treatment rate (rad / sec)	Distance from source (meters)	Distance range (meters)	Treatment Range (Gray)
0	0			-	-
5	500	0.0087	3.624	-	-
7.5	750	0.0130	3.045	-	-
10	1000	0.0174	2.690	-	-
20	2000	0.0347	1.997	-	-
40	4000	0.0694	1.482	-	-
80	8000	0.1389	1.100	-	-

D

Designed Treatment (Gray)	Total rad	Treatment rate (rad / sec)	Distance from source (meters)	Distance range (meters)	Treatment Range (Gray)
0	0	-	-	-	-
10	1000	0.0206	2.501	2.40 - 2.61	9.099 - 11.05
40	4000	0.0823	1.378	1.27 - 1.48	33.72 - 48.10

Table 2.4: Promoter sequences used in phytosensor constructs

These sequences include the entire promoter sequence used in the radiation phytosensor constructs including the first six amino acids of the native protein.

Promoter	Sequence 5' → 3'
StPCNA$_{pro}$	TGCTCTACTCTGCCTACTCCATCGCAATACCGGAACATTGAGTCATATTAAAGGTTCCCTAAATCCCATCTTATATTG CCCTCTATTAATTTGCCTTTTACCTTCTATTATTCCAGCAATTATCAAAGTAGAAAGTATAGTTCTCCTTGGTGATTAA AGGATAACAAACTATGCGACACTATCAAAGTTTGAAGTTTGTCAAACCAAGCAGACAACAACAATTAGCTACTGAT AAAAACAGAGGCGGATCAAGTACTAAAAGCTTTATTTATCCTGACATTTATTTAAGGATCATAGCACTGAACCAAT TGCACTTCTATACTGTAATTGTGAGTTCAAATCTAATAGTATAGTAAGGCTTTACACACACACACACACACATACAT ACATATATATATATATATGCTCCCTTGTAAGTTGGAAGTACTGGAACCCCGCCAATGTTTACAGTTTTCAAAAGGAT TAGCGTGAAAGCATTCATTGCTATATATCAAAACCATAAAACAACAAAATCACAAATAAGCTCAATTGCTCAAAGA CGAAGAATACACAATAAACAAAAATTCGACAGACTGTTTAGCTCTTTATGTTCTGGGTAAAAAATGAACGGAAGA ATCGTCTAATCCGCTCAGGTAATAGCAAATTCAATTTAAATCAAATATTGATGCCGATCACAAACGCAAATGACATA CAATCTCATCAACAATTAATATCTATAATTTTAGTTCATTCGTATCGAAGAAGAGAATTAAGAGAGAAAAAGCAGA CATGAAAAGAAAACTCACCGTGAAGAGATTATGGCGTAGTATCGAAATGCGTCTCTTTCTCTCTCTAATTAGCGAA GGCTCTCGAATGGGTTGCGTGTTGTGGGGAAAGGCTTATATATATACCTGTAGCGTAAAGAAGTTTCTAGACGAG GGACACGAAATCCTTTTTAATTGGACTTGAATTTGTCACATTATTCCACCAACCAAAAAAAATGAAATTTGTTTCAT ACTAGTAGATTTGATATGAGATTATATAATTTTAAAGGTTATATTAATATTTAATTAGCATTGTAATAAATGAATGT ACAAGACTCTACAAAGTGGACTCTCGATTCTTTATTATGATATGATCAAAAACAAAAAAGTTGGTTATTCTCTTTTTT TTTGAATAATTGATTAGTGAGTGACATCTGTTTGTCGTAGTAACTTATGTATCTTTTAGAAAACAATCTGAATATTCA TTTTGATCTATTGAAAATTATATAATAATACTTAAAATCACAATCTAAAAATTTATAGATATTAGATGACAATTTAAT GTTTTGTCAAGCCCAAAGCTATAGTTGCAACAAAAACAATGAGCAATCATTGTGTTTTCATAAGTAGGGTCTGAAA AGGAGGATATGTATGATGTACGTAATTTTTTCTCTACCTTGTAAAGATAGAGAAAGTGTTACAATAGTAAAAAAAA AACAGGCTGAAAACAGTGGAAAAGAAAATAAAAGCAACATTTAATAGGGACGAAAATTTAATGATAGCCTAAAA AGAGACATTTGCATAAATTAGCCTATTATCCTTCCTAGTAATTACTACTGAAAAAGAGTATAAAACTGTAATGGGTT TTAAAGCCCAAGACAACCCAAGGCCTTTTTCCGGAGCAGAGCCCACTGATTTATGGGCCAAAATAGGCAGTAGCC CAAAATCAAAATAAAGGCGGGAACTTATTTTATTTTCTGACAATTCATTTCCCGCCAATAGCGAGCCCTAAATTCTC GAGCACACTTTCCAGCAGCTATATAAACCCTAACCCCTTTTTTCCACTCATTTTCGCTCTATTTTTCATTCAGACACCT CTGTTTTCCCTCCTTCCCCATTTCAAAACCCTAACCCTAGTTTCCCGCAGAGAACAAAATGTTGGAACTACGTCTA
StUVH1$_{pro}$	ATTCGAGACAGTCCCTAGTGAATTCTGTCCTGAAATACGACGGGGTTCAGTTGCATGGGTTGGTTCTGGCCCTGAA TTCTTTATAAGCTTAGCAAACCATCAAGAATGGAAAAATGCGTACACTGTTTTTGGCTATGTGCTGCCGGAGGACT TGAAAATCGTAGAGAAAATAGCTCAGCTCCCCACGAAATCAGATATCTGGACCGGAGTTAACGTGACAATCTTGG AGAACCCTGTACCTTTGAATGTACGACGAATCAAGTCCAGCAATGATGATCTGAACCTCAGTAGTTAGCACTTATG GATCTGTATGATTTGCAAATTAGCACAATACTGCTACTTTGTATATTGAAATTATAGTTTTGAAACTGTTCTATGCAC ACTTCTATATCCATGTTGTAATCAATTTTGCAGAGCATGTTTTCATAATTTGGAAAGAAGAAATAACACCTTGAATT TTGTTGGCTCCAAGTGAATTGCCTATTACTATATGTTAGGTAAGACAAATATTTTTCGCAATTTATTTTTAGGGAAA AGGGCTTGATATACCCCTCAACTTTGCTATTTGGAGCTGATATGCCCCTTATTATGAAAGTGACTCATATATACCCTT ACCGTTATACAAACGGTTCACATATACCCCTACCGTTACAAAATGAGCTCACATATACCCTTCATTTAACGGAAGTG AAAAATTAGTTTTAAATTTATATTTTTGACTTTTAATTTTCTTCAAAATTATTTAGGGGTATATGATTCTTCTAGCAAA GTTAAAGGTATATTTTAATCTTTTTCATACATAAATTATTTTTTTACTTCTTTGATTATAATTATTTGAGTTTCTTATTC TTATTTTTTTTTTCTTTCATTCCTTAGGGTAAAGAAAAAATTTAAAACTATTTTTTGTGGCTATATTGTAATTTAAAAC TATTTTTTTTTGTCTATATTGTAATTTGAAGAAAAAAAAATTGGTCATCTATAATAAGTTTTACAAGAATATTAGTGAA ACATAAGTAAATTTGACCATCAAAATAATAAGTCTAAATTAGTCATTGAAACAAAAAAAGAGTCAAAAAAAAAAAT GTTTGAGGAGGATTAAATATACTCATATGGGATTATATATATATTTTTAAAAAATAATAAAAAATTAAACTAAAATT AATTTATTTCATTTCCGTTAGAGGAAAAGGGTATATGTGAGCCATTGGTATATAAATAGGGGTATATATGAGCCAC TTTCATAACGAGGGTATATCAGCTCTAAATGACAAAGTTGAGGGGTATATCAGACCCCTTATTTTTATATAACAATA TTTCATTGTAGCAGTCAAAAGTATCACATCAAATGACACTATTATAAAGAGATTAATTTTCTTCAAATGTGTGTAAA ATTCCACAAAATGGGTTTTGGGAGTGTAGAATGTACACAAATATTATCACTCTTCGGGTTTTGAAAGCGTAGAATG TATGCAGATCTTATCACTAGCTCATGGAGGTAGAGAGACTGTTTCTGAAAGAACTTCGGCTCAAGTGCAATCCAAG TGCAATAAAATTTCTAGATGAGTACATAAAAATGTTGAAAGGTTGTTCAAGTGACAAAAATGGAAGTATGGGTAG CAAAAGCAATACATTTTCAAACTGCAGGGGCTAAACTCAGATTTGAGATTTGGCTAAACCCCAATTTTGCAAATATT CTCATATATATATCATCACTTTGAATTTTTCCAACAAACTCCACAGCGACCTTCCCGCCACCACCATCTCCGCCATCA TCCACCATAATCGCCACCGCATAAGGCTGAAACCTAGATTTCAAAATATGGTGCAATTTCACGAA
AtRAD51$_{pro}$	ATAGCTCAGTGGTAGAGCAATTGACTGCAGATCAATAGGTCACCGGTTCGAACCCGGTTGGGCCCTATATGTTTTA GTTTACCAAAAAAAATTAAATATCATCTTGAATAAAGAAAATTGACAAATTTTGTGATATTTGTAATATTTTATTTTT GTTATAATAAGTGATTACTACATTGTTGGAATTGTGGTGGTTCTCGGCGGTCAAACACCTAGGTACCATTTGGTTG ACATTCAAACACCTAGGTATCACTCGGCGGTCAAACACCTATTGTTTTTACAAAACGTTAATTTAGTGTTTTAAAAA TATATAATTTTAAGTAAAAATAATTTAAAATAAAAAAATAATTTTGAGAATCCATAATTCGATCAACTTTGATAATAT CTAACATTTATAATTTCATGCATTTAACTGAAAATTTAAAATTACTATGGTACTTAATTAATAATAAAAATGAGGAG GATTTTGTTGTTGTTTTTGAGTATTTTATAGAATAAGAATTTGGGCTTTAATAGCCTTTAAAGCCCAATATGATCAA GGCCGAGGAAAAGCTGACCCAAACGTAATCGAGACTTGTTGAAGAAGCCTTTGCCCTCATCGTCGTCTTGTATAAT AATTTTGGTTGTGGCGCTTCTTTCAATTTGTTTTCAGTTTCGCCATTTCCCTCCACTCTCAAGCTCTCTTTTGCTTCTCT CGCTTTCTCTGGTGACCCGAATCTGCTCTGATTGAGAGAATGACGACGATGGAGCAA

Table 2.5: Primers used in the work.

Listed are the forward and reverse primers used for all DNA amplification in the work. These primers include those for extraction promoters from the genome, genotyping transgenic plants, conducting qRT-PCR, and generating a probe for southern blot.

Forward Primers		
ID	**Name**	**Sequence**
Fw 1	L4440-Long	GCGCAGCGAGTCAGTGAGCGAGGAAGCGGA
Fw 2	Genotyping1_Fw	GATCTAGTAACATAGATGACACCG
Fw 3	Genotyping2_Fw	CTATCCTTCGCAAGACCCTTC
Fw 4	Genotyping3_Fw	CGAAACGCTGTTCGGCCTGTGG
Fw 5	StEF1α_qPCR_Fw	ATTGGAAACGGATATGCTCCA
Fw 6	StPCNAα_qPCR_Fw	CCAGAGGTGACATCGGTACTGCA
Fw 7	StUVH1α_qPCR_Fw	CAGTAGATCAGGATGGACGTTGTCT
Fw 8	StUVR7α_qPCR_Fw	AAACACTTGTGCTCTTTATTTGAGC
Fw 9	mEmerald_qPCR_Fw	GACCACTACCAGCAGAACAC
Fw 10	mEmerald_southernblot_probe_Fw	CCTGAAGTTCATCTGCACCACCGGC

Reverse Primers		
ID	**Name**	**Sequence**
Rv 1	PARP1-5UTR-P1-RV	TGGGCTTGCCATTTCTCCGGTAAGAGACAATTACACAATGCGAGAGTACT
Rv 2	PARP1-5UTR-P2-RV	AGTACAGGTCTCACATTTTATGTGGGCTTGCCATTTCTCCGGTAAGA
Rv 3	RAD51-5UTR-P1-RV	AGTACAGGTCTCACATTTGCTCCATCGTCGTCATTCTCTCAATCAGAGCAGATTCGGGTCACCA
Rv 4	PCNA-5UTR-P1-RV	AGTACAGGTCTCACATTAGACGTAGTTCCAACATTTTGTTCTCTGCGGGAAACTAGGGTTAGGGTTTTGAAA
Rv 5	UVH1-5UTR-P1-RV	GAAATCTAGGTTTCAGCCTTATGCGGTGGCGATTATGGTGGATGATGGCGGAGATGGTGGTGGCGGGAAG
Rv 6	UVH1-5UTR-P2-RV	AGTACAGGTCTCACATTTCGTGAAATTGCACCATATTTTGAAATCTAGGTTTCAGCCTTATGCGGTGGCG
Rv 7	UVR7-5UTR-P1-RV	TTTCTGATTTTCACCCACCAAATACTATCACCAAACCGACCCGAATTTTTTATTTTATTTTTTTGCATAG
Rv 8	UVR7-5UTR-P2-RV	ATTTTCTCCTTCTGCTTTCTTTTCTGTTTCGCCGCTATTTTTTCTGATTTTCACCCACCAAATACTATCACCAAA
Rv 9	UVR7-5UTR-P3-RV	AGTACAGGTCTCACATTCGCTCTGCGTCTCCCATTTCGTTACTGTATTTTCTCCTTCTGCTTTCTTTTCTGTTTCGCCGC
Rv 10	Genotyping1_Rv	CACCATGGTGAGCAAGG
Rv 11	Genotyping2_Rv	TACTCAAACCGCCCCATATG
Rv 12	Genotyping3_Rv	GTTCAGCAGGCCGGCATCCTGG
Rv 13	StEF1α_qPCR_Rv	TCCTTACCTGAACGCCTGTCA
Rv 14	StPCNAα_qPCR_Rv	CACTGTGTTCGACAATGGAGATGCT
Rv 15	StUVH1α_qPCR_Rv	CACCAACTTCCAAGGTCACTGGT
Rv 16	StUVR7α_qPCR_Rv	CACAAAATTATGCGGAGTCTAAAGT
Rv 17	mEmerald_qPCR_Rv	TCTCGTTGGGGTCTTTGCTC
Rv 18	mEmerald_southernblot_probe_Rv	TCTTTGCTCAGCTTGGACTGGGTGC

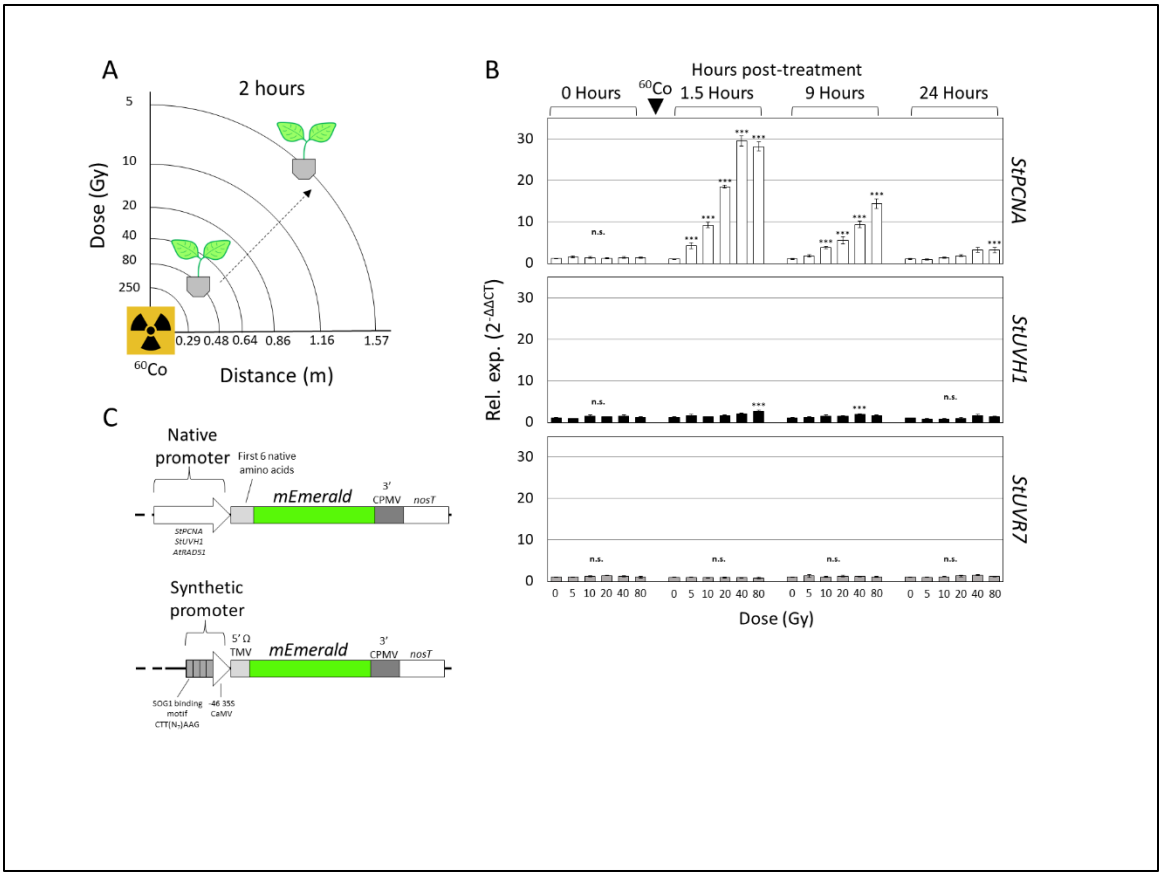

Figure 2.1 Radiation-inducible genes in *Solanum tuberosum* and design of radiation phytosensor constructs.

(A) Schematic representation of the gamma radiation facility used to treat whole potato plants grown potting mix. The indicated 250-5 Gy doses were obtained after 2 hours of treatment with plants placed 0.48-1.57 meters from the Cobalt 60 (^{60}Co) radiation source. **(B)** Expression time course of three putative radiation-inducible genes in four-week-old wild type potato treated (5-80 Gy) and non-treated with gamma radiation. Samples were taken before treatment (0 Hours), then 1.5, 9 and 24-hours post-treatment (^{60}Co, black arrow). Graphs represent RT-qPCR relative expression data ($2^{-\Delta\Delta CT}$) of the indicated radiation inducible genes (*StPCNA*, *StUVH1* and *StUVR7*) vs the endogenous reference gene, *StEF1α*. Data are expressed as mean ± standard error (SE) of 4 biological and three technical replicates. Data were analyzed using ANOVA ($p < 0.05$) and comparisons to 0 Gy were evaluated using Post-Hoc Dunnett's T3 test ($p < 0.05$). Statistical significance is indicated by "***" while non-significance with "n.s." **(C)** Design of radiation phytosensor constructs. The endogenous promoter-5'UTR sequence of *StPCNA* and *StUVHI*, and *AtRAD51* plus each gene's first six codons along with the synthetic 4xRAD51-min35S-TMVΩ promoter-5' TMV Ω UTR were used to design phytosensors. All phytosensor constructs contain the *mEmerald* reporter gene (green fluorescent protein variant) and the Cowpea Mosaic Virus (CPMV)-nos 3'UTR and terminator.

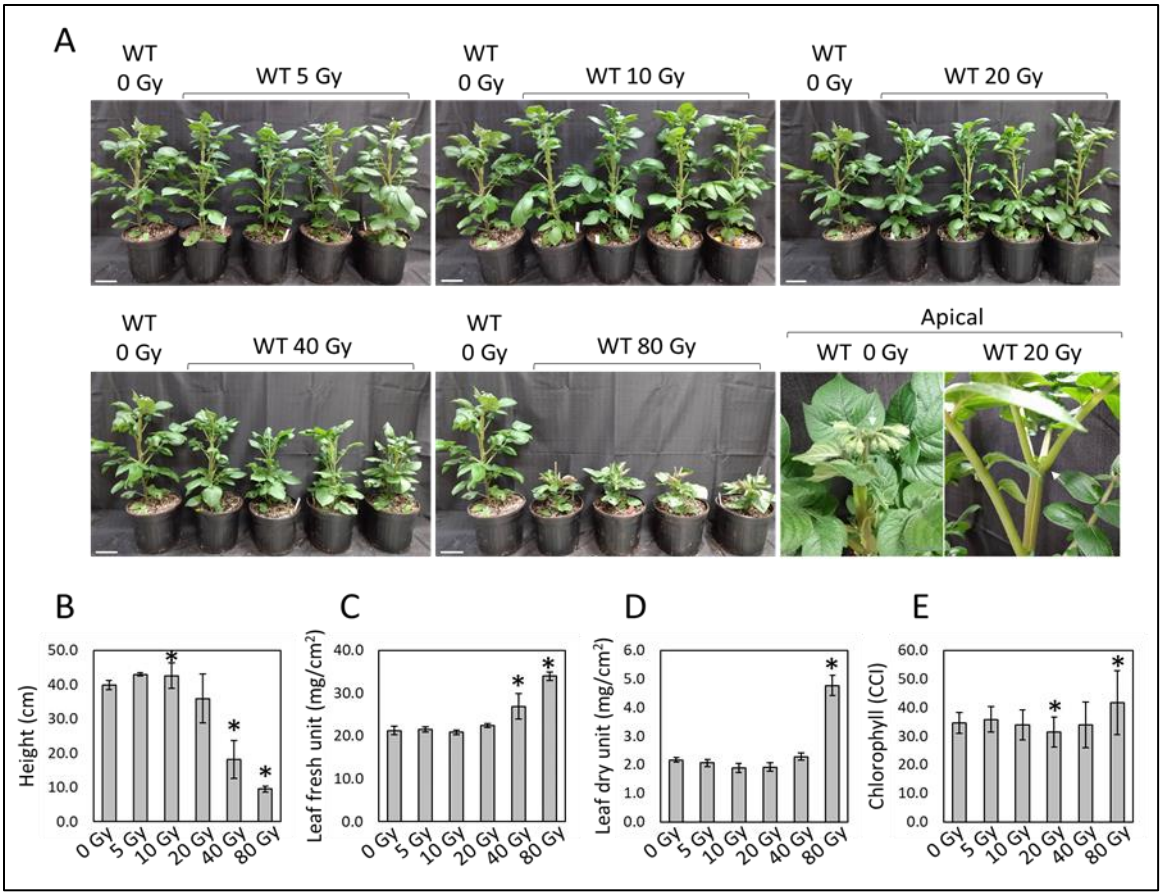

Figure 2.2: Phenotypic characteristics at anthesis of wild-type potato plants exposed to gamma radiation.

(A) Images showing 7-week-old wild-type potato plants in potting soil exposed to increased doses of gamma radiation (5-80 Gy) in comparison to non-treated control plants (0 Gy). Starting at 20 Gy doses, a severe inhibition of plant apical growth (white arrows) preventing anthesis was observed (apical). Graphs represent mean ± sd (standard deviation) of various plant phenotypic characteristics at anthesis of 4 plants per treatment: height **(B)**; ratio of either leaf fresh or dry weight to foliar area **(C and D, respectively)**; chlorophyll content index, CCI **(E)**. ANOVA ($p<0.05$) and a post-hoc Dunnett's t test ($p<0.05$) was used to evaluate means separation. Statistical significance in comparison to the control group (0 Gy) is indicated (*). Scale bars: 10 cm (A).

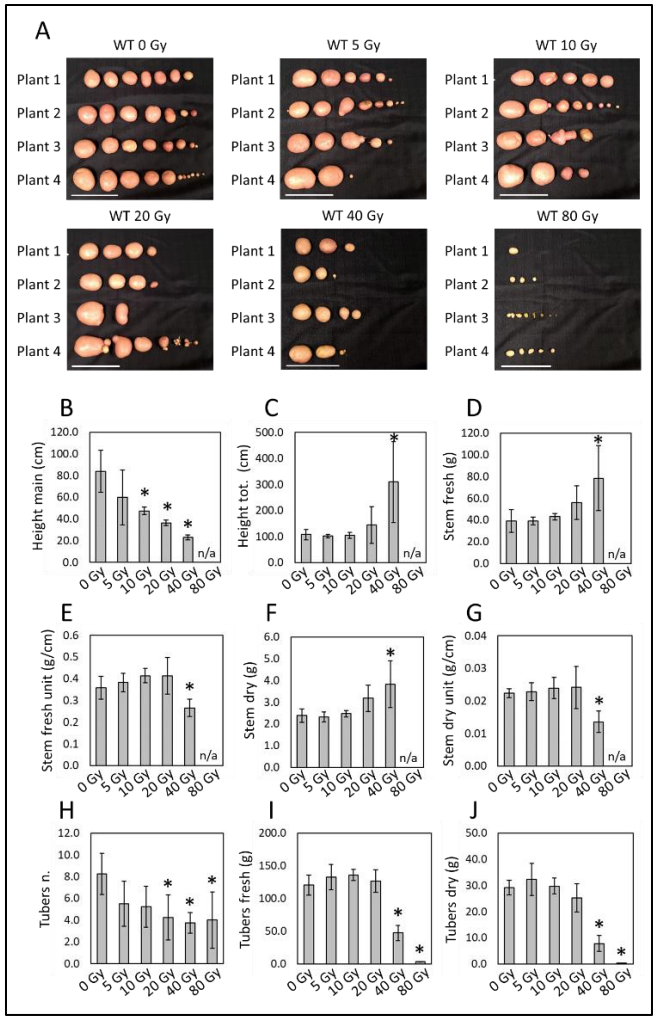

Figure 2.3: Phenotypic characteristics at tuberization stage of wild-type potato plants exposed to gamma radiation.

(A) Images showing tubers collected from ~11-weeks-old wild-type potato plants (1-4) exposed to increased doses of gamma radiation (5-80 Gy) in comparison to non-treated control plants (0 Gy). The same plants analyzed at anthesis were grown in the same environmental conditions and analyzed at the tuber maturity. Plants treated at 80 Gy were unable to survive to complete tuberization stage (n/a). Graphs represent mean ± sd (standard deviation) of various plant phenotypic characteristics of 4 plants per treatment: height of the main stem analyzed at anthesis **(B)**; high of the main stem plus the apical secondary stem **(**height tot., **C)**; total stem fresh weight **(D)**; stem fresh weight per unit of length **(E)**; total stem dry weight **(F)**; stem dry weight per unit of length **(G)**; total number of tubers per plant **(H)**; total fresh and dry weight of tubers per plant **(I** and **J**, respectively**)**. ANOVA Post-Hoc Dunnett ($p<0.05$) was used to evaluate means separation. Statistical significance in comparison to the control group (0 Gy) is indicated (*). Scale bars: 10 cm (A).

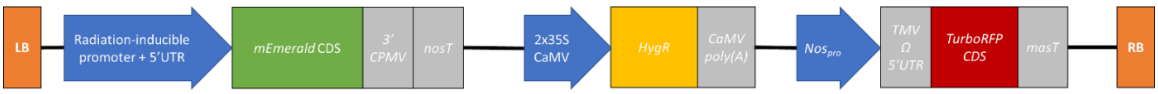

Figure 2.4: Full design of radiation phytosensor constructs used in the study.

This image displays all genetic information between the right and left borders of the radiation phytosensor constructs. The native and synthetic promoter + 5' untranslated region (UTR) described in Figure 1 drive expression of the mEmerald fluorescent protein, with the 3' UTR from cowpea mosaic virus (3'CPMV) and *Agrobacterium tumefaciens Nopaline synthase* terminator (nosT) used to direct efficient transcription and translation. Hygromycin resistance is conferred via constitutive expression of aminoglycoside phosphotransferase (HygR) from *Escherichia coli* using the double 35S promoter (2x35S) and poly(A) termination signal from cauliflower mosaic caulimovirus. A marker gene for screening was also included in the construct, in which the *A. tumefaciens Nopaline synthase* promoter drives expression of the TurboRFP red fluorescent protein, with the tobacco mosaic virus Omega 5' UTR and *A. tumefaciens Mannopine synthase* terminator (masT) aiding in efficient transcription and translation.

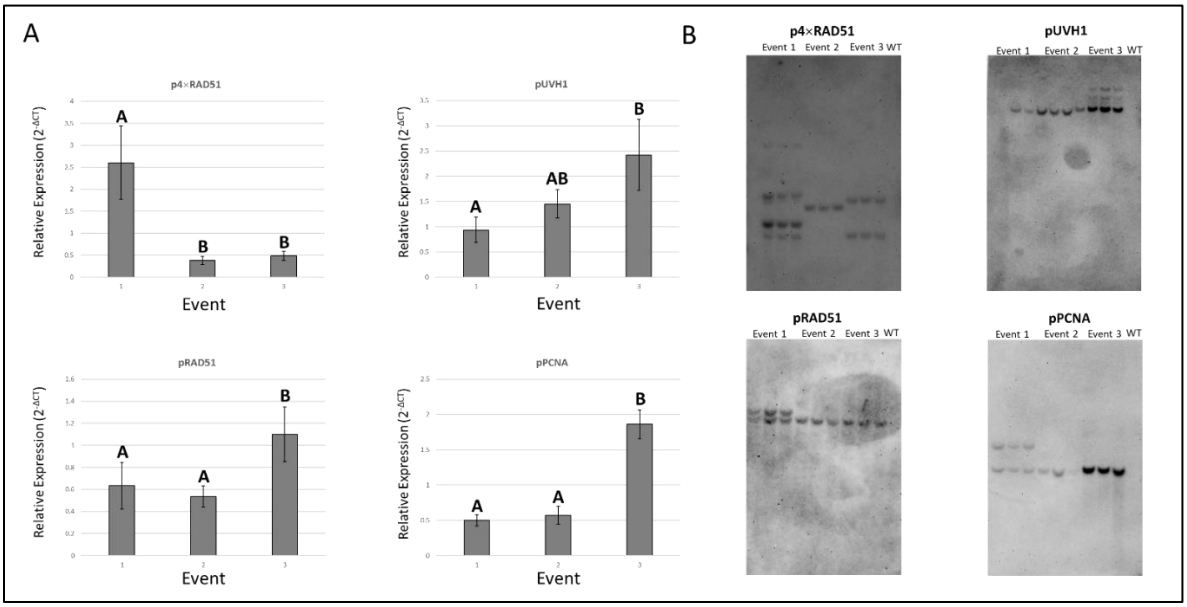

Figure 2.5: Basal expression and transgene copy number of the phytosensor events tested.

(A) Basal expression of the *mEmerald* mRNA in the three transgenic events harboring each phytosensor construct (pUVH1, pPCNA, pRAD51 and p4×RAD51) tested in Figure 2.6. Plants grown *in vitro* and graphs represent RT-qPCR relative expression data ($2^{-\Delta CT}$) of *mEmerald* coding sequence vs the endogenous reference gene, *StEF1α*. Data are expressed as mean ± standard error (SE) of 4 biological (exceptions: *UVH1* Lines 3 and 7 have three biological replicates) and three technical replicates. Data were analyzed using ANOVA ($p < 0.05$) and a post-hoc mean separation with Tukey's adjustment ($p < 0.05$). **(B)** Transgene copy number of the events tested in Figure 2 determined by Southern Blot. Three genomic DNA samples extracted from biological replicates of each phytosensor event were used, as well as one sample of wild type (WT) *Solanum tuberosum* DNA as a negative control for the probe. DNA was cut using AflII, BspHI, and KasI enzymes.

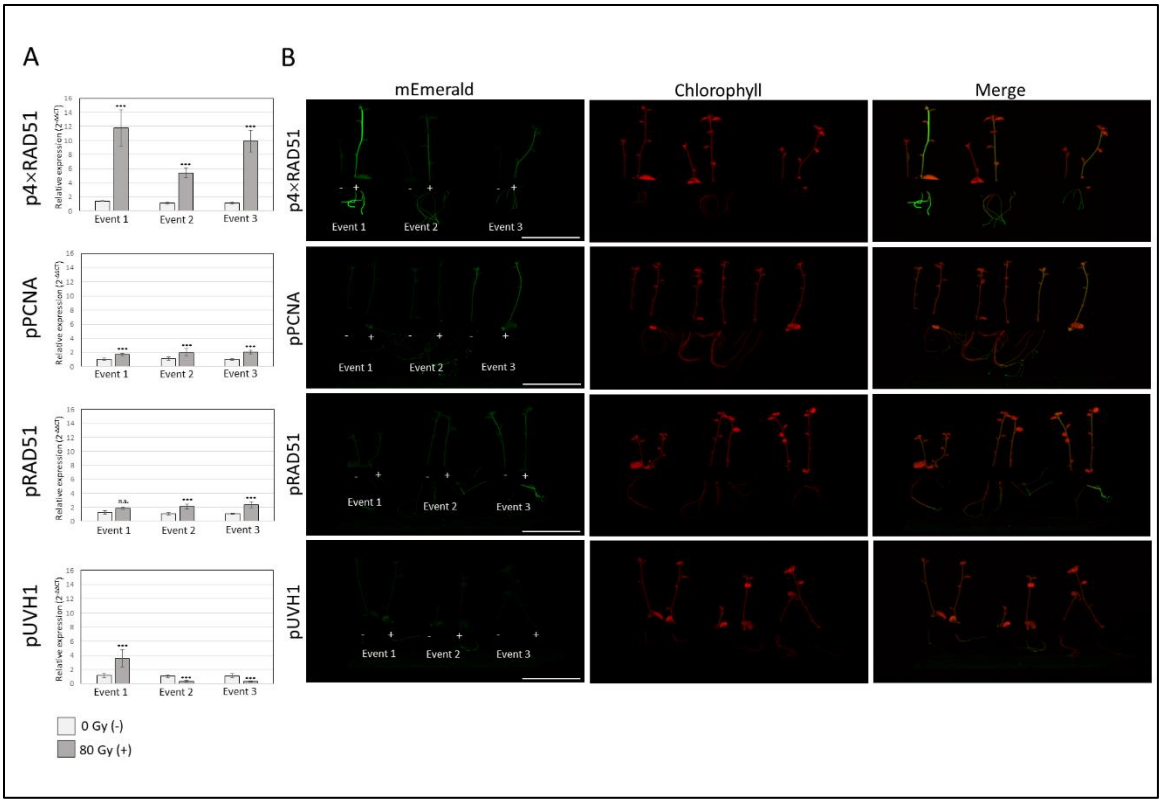

Figure 2.6: Testing of down-selected gamma radiation phytosensor lines with a high dose of radiation.

(A) Induction of expression of the reporter gene (*mEmerald*) in three phytosensor events of each construct (pUVH1, pPCNA, pRAD51 and p4xRAD51) grown *in vitro* and analyzed at 1.5 hours after dosing with 80 Gy of gamma radiation. Graphs represent RT-qPCR relative expression data ($2^{-\Delta\Delta CT}$) of *mEmerald* coding sequence vs the endogenous reference gene, *StEF1α*. Data are expressed as mean ± standard error (SE) of 4 biological (exceptions: pUVH1 Events 2 and 3, 0 Gy treatment have 3 biological replicates) and three technical replicates. Data were analyzed using ANOVA ($p < 0.05$) and statistical significance is indicated with "***" while non-significance with "n.s.". Wild type individuals were used as a negative control; 3 biological replicates and 3 technical replicates per treatment. No expression of the *mEmerald* coding sequence was detected. **(B)** Fluorescence-inducing laser projector (FILP) images of the same phytosensor plants lines (pUVH1, pPCNA, pRAD51 and p4xRAD51) treated (+; 80 Gy) and non-treated (-; 0 Gy) with gamma radiation and analyzed at 24 hours post-treatment. Images taken using the following settings: mEmerald fluorescence (2 watts, ex. 465 nm, em. 525/50 nm) (green), chlorophyll fluorescence (1-2 watts, ex. 465 nm , em. 645/75 nm). Scale bar = 10 cm.

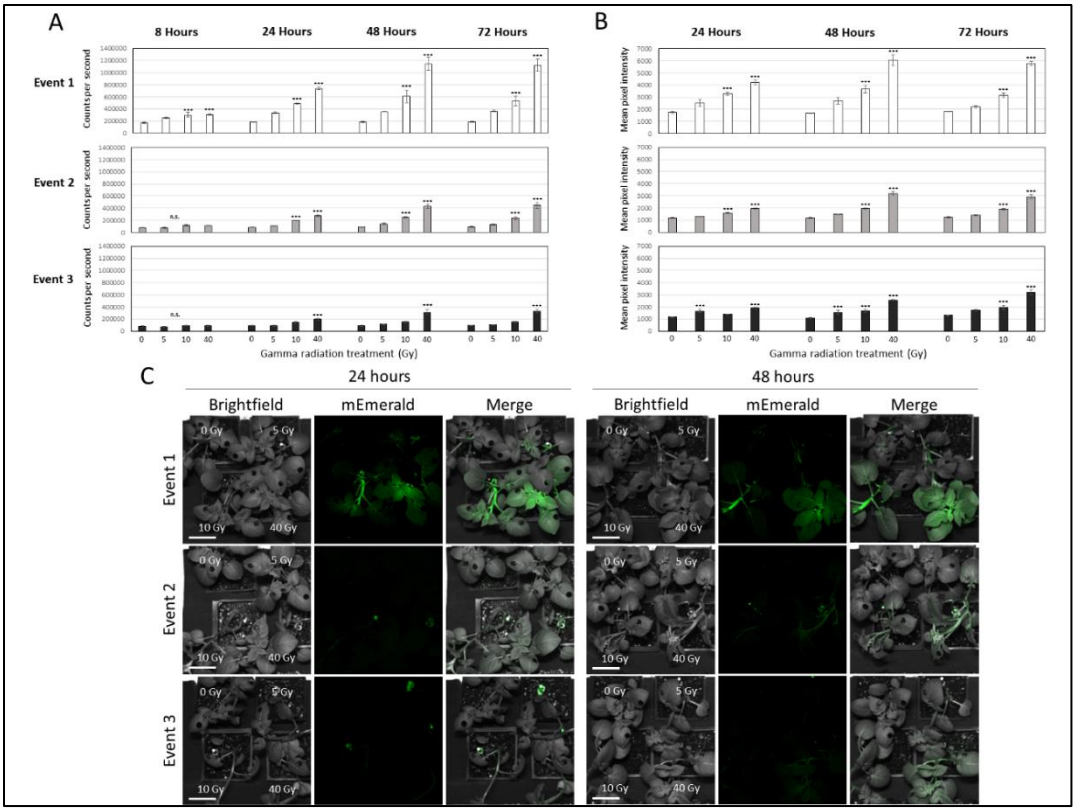

Figure 2.7: Performance of the p4xRAD51 phytosensor.

(A) Four-week-old p4xRAD51 radiation phytosensors grown in potting soil were treated at 0, 5, 10, or 40 Gy of gamma radiation. Graphs showing mEmerald fluorescence signal (cps, count per second) of phytosensor lines measured via spectrofluorometer (ex. 465 nm, em. 509-511 nm) at 8-, 24-, 48-, and 72-hours post-treatment. Background subtracted from mean using mean spectrofluorometer measurements of wild type which underwent the same treatment as the transgenic plants. Data are expressed as mean ± standard error (SE) of 3 biological and six technical replicates. Data were analyzed using ANOVA ($p < 0.05$) and comparisons to 0 Gy were evaluated using Post-Hoc Dunnett's test ($p < 0.05$). Significant difference from 0 Gy via the Dunnett's test is indicated by "***" and groups of comparisons where there was no significant effect of radiation treatment via ANOVA are marked with "n.s." **(B)** mEmerald pixel intensity of plant phytosensors collected using the fluorescence-inducing laser projector (FILP) apparatus. Data are expressed as mean ± standard error (SE) of 3 biological and 1 technical replicate. Data were analyzed using ANOVA ($p < 0.05$) and comparisons to 0 Gy were evaluated using Post-Hoc Dunnett's test ($p < 0.05$). Statistical significance via the Dunnett's test is indicated by "***" while non-significance is left unmarked. **(C)** FILP images of p4xRAD51 radiation phytosensors treated at 0, 5, 10, or 40 Gy of gamma radiation and acquired at 24- and 48-hours post-treatment. All images show plants treated with 0 Gy (top left), 5 Gy (top right), 10 Gy (bottom left), and 40 Gy (bottom right). Brightfield (gray), mEmerald fluorescence (green signal: 2 watts, ex. 465 nm, em. 525/50 nm), and merged images are shown. Scale bar: 5 cm.

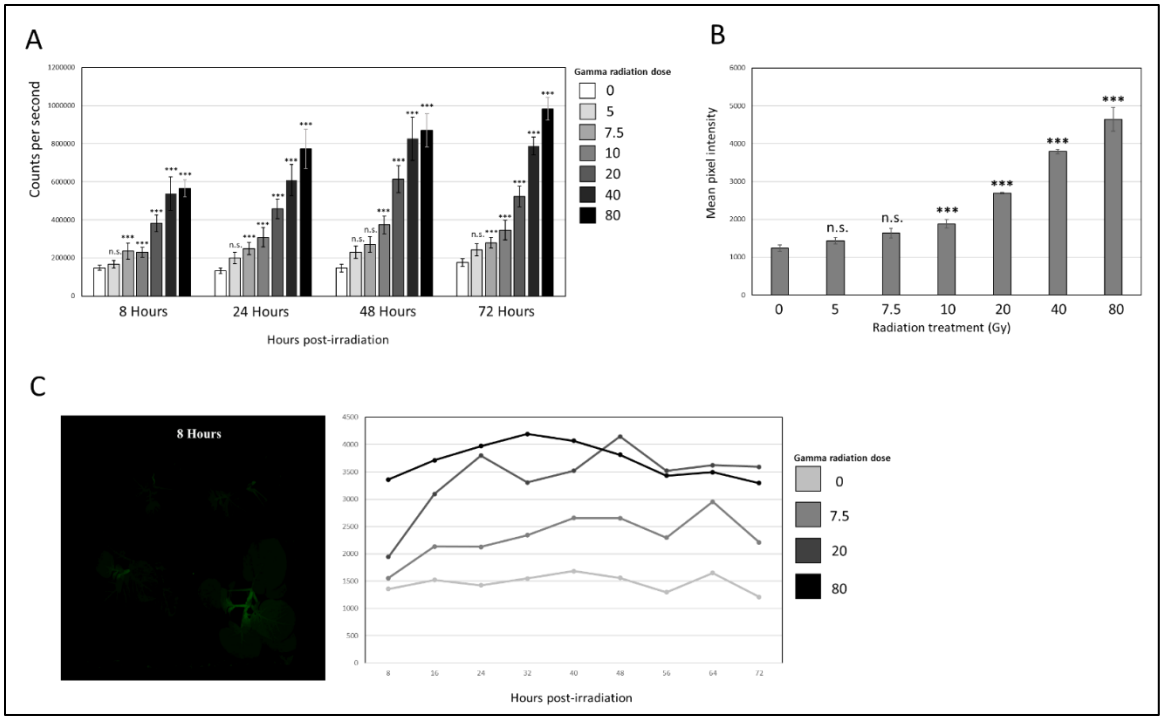

Figure 2.8: Full specification of p4xRAD51 event 1 gamma radiation phytosensing.

(A) Four-week-old p4×RAD51 event 1 radiation phytosensors were treated at 0, 5, 7.5, 10, 20, 40, or 80 Gy of gamma radiation. Graph shows mEmerald fluorescence signal (count per second) of phytosensor lines measured via spectrofluorometer (ex. 465 nm, em. 509-511 nm) from 8- to 72-hours post-treatment. Background subtracted from mean using mean spectrofluorometer measurements of wild type which underwent the same treatment as the transgenic plants. Data are expressed as mean ± standard error (SE) of 3 biological and six technical replicates. Data were analyzed using ANOVA ($p < 0.05$) and comparisons to 0 Gy were evaluated using Post-Hoc Dunnett's test ($p < 0.05$). Statistical significance is indicated by "***" while non-significance with "n.s." **(B)** Graphs showing mEmerald image pixel intensity of phytosensors collected using the fluorescence-inducing laser projector apparatus at 72-hours post-treatment. Data are expressed as mean ± standard error (SE) of 3 biological and 1 technical replicate. Data were analyzed using ANOVA ($p < 0.05$) and comparisons to 0 Gy were evaluated using Post-Hoc Dunnett's test ($p < 0.05$). Statistical significance is indicated by "***" while non-significance with "n.s." **(C)** Fluorescence-inducing laser projector images of p4×RAD51 event 1 plants taken every 8 hours until 72-hours post-treatment of plants treated with 0 (top left), 7.5 (top right), 20 (bottom left), and 80 Gy (bottom right) presented as a gif. Mean pixel intensity for the plants in these images are presented beside the figure, ($n = 1$). Images show all plants turning upwards against gravity over time because plants are turned 90 degrees to take canopy images. An exception is the individual treated with 80 Gy, which was unable to maintain gravitropic growth.

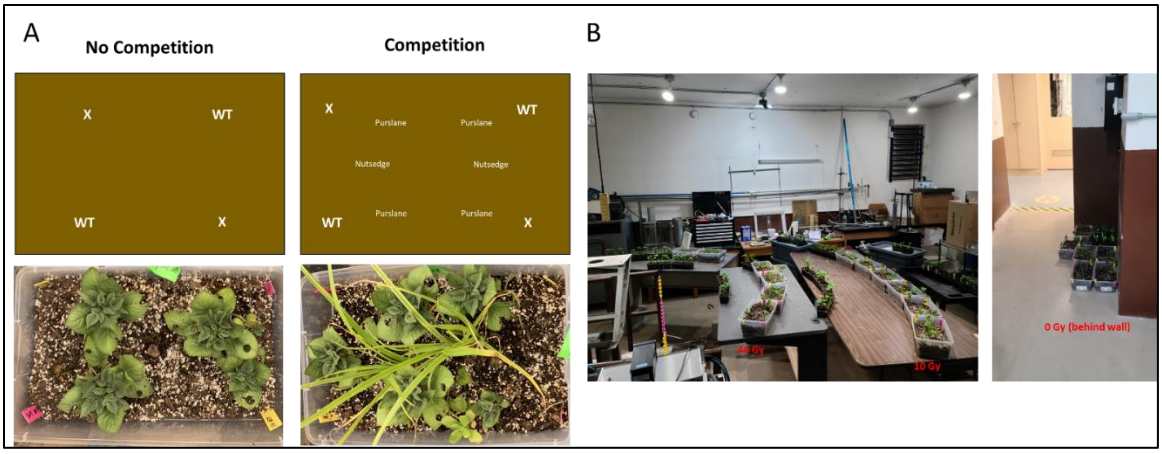

Figure 2.9: Simulated field site mesocosm layout and irradiation treatment.

(A) Diagrams and images showing the layout of mesocosms created for *in situ* testing of p4×RAD51 event 1. Diagrams note the location of wild type *Solanum tuberosum* (WT), transgenic p4×RAD51 event 1 plants (X), *Cyperus esculentus* (nutsedge), and *Portulaca oleracea* (purslane). **(B)** Images of the irradiation treatment of mesocosms. Mesocosms treated with 40 Gy (1.38 meters from source), 10 Gy (2.5 meters from source), or 0 Gy (mesocosms placed behind a concrete wall) over the course of 13.5 hours.

Figure 2.10: Specifications of p4xRAD51 event 1 and testing *in situ*.

(A) Time course of p4xRAD51 fluorescence in mesocosms with and without yellow nutsedge and common purslane competitors irradiated with 0, 10, or 40 Gy. Plants established in plastic bins with 50/50 field soil and potting mix. Graphs showing mEmerald fluorescence signal (cps, count per second) of phytosensor lines measured via spectrofluorometer (ex. 465 nm, em. 509-511 nm) for up to a month after treatment. Background subtracted from mean using mean spectrofluorometer measurements of wild type which underwent the same treatment as the transgenic plants. Data are expressed as mean ± standard error (SE) of six biological and six technical replicates. Data were analyzed using ANOVA ($p < 0.05$), mean comparisons between 0-, 10-, and 40-gray treated plants are made with a post hoc Dunnett's t test ($p < 0.06$) while later comparisons between 0 and 40-gray treated plants made with a student's t-test ($p < 0.05$). Statistical significance is indicated by "***" while non-significance indicated with "n.s." **(B)** Time course of p4xRAD51 fluorescence in mesocosms with and without competitors irradiated with 0, 10, or 40 Gy. Fluorescence measured by extracting fluorescence-inducing laser projector image pixel data. Error bars represent the mean ± 1 standard error. Data analyzed using ANOVA ($p < 0.05$) and a post hoc Dunnett's test when comparing 10 Gy and 40 Gy treated plants to 0 Gy, while comparisons between 0 and 40 Gy treated plants made with a student's t-test ($p < 0.05$). Statistical difference from 0 Gy using the Dunnett's or t-test are indicated by "***" while non-significance indicated with "n.s.". **(C)** Images of mesocosms with and without weedy competitors 48 hours after treatment. Plants labelled "X" are p4xRAD51 event 1 while plants while those labelled "WT" are wild type *Solanum tuberosum* plants. Images shown include brightfield (gray), mEmerald (2 watts, ex. 465 nm, em. 525/50 nm) with brightness increased 40% and contrast decreased 40% on all images for clarity, and a stack of the mEmerald fluorescence image on top of the brightfield. Scale bar = 2.5 cm.

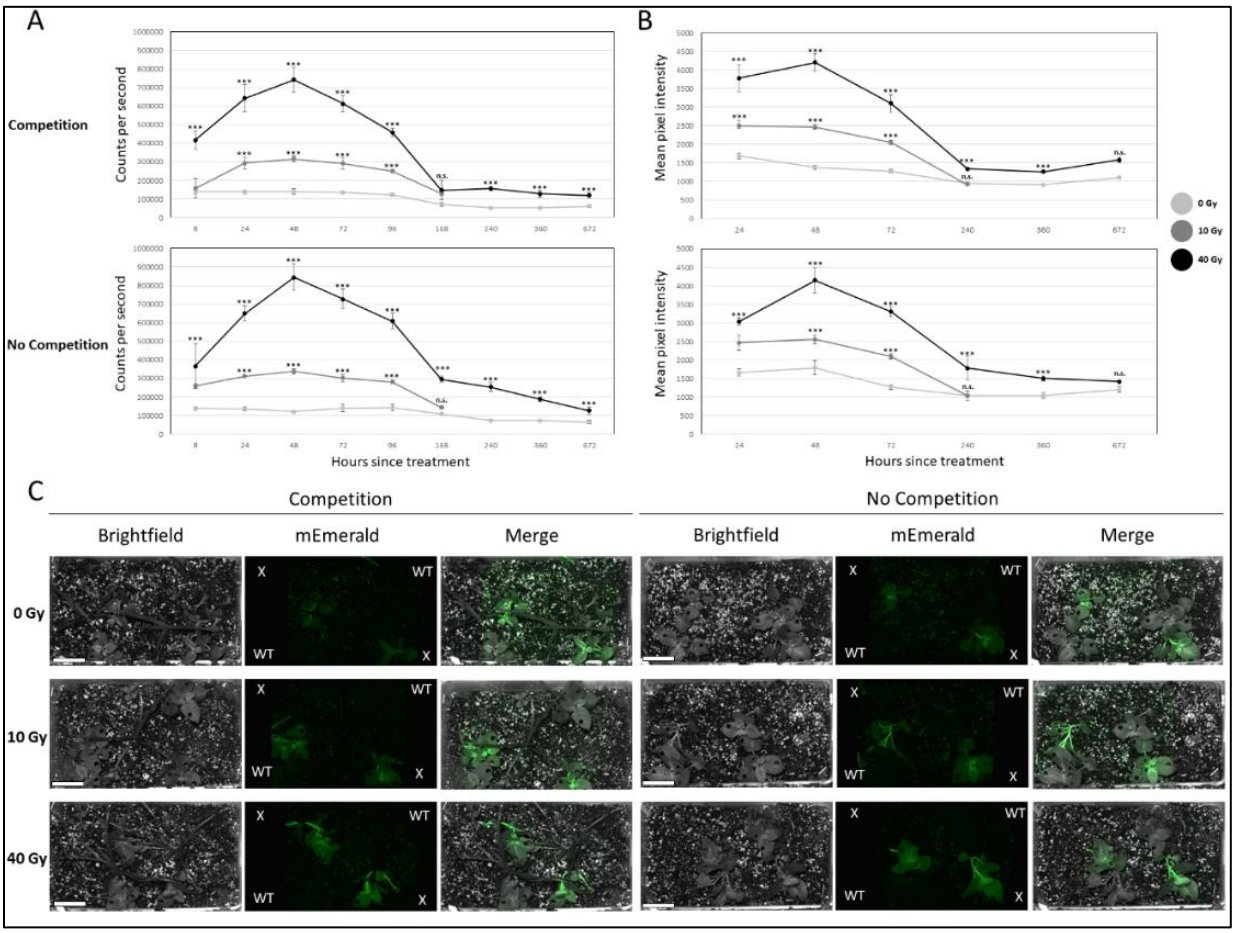
A
Competition
No Competition
Counts per second
Hours since treatment
B
Mean pixel intensity
Hours since treatment
0 Gy
10 Gy
40 Gy
C
Competition
No Competition
Brightfield
mEmerald
Merge
0 Gy
10 Gy
40 Gy
X
WT

Figure 2.11: Effect of mesocosm community and radiation dose on phenotypes at harvest. Community type (grown alone or under competition with neighbors) is shown on the x-axis, while the following trait values are plotted on the y-axis: number of leaves, number of tubers, fresh aboveground biomass, and fresh tuber mass. Wild type is shown on the left column, while the p4×RAD51 event 1is shown on the right column. Radiation dose is demonstrated by the fill of the boxplot; see the legend. Median trait value is shown as the horizontal black line within the box, quartiles are shown as the bars, and vertical lines demonstrate the range of the values. Brackets over the boxes demonstrate the significance of the comparison of radiation doses within each community type for each genotype, separately, via Dunnett's Test; "ns" denotes no significant difference between the doses, while significant p values are denoted as follows: * < 0.05, ** < 0.01. Only the significant effects of community type (alone versus competition) are shown by the asterisks within the boxes of the competition panel for each genotype, calculated by pairwise comparisons of estimated marginal means, using the same values as shown above.

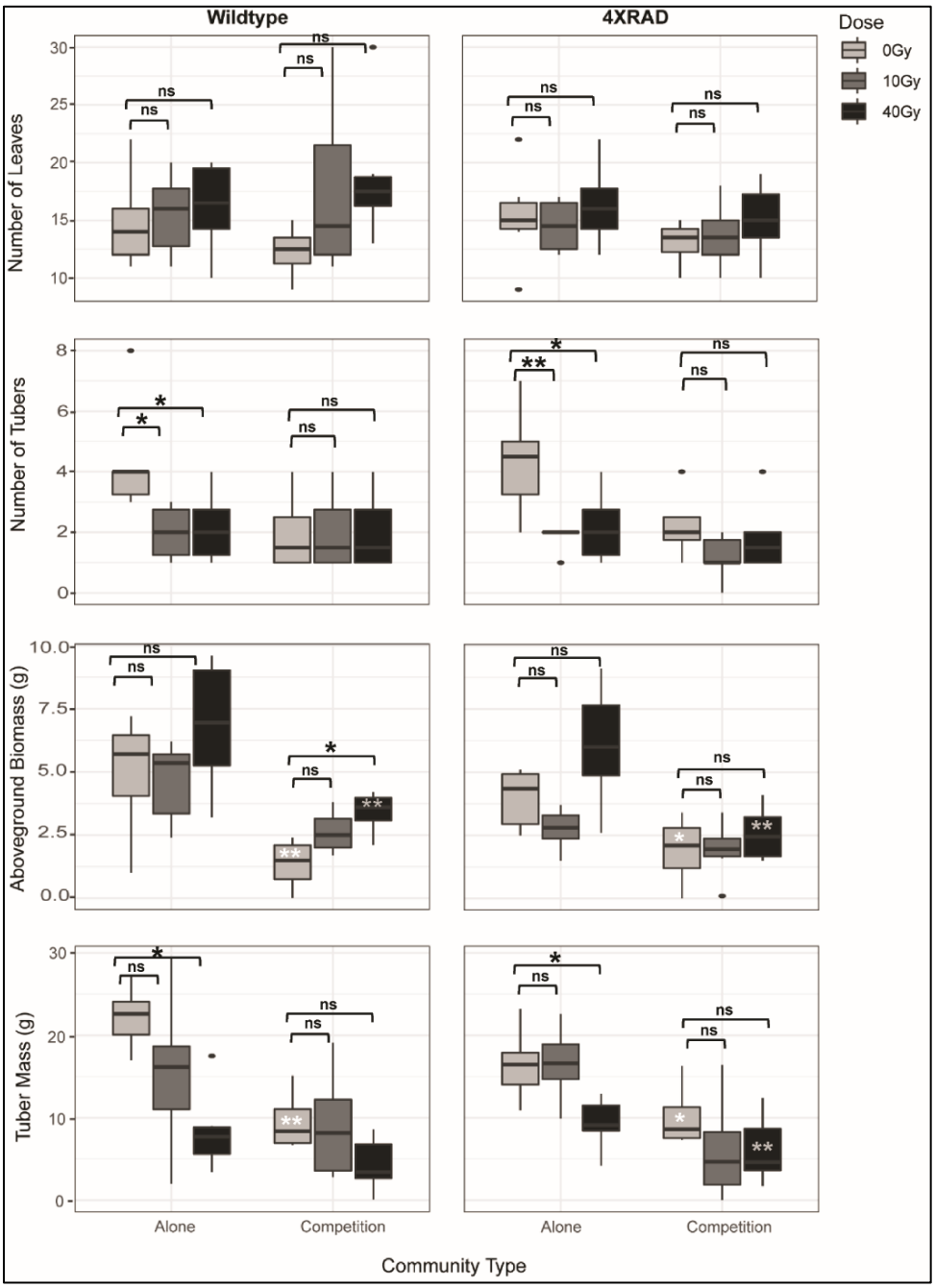
Wildtype
4XRAD
Dose
0Gy
10Gy
40Gy
Number of Leaves
Number of Tubers
Aboveground Biomass (g)
Tuber Mass (g)
Alone
Competition
Community Type

CHAPTER III: CONSTITUTIVE EXPRESSION OF TARDIGRADE 'DAMAGE SUPPRESSOR' GENE IN POTATO PROVIDES LIMITED INCREASES IN HOST PLANT RADIOTOLERANCE

Abstract

Increasing radiotolerance in plants above their normal basal tolerance levels would help ensure their long-term survival in environments with inherent ionizing radiation stress such as space. Overall, land plants are some of the most radiotolerant macroorganisms. Most examples of improved radiotolerance mechanisms belong to microscopic Prokaryotes and Eukaryotes. One such mechanism is the expression of a 'damage suppressor' (Dsup) protein by tardigrades such as *Ramazzottius varieornatus*, which confers radiotolerance through the protection of chromatin from reactive oxygen species. To determine whether this protein can confer increased radiotolerance in plants, potato was engineered to constitutively express Dsup. Transgenic plant responses to gamma radiation treatment were compared to those of non-transgenic plants. Dsup expression resulted in significantly reduced expression of DNA damage response genes as well as improved apical dominance phenotypes after ionizing radiation treatment, but did improve aboveground or tuber biomass production after treatment. Expression of *R. varieornatus* Dsup may produce population-level effects in space and bioremediation applications, though reliable increases in radiotolerance for phytosensor applications is limited.

Introduction

Radiotolerance is achieved in many distantly-related species and the mechanisms behind each species' tolerance of ionizing radiation can vary wildly. When comparing all life, organisms that are small, maintain simple genomes, and that live in already-stressful environments tend to be more radiotolerant[1]. In many ways, plants are the exception to these rules. Plants are an incredibly radiotolerant group of macroorganisms, with mechanistic explanations often referring to their large (often polyploid) genomes[2] and large number of antioxidant compounds[3]. Plant cells' propensity for totipotency and modular body plan also likely allow for quick recovery after an acute dose of ionizing radiation. Despite inherent radiotolerance, interest in long term food production in space[4] may require novel traits in order to ensure food security for astronauts. Constant exposure to ionizing radiation causes mutations to increase over time and across generations, resulting in reduced reproductive efficiency[5, 6], meaning there may be a finite number of generations a plant species can survive in space unless radiotolerance is increased. Many microorganisms are credited with surviving ionizing radiation doses over ten times greater than those survived by most plants[7, 8]. This begs the question, "Can radiotolerance mechanisms from microbes or other organisms that follow the radiotolerance 'rules' be effectively transferred to plants?" This work aims to address that question by expressing the 'damage suppressor' protein from *Ramazzottius varieornatus* in potato and assessing whether increased tolerance of ionizing radiation is conferred.

R. varieornatus, a common species of tardigrade or water bear, are microscopic animals commonly found in soil. Due to the large environmental extremes associated with life in soil, tardigrades commonly undergo anhydrobiosis to survive extremely dry or cold conditions[9]. During the dehydration process, many reactive oxygen species (ROS) are formed that could destroy many parts of the cell, with the most dangerous target being the genome. To protect its genome, *R. varieornatus* expresses a damage suppressor protein to reduce oxidative damage to its genome. The protein protects chromatin by binding nucleosomes with its C-terminal nucleosome-binding domain of high mobility group N-like region[10], likely blocking interactions between ROS and the minor groove of DNA[11]. DNA damage protection through Dsup expression has been studied in human cells[12], *Escherichia coli*[13], mice[14], and tobacco[15]. Results

in tobacco also suggest that Dsup expression lowers the expression of key DNA damage response genes in response to genotoxic stress[15]. This body of evidence suggests that expression of Dsup should reduce DNA damage induced by ionizing radiation in potato plants, given that Dsup reduces genotoxic stress many species that are distantly related to tardigrade. In this study, we assessed the radioprotective capabilities of Dsup expression in potato faced that was treated with gamma radiation from a cobalt-60 source, as this highly penetrative ionizing radiation is the most prevalent in contaminated areas and in space.

Results

Generation and downselection of potato plants expressing tardigrade 'Damage suppressor.'

The published coding sequence of RvDsup was made compatible to Golden Gate cloning and synthesized[12]. Constitutive expression of the coding sequence achieved with a Cauliflower mosaic virus double 35S promoter and the *Agrobacterium tumefaciens nopaline synthase* terminator. The Dsup expression cassette was combined with a constitutive hygromycin resistance cassette to complete the Dsup expression construct (Figure 3.1A). All figures and tables are located in an appendix at the end of the chapter. Ten independent transgenic events were generated, although four of these had poor growth in tissue culture and were discarded. The transgene expression levels of the remaining six events were then compared using qRT-PCR (Figure 3.1B). Events 1, 5 and 10 were selected because they represented low-expressing, mid-expressing, and high-expressing events of those assayed and each presented growth phenotypes similar to the non-transgenic parent plant. Stratification of expression profiles was selected to allow for any dosage effects of Dsup expression to be observed in any radiotolerance phenotypes observed after dosing. Confirmation of Dsup protein in the nucleus was achieved via mass spectroscopy analysis of chromatin-bound proteins.

Challenging potato plants expressing the 'damage suppressor' gene with a gamma radiation kill-curve.

Once generated and characterized, Dsup-expressing potato plants were challenged with a previously described gamma radiation kill curve from zero to 80 Gray[16]. Phenotypic effects of radiation treatment appeared to emerge at three weeks post-treatment, with a significant decrease in surviving leaf area that increased with increased Dsup expression (Figure 3.2). Dsup expression did not have a significant effect on leaf number or height increase since radiation treatment (Figure 3.2), indicating that apical growth or whole leaf senescence were unaffected by Dsup expression. Radiation treatment did significantly increase leaf number at 20 Gy, decrease leaf number at 80 Gy, and decrease apical growth since treatment (40 and 80 Gy) ($p < 0.05$), though there was no significant effect of Dsup expression within individual radiation treatments for these measurements (Figure 3.2A). This indicates that Dsup expression did not have a measurable effect on apical growth or whole leaf senescence.

After three weeks, plants were transferred to 3.79 liter pots in a greenhouse setting so that harvest phenotypes could be assayed. After two months in a greenhouse setting, aboveground and tuber mass were harvested, and branching phenotypes were assessed. Gamma radiation treatment had a significant effect (ANOVA $p < 0.05$) on all aboveground phenotype measures (stem fresh weight, dry weight, total stem length, number of branches, and number of 'sub' branches) (Table 3.1). Stem fresh weight is significantly (Dunnett's test $p < 0.05$) lower at 10 Gy, higher at 40 Gy, and almost nonexistent at 80 Gy. This trend is matched in the stem dry weight data, with 5 Gy also having significantly lower stem biomass. Regarding aboveground

morphology, 40 Gy plants had significantly higher stem length while 80 Gy plants had significantly lower stem length. This trend corresponds to that of branch number data. An interesting phenotype emerged in 40 Gy treated plants, where branching was extreme and many offshoots from the main stem had even more side branches, resulting in the significantly higher branch number seen in 40 Gy-treated plants (Table 3.1). This was only observed in 40 Gy treated plants, indicating this treatment has lasting effects on apical dominance. Radiation treatment had a negative impact on tuber yield, with marked decrease of tuber biomass and tuber fresh weight at 40 Gy and tuberization completely abolished at 80 Gy (Table 3.1).

Despite the clear effect of radiation treatment, there was rarely an effect of Dsup expression on aboveground biomass, tuber biomass, or aboveground structure (Figure 3.3). Dsup expression showed no significant effect (ANOVA $p < 0.05$) on stem length, stem fresh weight, branch number, tuber number at any treatments. The two effects of Dsup expression observed: first, for stem dry weight at 80 Gy, where Event 1 is significantly lower than wild type and Event 10 is significantly higher; second, for tuber fresh weight, Event 5 had significantly higher tuber mass when untreated and Events 1 and 5 had significantly lower tuber mass at 5 Gy compared to wild type. While interesting that Dsup Event 5 has significantly higher tuber mass yield compared to wild type, harvest data does not suggest that Dsup expression has an impact on plant survival aboveground morphology in the long term after a gamma radiation treatment. The only observed difference in aboveground phenotype between wild type and Dsup-expressing plants was observed in leaf area after three weeks, suggesting that Dsup expression could reduce radiation-induced cell death at 80 Gy and doses between 40-80 Gy.

Reduced leaf senescence is not maintained in potato plants expressing tardigrade 'Damage suppressor' protein when treated with 40 – 80 Gray.

To confirm the phenotype observed in the initial gamma radiation kill curve and to explore its exact threshold, four-week-old wild type and Dsup-expressing plants were irradiated with 40 – 80 Gy of gamma radiation in 10 Gy increments, with untreated plants used as a control. Four-week-old potato plants in soil were irradiated with the described treatments and monitored for leaf senescence. Three weeks post treatment, leaf area data was collected (Figure 3.4A). Radiation treatment significantly reduced leaf area in all plants at 70 and 80 Gy (ANOVA $p < 0.05$, Dunnett's test $p < 0.05$), indicating that radiation-induced senescence occurs high in the 40 – 80 Gy range. Dsup Events 5 and 10 have a higher mean leaf area than wild type at these doses, though no significant effect of Dsup expression on leaf area was detected at 70 or 80 Gy ($p = 0.17$ and 0.36, respectively).

Similar to the previous experiment, plants were transferred to 3.79 liter pots in a walk-in growth chamber setting. Plants were grown to maturity in this growth chamber, although plants underwent additional biological pest stress due to sharing the growth chamber with soybean harboring thrips. Plants closest to the soybean introduced high variation into the aboveground biomass harvest data, therefore this data was discarded. Belowground biomass data indicates that Dsup Event 5 produced significantly higher tuber numbers than wild type (ANOVA $p < 0.05$, Dunnett's test $p < 0.05$), though this was true in the 0 Gy treatment group (Figure 3.4C) and consistent with the previous tuber yield data (Figure 3.3).

The results of this experiment clarify the gamma radiation treatment range that induces senescence (70 – 80 Gy) but contradicts previous results that suggested Dsup expression prevented this effect. Without aboveground data to reveal any effects of Dsup expression on biomass accumulation and apical dominance in this treatment, the only conclusion from this

experiment is that Dsup expression does not reduce leaf senescence three weeks after gamma radiation treatment in the 40 – 80 Gy range.

Dsup expression lowers expression of DNA damage response genes after irradiation and helps maintain apical dominance in vitro.

Because of inconsistency in leaf senescence phenotype and complications associated with greenhouse studies, experiments that involve whole plants in soil were abandoned. The remaining phenotype of interest from the first study is the amount of branching induced by radiation treatment. To address apical dominance and remove the possibility of other stressors, wild type potato and Dsup events 1, 5, and 10 were propagated *in vitro* and irradiated with 0, 20, 40, 60, or 80 Gy. To detect any effects of Dsup on DNA repair at the molecular level, leaf tissue samples of 0, 20, 40, and 80 Gy irradiated plantlets were taken 1.5 hours post-treatment for qRT-PCR analysis (Figure 3.5A). Expression of the DNA damage response genes *RAS associated with diabetes protein 51 (RAD51)* and *Proliferating cell nuclear antigen (PCNA* were equal in wild type and transgenic plantlets at 0 Gy (ANOVA $p < 0.05$). *RAD51* transcript increases with Dsup expression in the transgenic events at 20 and 40 Gy, with Event 1 having significantly lower *RAD51* transcript than wild type at 20 Gy and 40 Gy while Event 5 having significantly lower transcript than wild type at 40 Gy (ANOVA $p < 0.05$, Dunnett's test $p < 0.05$). No significant differences in *RAD51* transcript between wild type and transgenic plants were observed at 80 Gy (Figure 3.5A). *PCNA* transcript was significantly lower in Event 1 plantlets compared to wild type at 20, 40, and 80 Gy (Figure 3.6A). Event 10 had significantly higher *PCNA* expression at 20 Gy but significantly lower expression at 40 Gy, compared to wild type. Event 5 showed no significant differences in *PCNA* expression compared to wild type. These results suggest that Dsup expression may reduce expression of key DNA damage response genes, but this reduction is greatest in the lowest-expressing Dsup event. Additionally, Event 10 displays significantly higher *PCNA* expression compared to wild type at 20 Gy, indicating that Dsup expressing events can have a larger DNA damage response than wild type in this treatment range.

Five weeks post-irradiation, plantlets were removed from tissue culture and surveyed for radiation-induced meristem phenotypes. Like the greenhouse experiment, irradiation of plantlets disturbed apical tissue and induced many new meristems to emerge from the location of the previous meristem (Figure 3.5B,C). The number of newly emerged meristems was measured to determine if apical dominance was better-maintained in Dsup-expressing plants. Dsup Event 1 plantlets had significantly less recovered meristems than wild type at 20 Gy and 80 Gy, though not at 40 and 60 Gy (ANOVA $p < 0.05$, Dunnett's test $p < 0.05$). Event 5 had significantly fewer recovered meristems than wild type at 40 Gy, while Event 10 had significantly fewer at 20 Gy. No significant effect of Dsup expression was detected at 60 Gy (ANOVA $p < 0.05$). Dsup expression tended to confer fewer recovery meristems in this experiment, and certainly wild type was never observed to have significantly fewer than any Dsup event, but the high variation in significance between treatment groups does not inspire confidence that Dsup expression is always effective at preserving apical dominance.

Discussion

The three experiments described here suggest that expression of the tardigrade Dsup protein may increase radiotolerance in potato, though its effect was unreliable at best. In the first experiment,

leaf senescence three weeks after radiation treatment appeared to be greater in wild type tissues and lowest in the highest-expressing Dsup event (Figure 3.2C,D). The increased senescence observed in this experiment goes against other observations in Arabidopsis[17] and potato[16] treated with acute gamma radiation treatments (≥ 80 Gy). In Arabidopsis, expression of developmental leaf senescence genes was lowered[17], while senescence of lower leaves was delayed and apical growth was abolished in both studies. This experiment utilized a 13.5 hour treatment time while the cited studies used 2 – 4 hour treatments, indicating there may be a treatment rate effect on senescence. At harvest, it is unsurprising that gamma radiation treatments below 40 Gy simultaneously disrupted apical dominance and lead to increased aboveground biomass (Figure 3.3). Disruption of apical dominance is widely reported in ionizing radiation literature focused on mature plants[18-20], with hormesis often observed after irradiation in mature plants as well as seeds[16, 21-23]. Despite aboveground gains, tuber number or biomass was not increased with aboveground tissue, consistent with early reports of potato irradiation[24]. Dsup expression had no significant effect on any traits at harvest, indicating that if Dsup was reducing DNA damage events during irradiation, less DNA damage did not improve repair and recovery processes. This is surprising given the importance of genome stability during stress[25], though may indicate that DNA repair mechanisms are carried out quickly and efficiently at ≤ 20 Gy while at 40 Gy and above there is lasting damage that is disruptive with or without Dsup protection. If expression of Dsup were an effective overall radiotolerance strategy, it would be expected that the transgenic plants in this study would show a phenotypic difference from wild type at doses that affect wild type phenotype (5 – 80 Gy), but this was not detected.

The second experiment's leaf area results (Figure 3.4) failed to find a significant effect of Dsup expression, adding further evidence that Dsup expression does not confer increased radiotolerance. All treatment groups in experiment two retained greater leaf area than Dsup event 10 in the first study with a small difference in treatment time, indicating that other environmental factors may help facilitate the senescence phenotype. Additionally, transgene silencing on the individual level[26] as well as somaclonal variation caused associated with propagation in tissue culture[27] could have introduced variation among biological replicates that masked the effect of Dsup expression in this experiment. This experiment did confirm that Dsup Event 5 displays desirable tuber yield phenotypes that may be of interest to the breeding community, highlighting that every study that utilizes nuclear transformation is inherently a random mutagenesis study.

The third experiment utilized plantlets in tissue culture to reduce impacts of environmental variation that may be affecting greenhouse and growth chamber experiments. qRT-PCR data generally confirms that Dsup expression lowers the expression of DNA damage response genes in response to genotoxic stress in plants[15](Figure 3.5A), though this effect has an inverse relationship with Dsup expression that contradicts the relationship observed in the first experiment's leaf area data as well as the rationale of this study. Recovered meristem data suggests that Dsup expression can help maintain apical dominance, aligning with data from human cell lines that indicate Dsup expression helps maintain mitotic capability[12]. It should be noted that ionizing radiation causes mutations randomly within a cell's genome, meaning that the high variation in phenotypic measures observed within experiments is not surprising. Random mutation paired with the variation between biological replicates discussed above could lead to the inconsistency in the effect of Dsup and transgenic event observed here.

Interestingly, Kirke et al. report that Dsup-expressing tobacco have favorable growth phenotypes compared to wild type when exposed to bleomycin and ethylmethane sulfonate but not irradiated with UV-C and X-ray genotoxic stressors[15]. Hashimoto et al. report that human

cells that express Dsup have a favorable growth rate when irradiated with X-rays[12]. The fact that Dsup expression does not impact growth phenotypes after ionizing radiation treatment in plants but does in animal cells could indicate a difference in how genotoxic stress from photons is processed in plants compared to animals. Adaptation and growth during high light and UV stressors are key adaptations for early land plants[28, 29], as high light stress can drive the production of ROS[30] and UV inherently causes DNA lesions[31]. It is possible that the evolutionary pressures that shaped modern land plants produced mechanisms of growth resilience under conditions of oxidative stress and genomic instability caused by high energy photons. This would certainly explain the effectiveness of Dsup in animal cells[12, 14] and microbes[13] that was fleetingly observed in this analysis.

In conclusion, expression of the tardigrade Dsup protein confers a limited increase in radiotolerance to potato. Expression of DNA damage response genes was lower in some Dsup-expressing events compared to wild type, which corresponded to fewer meristematic aberrations after treatment across multiple gamma radiation treatments. Dsup-expressing potato plants were not observed to survive and grow after treatments where wild type potato growth was abolished, suggesting that Dsup expression does not raise the lethal dose of gamma radiation for potato. The effect of Dsup expression may be more easily detected in long term, chronic exposure such as generational growth on the ISS or in areas in need of bioremediation where mutation is the main concern, though this type of examination would require a large investment of time and resources. Increasing the number of biological replicates per treatment may also resolve some of the variation observed in this work. For phytosensor applications, the expression of the Dsup protein provided limited radioprotection and other strategies for increasing radiotolerance should be pursued.

Materials and methods

Plant material and growth conditions

Wild type *Solanum tuberosum* cv. 'Desiree' was procured from the Wisconsin Seed Potato Certification Program at the University of Wisconsin - Madison and kept in sterile culture on modified Murashige and Skoog media for transformation[32]. After transformation and qRT-PCR analysis for transcript abundance, events were maintained in tissue culture.

For experiments where plants were in pots, plants were removed from tissue culture and placed into a 10 cm plastic pot filled with a soilless media and allowed to adjust to ambient humidity for one week under a closed lid inside of a growth chamber. After this the lid was removed, plants were grown within the growth chamber an additional three weeks until radiation treatment. Growth chambers were set to a 16-hour light / 8-hour dark daylight regime, with daytime temperature set to 20 ºC and nighttime temperature set to 18 ºC. Plants were fertilized with Peter's 20-20-20 fertilizer after hardening and after 3 weeks in soil. For experiments that were moved to greenhouse and walk-in growth chamber settings, 16-hour light / 8-hour dark daylight settings were maintained with supplemental lighting but temperature regime was increased to 29 ºC in the daytime and 21 ºC at night. Plants were fertilized with Peter's 20-20-20 fertilizer at recommended concentration once every two weeks until harvest.

Gamma radiation treatment

Gamma radiation treatment was done by adjusting plants' distance and dosage time from a Cobalt-60 source to reach a total dose (reported in this paper in Gray). Treatment times and distances can be found for each of the experiments in Table 3.2.

Construct design and cloning

The *R. varieornatus* 'damage suppressor' protein's coding sequence was made compatible with Golden-Gate cloning and the gene was chemically synthesized by GeneArt (Invitrogen, Thermo Fisher Scientific). The Dsup coding sequence was fused with the CaMV 35S promoter + TMV 5'UTR (pICH51288) and nopaline synthase 3'UTR and terminator (pICH41421) into a modified pICH86966 destination plasmid with a hygromycin resistance cassette rather than the original kanamycin using Golden-Gate cloning as described before[33, 34].

Plant transformation

Transformation of *Solanum tuberosum* cv. 'Desiree' was performed using an established method[32]. At least ten shoots from separate calli were recovered and propagated separately per construct, with ten being kept after successful genotyping via PCR. Four of these events had very poor phenotype in tissue culture, therefore three events from the remaining six were selected for further testing based on vigorous growth phenotype and a range of basal fluorescence.

qRT-PCR analysis

RNA was extracted from tissue samples stored in RNAlater solution (Sigma-Aldrich) after dosing and extracted using a TRI Reagent extraction protocol (Molecular Research Center) and RNA Clean and Concentrator kit (Zymo) with a DNase I treatment. Two thousand nanograms of RNA from each sample was used to generate cDNA with the Applied Biosystems™ High-Capacity cDNA Reverse Transcription Kit (Fisher). The cDNA was generated, then 1.08 ng cDNA was used for qPCR a single 5 µl qPCR reaction using the PowerUp™ SYBR™ Green Master Mix (Fisher) and its associated protocol. An Applied Biosystems QuantStudio 6 Flex qPCR instrument and its associated software were used. The primers used for native genes, Dsup, and *StEF1α* can be found in Table 3.3. For all primer sets, qPCR settings include 2 minutes at 50ºC, 10 minutes at 95ºC, then 40 cycles where temperature begins at 95ºC for fifteen seconds, descends 1.6ºC per second to 60ºC where it holds for one minute, then ascends to 95ºC at the same rate. Results were analyzed using the $2^{(-\Delta C_T)}$ and $2^{(-\Delta\Delta C_T)}$ methods, with mEmerald C_T values first being set relative to *EF1α* expression ($2^{(-\Delta C_T)}$), then relative to the appropriate average 0 Gy ΔC_T value to calculate fold change induced by gamma radiation treatment($2^{(-\Delta\Delta C_T)}$)[35]. Primer efficiencies were equal and therefore not included in $2^{(-\Delta\Delta C_T)}$ calculations.

Plant phenotype measurements

Phenotypic measures of plants in soil were conducted at three weeks post-treatment and at harvest, when flowering was complete and plants began to senesce. All flowers were removed before anthesis to prevent gene flow. For dry stem weight, stems were dried in a 55 ºC oven for two weeks before weighing.

Leaf area measurements two weeks post-treatment were taken using a Samsung S20 phone camera and scaled to a 10 cm reference within the image. All images were processed and analyzed for pixel intensity using the ImageJ program[36]. Pixel area data was analyzed in ImageJ by identifying plant tissue in the image using the Image > Adjust > Color Thresholding function for green tissue. Once selected via threshold, images were converted to black and white using Process > Binary > Make Binary. Then, Analyze > Analyze particles was used to generate ROIs

for the plants in the image. Once generated, the ROIs were measured to gather pixel area data and pixel data was converted to cm^2 using the size of the reference in the image.

Statistical analysis

Phenotypic and qPCR data statistics were analyzed using JMP Pro 15 software (SAS, Cary, NC) ANOVA function ($p < 0.05$) and mean separation with either a post-hoc Dunnett's test ($p < 0.05$) or a Tukey's HSD ($p < 0.05$).

References

1. Shuryak, I. Review of resistance to chronic ionizing radiation exposure under environmental conditions in multicellular organisms. *Journal of Environmental Radioactivity* **212**, 106128 (2020).
2. Gartenbach, K. et al. Present results of the joint radiobiological ESA/IBMP experiments "seeds" aboard Cosmos 2044 and 2229 — correlation of micro-dosimetric data and damage endpoints in *Arabidopsis thaliana* plants. *Advances in Space Research* **18**, 215-220 (1996).
3. De Micco, V. et al. Effects of sparsely and densely ionizing radiation on plants. *Radiation and Environmental Biophysics* **50**, 1-19 (2011).
4. Mousseau, T. & Møller, A. Plants in the light of ionizing radiation: what have we learned from Chernobyl, Fukushima, and other "hot" places? *Frontiers in Plant Science* **11**, 552 (2020).
5. Spampinato, C. Protecting DNA from errors and damage: an overview of DNA repair mechanisms in plants compared to mammals. *Cellular and Molecular Life Sciences* **74**, 1693-1709 (2017).
6. Real, A. et al. Effects of ionising radiation exposure on plants, fish and mammals: relevant data for environmental radiation protection. *Journal of Radiological Protection* **24**, A123-A137 (2004).
7. Horikawa, D. et al. Radiation tolerance in the tardigrade *Milnesium tardigradum. International Journal of Radiation Biology* **82**, 843-848 (2006).
8. Moseley, B. & Mattingly, A. Repair of irradiated transforming deoxyribonucleic acid in wild type and a radiation-sensitive mutant of *Micrococcus radiodurans. Journal of Bacteriology* **105**, 976-983 (1971).
9. Møbjerg, N. et al. Survival in extreme environments – on the current knowledge of adaptations in tardigrades. *Acta Physiologica* **202**, 409-420 (2011).
10. Mínguez-Toral, M. et al. A computational structural study on the DNA-protecting role of the tardigrade-unique Dsup protein. *Scientific Reports* **10**, 13424 (2020).
11. Chavez, C. et al. The tardigrade damage suppressor protein binds to nucleosomes and protects DNA from hydroxyl radicals. *Elife* **8**, e47682 (2019).
12. Hashimoto, T. et al. Extremotolerant tardigrade genome and improved radiotolerance of human cultured cells by tardigrade-unique protein. *Nature Communications* **7**, 12808 (2016).
13. Puig, J. et al. DNA damage protection for enhanced bacterial survival under simulated low earth orbit environmental conditions in *Escherichia coli. Frontiers in Microbiology* **12**, 789668 (2021).
14. Escarcega, R. et al. The tardigrade damage suppressor protein Dsup promotes DNA damage in neurons. *Molecular and Cellular Neuroscience* **125**, 103826 (2023).
15. Kirke, J. et al. Expression of a tardigrade Dsup gene enhances genome protection in plants. *Molecular Biotechnology* **62**, 563-571 (2020).
16. Sears, R. et al. Engineered gamma radiation phytosensors for environmental monitoring. *Plant Biotechnology Journal* **21**, 1745-1756 (2023).
17. Kim, J. et al. Characterization of metabolic disturbances closely linked to the delayed senescence of Arabidopsis leaves after γ irradiation. *Environmental and Experimental Botany* **67**, 363-371 (2009).

18. Sax, K. & Schairer, L. The effect of chronic gamma irradiation on apical dominance of trees. *Radiation Botany* **3**, 283-285 (1963).
19. Arkhipov, N. et al. Acute and long-term effects of irradiation on pine (*Pinus silvestris*) strands post-Chernobyl. *Science of the Total Environment* **157**, 383-386 (1994).
20. Yoschenko, V. et al. Morphological abnormalities in Japanese red pine (*Pinus densiflora*) at the territories contaminated as a result of the accident at Fukushima Dai-Ichi Nuclear Power Plant. *Journal of Environmental Radioactivity* **165**, 60-67 (2016).
21. Taha, E. & Shoaib, R. Impact of gamma irradiation on tomato and pepper growth parameters, phytochemical, nematode infectivity and detection of DNA damage by comet assay. *Journal of Plant Protection and Pathology* **12**, 599-608 (2021).
22. Volkova, P. et al. Metabolic profiling of γ-Irradiated barley plants identifies reallocation of nitrogen metabolism and metabolic stress response. *Dose-Response* **18**, 1559325820914186 (2020).
23. Jaipo, N. et al. Low dose gamma radiation effects on seed germination and seedling growth of cucumber and okra. *Journal of Physics: Conference Series* **1380**, 012106 (2019).
24. Sax, K. The stimulation of plant growth by ionizing radiation. *Radiation Botany* **3**, 179-186 (1963).
25. Raina, A. et al. Mechanisms of genome maintenance in plants: playing it safe with breaks and bumps. *Frontiers in Genetics* **12**, 675686 (2021).
26. Vaucheret, H. et al. Transgene-induced gene silencing in plants.*The Plant Journal* **16**, 651–659 (1998).
27. Bairu, M. et al. Somaclonal variation in plants: causes and detection methods. *Plant Growth Regulation* **63**, 147-173 (2011).
28. Gray, D. et al. Photosynthetic recovery following desiccation of desert green algae (*Chlorophyta*) and their aquatic relatives. *Plant, Cell & Environment* **30**, 1240-1255 (2007).
29. de Vries, J. & Archibald, J. Plant evolution: landmarks on the path to terrestrial life. *New Phytologist* **217**, 1428-1434 (2018).
30. Li, M. & Kim, C. Chloroplast ROS and stress signaling. *Plant Communications* **3**, 100264 (2022).
31. Takahashi, M. et al. Cyclobutane pyrimidine dimer (CPD) photolyase repairs ultraviolet-B-induced CPDs in rice chloroplast and mitochondrial DNA. *The Plant Journal* **66**, 433-442 (2011).
32. Chronis, D. et al. Potato transformation. *Bio-Protocol* **4**, e1017-e1017 (2014).
33. Engler, C. et al. A Golden Gate modular cloning toolbox for plants. *ACS Synthetic Biology* **3**, 839-843 (2014).
34. Occhialini, A. et al. MoChlo: A versatile, modular cloning toolbox for chloroplast biotechnology. *Plant Physiology* **179**, 943-957 (2019).
35. Livak, K. & Schmittgen, T. Analysis of relative gene expression data using real-time quantitative PCR and the $2^{-\Delta\Delta CT}$ method. *Methods* **25**, 402-408 (2001).
36. Schneider, C., Rasband, W. & Eliceiri, K. NIH Image to ImageJ: 25 years of image analysis. *Nature Methods* **9**, 671-675 (2012).

Appendix

Table 3.1 : Overall effect of gamma radiation on harvest phenotype in potato.
Results of phenotypic analysis of wild type and three events of Dsup-expressing plants after irradiation with various total doses of gamma radiation. Data shown is the mean value for each phenotype among wild type and Dsup-expressing potato events (n = 3) and the standard error of the mean. All phenotypes are significantly affected by gamma radiation treatment but not Dsup expression (ANOVA $p < 0.05$). The results of a post-hoc Dunnett's test for the effect of radiation treatment and Dsup expression are shown comparing all treatments to 0 Gy. Significant difference from the 0 Gy mean ($p < 0.05$) is denoted with "*" while lack of significance is denoted with "ns".

Stem fresh weight (g)										
Treatment	Wild Type		Event 1		Event 5		Event 10		Effect of radiation treatment	Effect of Dsup expression
	Mean	Standard Error	Mean	Standard Error	Mean	Standard Error	Mean	Standard Error		
0 Gray	12.82	1.87	20.86	7.49	18.60	1.60	20.35	4.86	-	-
5 Gray	11.74	1.20	10.13	5.11	14.45	3.31	17.45	1.84	ns	ns
10 Gray	14.75	2.60	11.99	1.16	9.01	1.28	12.31	1.44	*	ns
20 Gray	20.17	4.31	18.60	2.48	20.59	3.70	25.22	5.35	ns	ns
40 Gray	23.74	2.53	24.47	2.00	22.02	1.30	25.32	2.44	*	ns
80 Gray	0.55	0.20	0.38	0.03	0.68	0.12	0.77	0.09	*	ns
Stem dry weight (g)										
Treatment	Wild Type		Event 1		Event 5		Event 10		Effect of radiation treatment	Effect of Dsup expression
	Mean	Standard Error	Mean	Standard Error	Mean	Standard Error	Mean	Standard Error		
0 Gray	1.65	0.26	2.21	0.69	1.78	0.16	2.24	0.79	-	-
5 Gray	1.33	0.13	1.30	0.50	1.27	0.38	1.83	0.30	*	ns
10 Gray	1.72	0.26	1.31	0.16	0.91	0.11	1.42	0.39	*	ns
20 Gray	2.06	0.39	2.23	0.29	2.01	0.38	2.41	0.78	ns	ns
40 Gray	2.84	0.15	3.18	0.26	2.35	0.10	3.02	0.37	*	ns
80 Gray	0.44	0.09	0.14	0.02	0.44	0.07	0.75	0.13	*	ns
Total stem length (cm)										
Treatment	Wild Type		Event 1		Event 5		Event 10		Effect of radiation treatment	Effect of Dsup expression
	Mean	Standard Error	Mean	Standard Error	Mean	Standard Error	Mean	Standard Error		
0 Gray	67.97	7.84	155.60	55.08	87.77	9.92	107.43	24.51	-	-
5 Gray	86.07	2.42	80.30	27.28	90.93	13.99	106.63	6.21	ns	ns
10 Gray	85.73	11.68	99.43	11.47	59.33	8.58	82.87	3.41	ns	ns
20 Gray	121.57	8.05	102.60	13.74	113.10	20.38	115.30	13.96	ns	ns
40 Gray	135.27	18.80	171.70	17.79	129.13	19.81	158.17	19.95	*	ns
80 Gray	11.67	5.84	0.00	0.00	2.20	2.20	0.00	0.00	*	ns
Branch number										
Treatment	Wild Type		Event 1		Event 5		Event 10		Effect of radiation treatment	Effect of Dsup expression
	Mean	Standard Error	Mean	Standard Error	Mean	Standard Error	Mean	Standard Error		
0 Gray	5.00	0.58	7.67	1.67	6.33	0.88	5.33	1.33	-	-
5 Gray	8.33	2.03	5.67	2.85	7.67	1.67	5.33	2.19	ns	ns
10 Gray	6.00	1.15	6.67	0.88	3.67	1.20	5.33	0.67	ns	ns
20 Gray	6.00	0.58	4.67	1.20	4.67	0.33	4.00	0.58	ns	ns
40 Gray	8.67	1.45	14.67	2.19	8.67	1.76	14.33	2.19	*	ns
80 Gray	0.00	0.00	0.00	0.00	0.00	0.00	0.00	0.00	*	ns
Tertiary branch number										
Treatment	Wild Type		Event 1		Event 5		Event 10		Effect of radiation treatment	Effect of Dsup expression
	Mean	Standard Error	Mean	Standard Error	Mean	Standard Error	Mean	Standard Error		
0 Gray	0.00	0.00	0.00	0.00	0.00	0.00	0.00	0.00	-	-
5 Gray	0.00	0.00	0.00	0.00	0.00	0.00	0.00	0.00	ns	ns
10 Gray	0.00	0.00	0.00	0.00	0.00	0.00	0.00	0.00	ns	ns
20 Gray	0.00	0.00	0.00	0.00	0.00	0.00	0.00	0.00	ns	ns
40 Gray	4.67	1.33	8.33	0.88	3.67	2.03	7.00	0.58	*	ns
80 Gray	0.00	0.00	0.00	0.00	0.00	0.00	0.00	0.00	ns	ns
Tuber fresh weight (g)										
Treatment	Wild Type		Event 1		Event 5		Event 10		Effect of radiation treatment	Effect of Dsup expression
	Mean	Standard Error	Mean	Standard Error	Mean	Standard Error	Mean	Standard Error		
0 Gray	16.21	3.73	21.99	3.93	31.35	1.78	25.48	1.53	-	-
5 Gray	28.06	6.16	12.34	4.96	15.42	7.73	15.09	3.95	ns	ns
10 Gray	15.46	2.90	26.84	3.31	30.71	4.39	19.30	2.44	ns	ns
20 Gray	17.60	5.82	17.12	1.87	24.38	2.06	29.25	4.69	ns	ns
40 Gray	6.08	3.66	3.88	3.08	10.84	3.98	11.77	0.18	*	ns
80 Gray	0.00	0.00	0.00	0.00	0.00	0.00	0.00	0.00	*	ns
Tuber number										
Treatment	Wild Type		Event 1		Event 5		Event 10		Effect of radiation treatment	Effect of Dsup expression
	Mean	Standard Error	Mean	Standard Error	Mean	Standard Error	Mean	Standard Error		
0 Gray	5.00	0.58	3.67	0.88	5.67	0.33	5.00	1.15	-	-
5 Gray	5.33	1.33	5.67	2.03	5.67	2.96	5.00	1.53	ns	ns
10 Gray	7.33	2.03	5.33	1.20	5.67	0.67	4.67	0.88	ns	ns
20 Gray	4.00	1.00	6.00	1.53	6.00	1.15	3.67	1.67	ns	ns
40 Gray	2.67	0.67	1.33	0.33	3.00	0.58	2.33	0.67	*	ns
80 Gray	0.00	0.00	0.00	0.00	0.00	0.00	0.00	0.00	*	ns

Table 3.2: Gamma radiation treatment time and distance calculations.
The tables below describe the intended absorbed dose in Gray, the required dose rate to meet the total dose in a given amount of time (rad / sec), and the calculated distance from the source to receive the desired rate. Dose tables below correspond with the following experiments: (A) – Figures 2.2-4, Table 2.1; (B) – Figure 2.5; (C) – Figure 2.6.

A	**Treatment (Gray)**	**Total Rad**	**Treatment rate (rad / second)**	**Distance from source (meters)**
	0	0	-	-
	5	500	0.0103	3.369
	10	1000	0.0206	2.501
	20	2000	0.0412	1.856
	40	4000	0.0823	1.378
	80	8000	0.1646	1.023
B	**Treatment (Gray)**	**Total Rad**	**Treatment rate (rad / second)**	**Distance from source (meters)**
	0	0	-	-
	40	4000	0.0694	1.482
	50	5000	0.0868	1.347
	60	6000	0.1042	1.245
	70	7000	0.1215	1.165
	80	8000	0.1389	1.100
C	**Treatment (Gray)**	**Total Rad**	**Treatment rate (rad / second)**	**Distance from source (meters)**
	0	0	-	-
	20	2000	0.0285	2.174
	40	4000	0.0570	1.614
	60	6000	0.0855	1.356
	80	8000	0.1140	1.198

Table 3.3: Primers used in the work.
Listed are the forward and reverse primers used for all DNA amplification in the work. These primers include those genotyping transgenic plants and conducting qRT-PCR.

Forward Primers		
ID	**Name**	**Sequence**
Fw 1	Genotyping1_Fw	CTATCCTTCGCAAGACCCTTC
Fw 2	Genotyping2_Fw	CGAAACGCTGTTCGGCCTGTGG
Fw 3	StEF1α_qPCR_Fw	ATTGGAAACGGATATGCTCCA
Fw 4	StPCNAα_qPCR_Fw	CCAGAGGTGACATCGGTACTGCA
Fw 5	StRAD51_qPCR_Fw	CGCAGACAGGTATGGATTGA
Fw 6	Dsup_qPCR_Fw	CTACACCTACCGACCCGAAA

Reverse Primers		
ID	**Name**	**Sequence**
Rv 1	Genotyping1_Rv	CATCCTCTAGTAGCGTCGAT
Rv 2	Genotyping2_Rv	GTTCAGCAGGCCGGCATCCTGG
Rv 3	StEF1α_qPCR_Rv	TCCTTACCTGAACGCCTGTCA
Rv 4	StPCNAα_qPCR_Rv	CACTGTGTTCGACAATGGAGATGCT
Rv 5	StRAD51_qPCR_Rv	AGCTGCCTCAAGCAAAAGTC
Rv 6	Dsup_qPCR_Rv	CTTTGACAGCTCCGATGACA

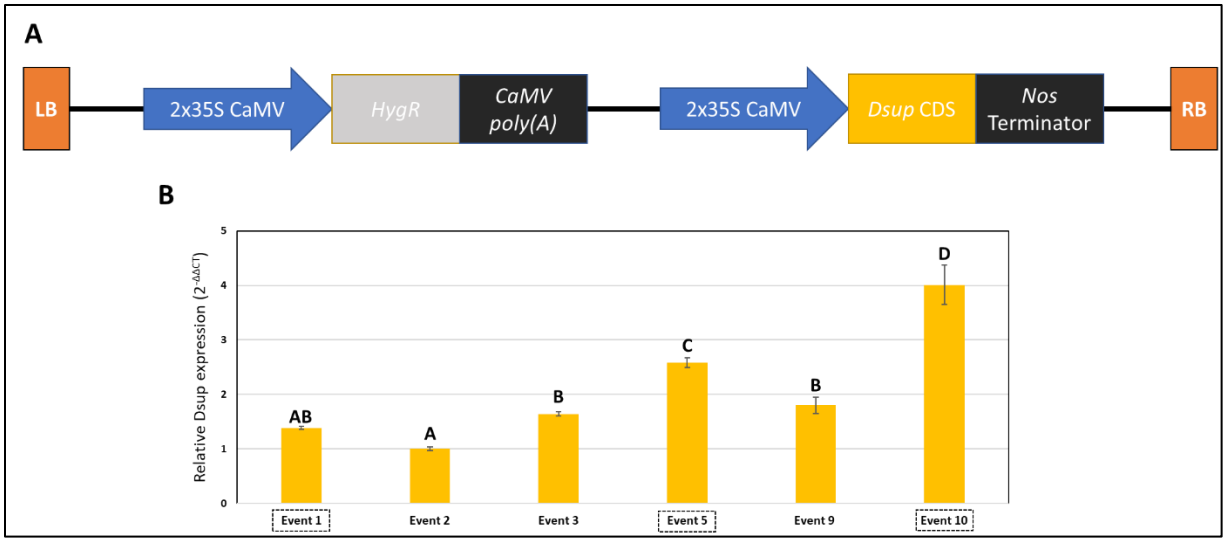

Figure 3.1: Design of a constitutive 'Damage suppressor' expression construct and down selection of transgenic events.

(A) The design of a constitutive Dsup-expression construct, with all components between the left and right borders shown. Hygromycin resistance was conferred via constitutive expression of aminoglycoside phosphotransferase (HygR) from *Escherichia coli* using the double 35S promoter (2x35S) and poly(A) termination signal from cauliflower mosaic caulimovirus. Constitutive Dsup gene expression was achieved using the same double 35S promoter and the *A. tumefaciens nopaline synthase* terminator (nosT). **(B)** Downselection of transgenic events based on capturing the greatest range of Dsup expression relative to the reference gene, *StEF1α*. Plants grown *in vitro* and graphs represent qRT-PCR relative expression data ($2^{-\Delta\Delta CT}$) compared to the reference gene and then to the lowest expressing event, Event 2. Data are expressed as mean ± standard error (SE) of three biological and three technical replicates. Data were analyzed using ANOVA ($p < 0.05$) and a post-hoc mean separation with Tukey's adjustment ($p < 0.05$), with significantly different expression denoted by differing letters.

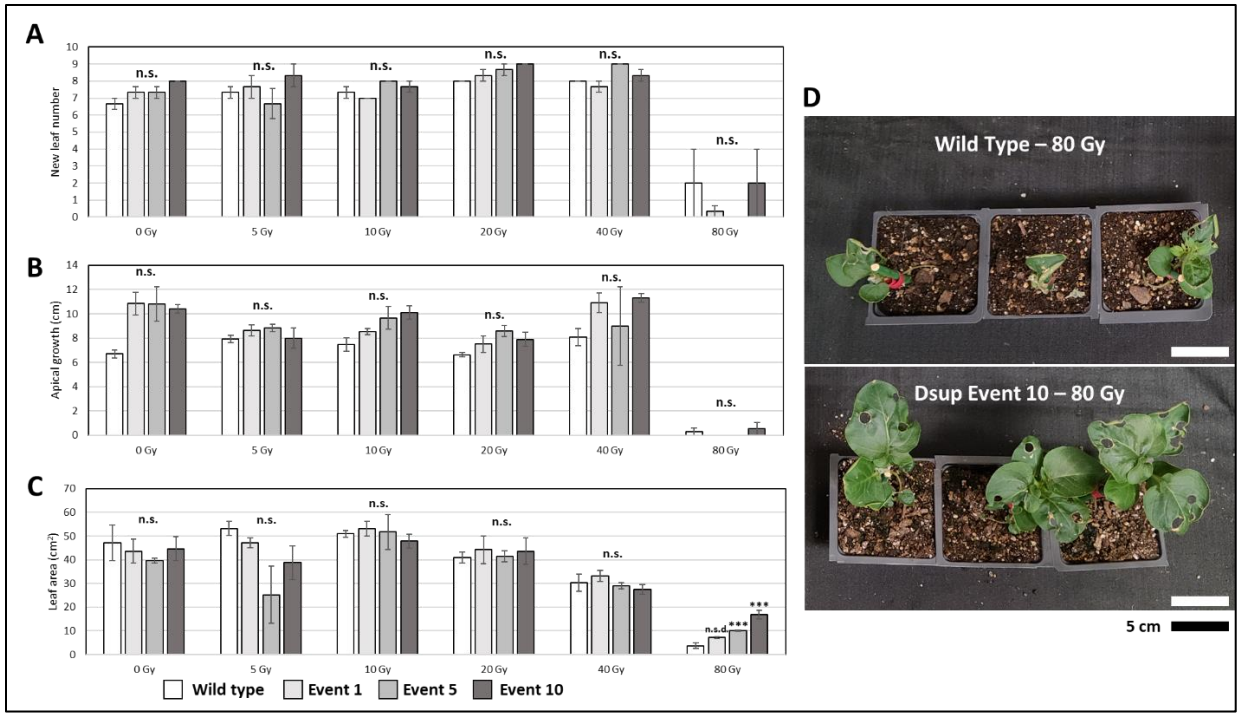

Figure 3.2: Effect of radiation three weeks post treatment in Experiment 1.
(A-C) Aboveground phenotype of wild type and Dsup-expressing (Events 1, 5, and 10) plants three weeks after treatment at 0 – 80 Gy. Graphs represent mean ± standard error of the mean of three aboveground phenotypes in three biological replicates per transgenic event (or wild type) and treatment. Traits include number of new leaves since treatment **(A)**, apical growth since treatment (plant height right before treatment – height at three weeks post treatment) **(B)**, and leaf area in square centimeters **(C)**. ANOVA ($p < 0.05$) with a post-hoc Dunnett's test ($p < 0.05$) was used to evaluate means separation. Lack of significant effect of "event" on the response variable marked with a "n.s." Statistical significance in comparison to the control group (0 Gy) is indicated (***). (**D)** Images of wild type and Dsup Event 10 showing the difference in leaf area remaining three weeks after treatment with 80 Gy. Scale bar = 5 cm.

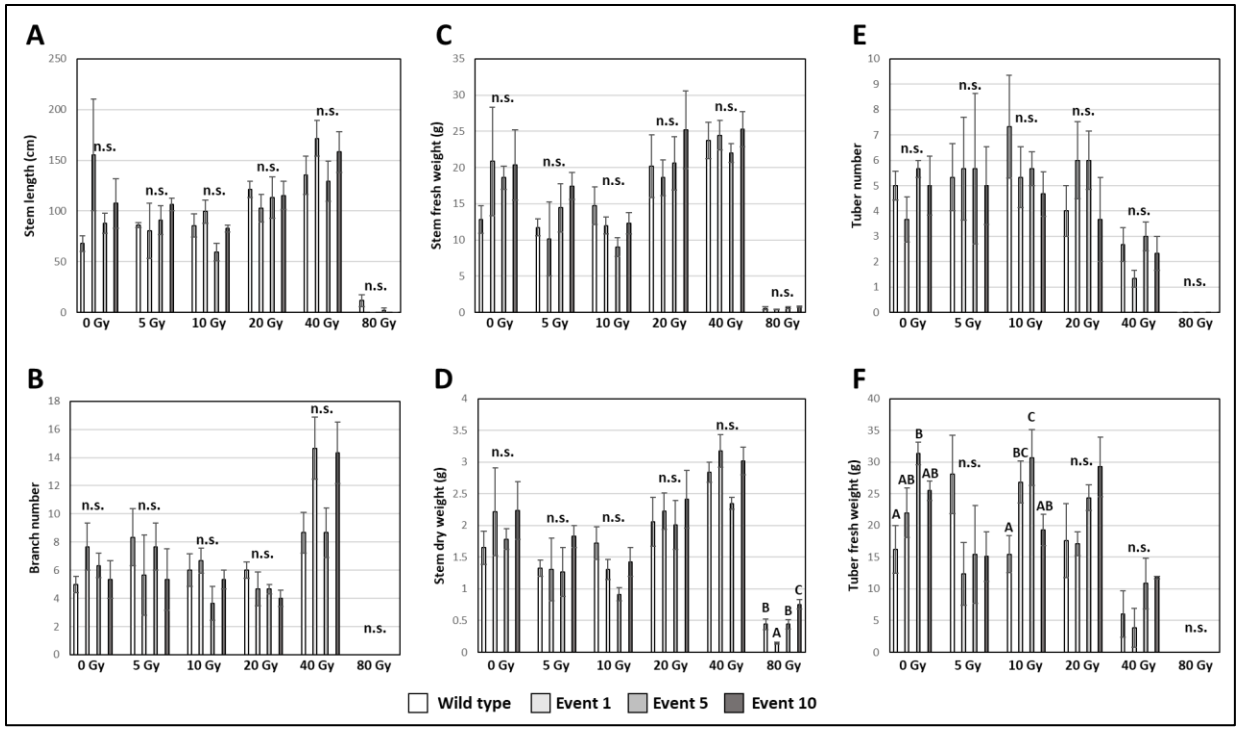

Figure 3.3: Effect of Dsup expression on phenotype at harvest from 0 – 80 Gray.
(A-F) Aboveground and belowground phenotypes of wild type and Dsup-expressing (Events 1, 5, and 10) plants three weeks after treatment at 0 – 80 Gy. Graphs represent mean ± standard error of the mean in three biological replicates per transgenic event (or wild type) and treatment. Traits include total stem length (**A)**, number of branches **(B)**, stem fresh weight in grams **(C)**, stem dry weight after two weeks in a 55 ºC oven, **(D)**, tuber number **(E)**, and tuber fresh weight in grams **(F)**. ANOVA ($p < 0.05$) and mean separation with a Tukey's adjustment ($p < 0.05$) were used to evaluate means separation. Lack of significant effect of "event" on the response variable marked with a "n.s." Statistical significance of "event" on the dependent variable and mean separation are marked with letters, with different letters representing significant differences between means.

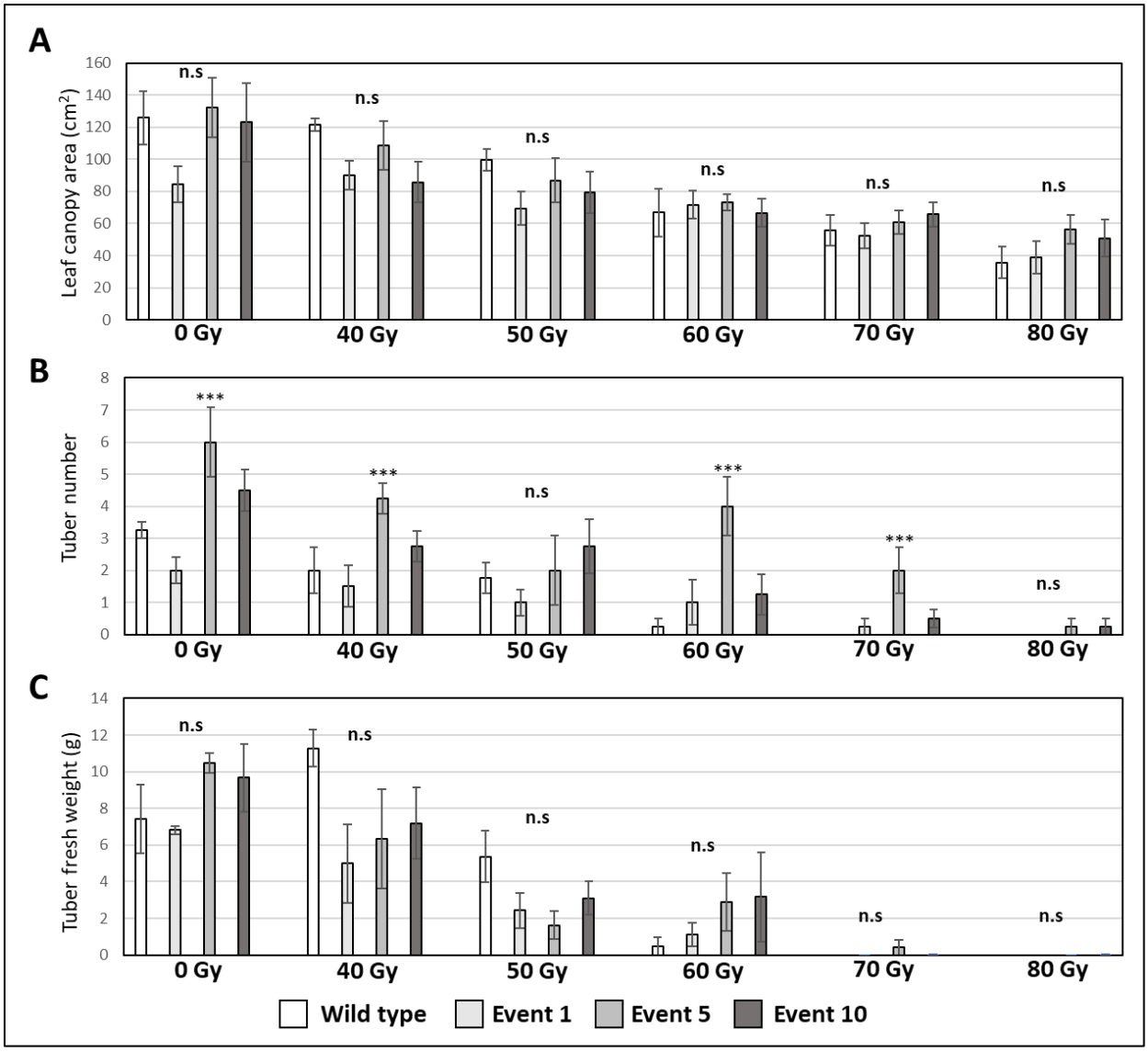

Figure 3.4: Phenotypic effects of Dsup expression on plants irradiated with a high dose range of gamma radiation.
(A) Leaf area in square centimeters three weeks post-treatment (40-80 Gy, 0 Gy as control) in wild type and Dsup-expressing plants. **(B,C)** Tuber number and fresh weight data in grams for plants the plants treated with a high range of gamma radiation. Graphs represent mean ± standard error of the mean in four biological replicates per transgenic event (or wild type) and treatment. ANOVA ($p < 0.05$) with a Post-Hoc Dunnett's test ($p < 0.05$) was used to evaluate means separation. Lack of significant effect of "event" on the response variable marked with a "n.s." Statistical significance in comparison to the control group (0 Gy) is indicated (***).

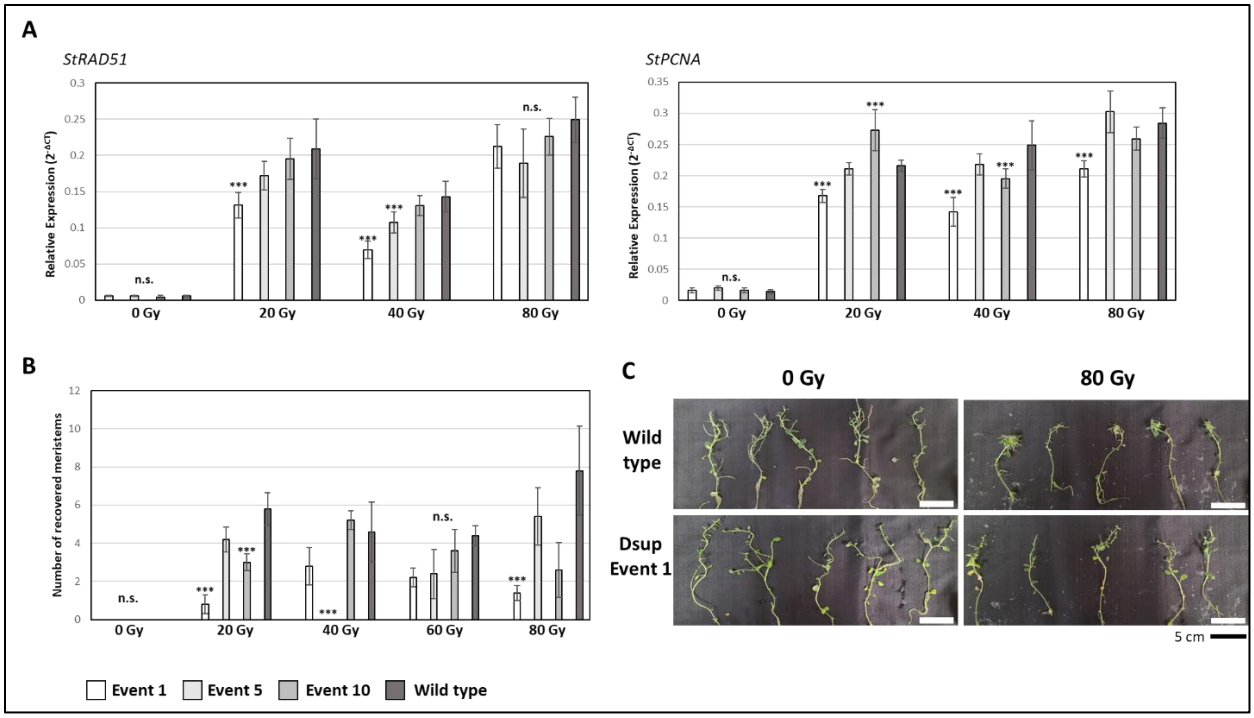

Figure 3.5: Effect of Dsup expression on DNA damage response genes and maintenance of apical dominance.

(A) Induction of expression of the DNA damage response genes *RAS associated with diabetes protein 51 (RAD51)* and *Proliferating cell nuclear antigen (PCNA)* in leaves of three Dsup-expressing events (Event 1, 5 and 10) and wild type *in vitro* at 1.5 hours after dosing with 20, 40, or 80 Gy of gamma radiation. Graphs represent qRT-PCR relative expression data ($2^{-\Delta CT}$) of the gene-of-interest transcript vs the endogenous reference gene, *StEF1α*. Data are expressed as mean ± standard error (SE) of five biological and three technical replicates. Data were analyzed using ANOVA ($p < 0.05$) with a Post-Hoc Dunnett's test ($p < 0.05$) for mean separation. Statistical significance is indicated with "***" while non-significance with "n.s.". **(B)** Number of recovered meristems that emerged from the original meristem five weeks after treatment with 0, 20, 40, 60, or 80 Gy, indicating the severity of apical dominance disturbance. Data represents mean ± standard error (SE) of five biological replicates. Data were analyzed using ANOVA ($p < 0.05$) with a Post-Hoc Dunnett's test ($p < 0.05$) for mean separation. Statistical significance is indicated with "***" while non-significance of the effect of Dsup expression is denoted with "n.s.". **(C)** Images of plantlets five weeks after treatment in wild type and Dsup Event 1 plants. Dsup Event 1 is pictured because it most commonly had significantly lower expression of *RAD51* and *PCNA* as well as fewer recovered meristems. Images show the meristems quantified in figure 2.5B. Note the normal branching from multiple side nodes in 0 Gy plants and the concentration of shoots from the top of the plantlet in 80 Gy treated plants. Scale bar = 5 cm.
***Note**: order and color of the transgenic and wild type bars has been changed in this figure to reflect the change in hypothesis. In previous figures, wild type values were expected to be lower than transgenic. In this figure, wild type values are expected to be higher if Dsup is increasing radiotolerance.

CHAPTER IV: ASSESSING THE MOLECULAR MECHANISMS OF POTATO RADIOTOLERANCE AND DESIGNS FOR IMPROVED RADIATION PHYTOSENSORS

Abstract

Land plants demonstrate much higher tolerance of acute ionizing radiation than most macroorganisms and few studies have investigated their mechanisms of survival in human-relevant dose ranges. An understanding of plants' responses to relatively low doses of gamma radiation would create a path towards low dose gamma radiation sensors and improved radiotolerance in space and radionuclide-contaminated areas on Earth. To address this, phenotypic effects of low dose (0.5 – 5 Gray) gamma radiation treatment and transcriptomic responses were measured in potato plant leaf tissue. Treatments in this range caused little lasting damage to cells and small effects on growth phenotype, but transcriptomic analysis revealed a response that encompassed over ten percent of the potato transcriptome in response to 5 Gray. Gene ontology analysis revealed that gamma radiation response is focused in the chloroplast, cell membrane, and nucleus. Based on this analysis, engineering strategies for increased radiotolerance to protect these key organelles and for the creation of low dose gamma radiation phytosensors were designed.

Introduction

Land plants have a well-established reputation for radiotolerance in the field of radiobiology. Studies regarding the impact of ionizing radiation on plants were being conducted as early as 1904[1], with interest increased steadily to current day[2]. Early observations suggested that radiation treatment could both promote or inhibit plant growth depending on the strength of treatment[1, 3-5], exciting the possibility of increased yields and better crop breeding[6] through use of mutagenic radiation. Interest in plant responses to radiation and their high radiotolerance compared to humans[7] has only continued to climb[2, 8] since the Chernobyl[9] and Fukushima[10] powerplant disasters. Ionizing radiation has captured humanity's interest since its discovery because of both its inherent power and danger. Plants' radiotolerance stands in stark contrast to humans and other mammals, making them a focal point of radiobiology research since nearly the discovery of ionizing radiation itself[11] and resulting in over 150,000 scientific publications[2].

Despite the large number of ionizing radiation publications involving plants, there are very few instances of studies on the effects of low total dose, and even fewer of these have investigated acute low doses. Studies focused on high, acute doses (≥ 50 Gray (Gy)) to observe severe detrimental vegetative phenotypes[12-14] or mechanisms of increased growth in the highly radiotolerant seed tissues[15, 16]. Studies that focused on low total doses typically mimic environmental contamination scenarios surrounding powerplants[17-20]. The high, acute dose studies revealed the effects of gamma radiation levels above those that are quenchable by the plant system and the low dose studies revealed how plants adapt over time to oxidative stress, but none of these address the low, acute doses that have little phenotypic effect on plants[2] but outright kill humans (severe acute radiation sickness, ~ 5 Gy)[21]. Aspects of plant molecular and cellular physiology allow naïve individuals from nearly all reported plant species to survive 5 Gy with little phenotypic effect, while a population of humans experience cell death in all three major blood cell types, severe bone marrow damage, and gastrointestinal damage with death almost certain within three weeks[21]. Plants and animals absorb the same amount of energy, resulting in reactive oxygen species generation[22], lipid peroxidation[23, 24], protein oxidation[25, 26], and DNA damage[27, 28] but these forms of damage lead to completely different outcomes for the respective organisms. Uncovering the mechanisms behind plant tolerance of 0.5 – 5 Gy of radiation would answer a historical curiosity of radiobiology and be directly applicable to long-term spaceflight and phytosensor applications.

Of the 150,000+ publications studying the impact of ionizing radiation on vegetative plant tissues, seed tissues, and callus cultures, few have studied the transcriptome of plant radiation response[29-32] and only Kovalchuk et al. 2007 studied low, acute doses of gamma radiation (1 Gy). Understanding transcriptomic responses to acute gamma radiation in the 0.5 – 5 Gy range, where overall plant phenotype is generally unaffected, would reveal new information on inherent plant radiotolerance that humans lack. This information could be applied to create low dose gamma radiation phytosensors that perform better than previous iterations[33, 34] and design plant-specific radiotolerance mechanisms that enhance already-present ionizing radiation mitigation and repair processes. Therefore, the goal of this study is to generate and evaluate deep transcriptomes of potato plants after acute, low dose ionizing radiation treatment. Potato (*Solanum tuberosum* cv. 'Desiree') was chosen based on previous evaluation of its radiotolerance and ideal phytosensor characteristics, making the findings of this study directly applicable to the improvement of existing gamma radiation phytosensor strategies.

Results and Discussion

Potato is capable of mitigating and/or repairing all damage caused by ≤ 5 Gray of gamma radiation.

To investigate the mechanisms of radiotolerance in plants and generate data that is relevant to most nuclear emergency scenarios, four-week-old wild type potato was irradiated with a low range of gamma radiation treatments (0.5 – 5 Gy). These doses were delivered in the same amount of time with dose rate adjusted by distance from source. It was expected that this range of treatments would result in little to no physiological effect, other than the typical hormesis[35] reported with low-dose radiation. H_2DCFDA analysis of leaf extracts collected right after treatment found no significant effect of radiation treatment on fluorescence per mg tissue (ANOVA $p < 0.05$), suggesting that no reactive oxygen species are unquenched at the end of treatment (Figure 4.1A,B). All figures and tables are located in an appendix at the end of the chapter. Doses just above the range tested here generated appreciable increases in H_2DCFDA in *Chlamydomonas*[36] and human cells[37], but not in Arabidopsis[38]. This suggests higher antioxidant capabilities in land plants compared to near and distant relatives. This also clarifies that cellular damage from radiation-induced reactive oxygen species may not continue after treatment, meaning all expression changes after treatment are done under normal cellular redox conditions. This is important to note, since ROS are involved in a variety of cellular responses and random, radiation-induced protein oxidation could lead to a myriad of pathways responding at the transcript level[39]. It should be noted that the H_2DCFDA assay used here is common in the literature but does homogenize tissue, which can cause spurious reactions that either quench or generate ROS[40]. *In situ* observation of H_2DCFDA fluorescence would be preferable and is also used widely[41], though samples could not be observed directly post-treatment and therefore were flash frozen, introducing inherent disruption even before homogenization. To further investigate the dynamics of ROS generation and quenching in wild type potato, an ideal assay would utilize fumigation of plants with H_2DCFDA as they are irradiated, allowing for real-time whole plant imaging of reactive oxygen species[42]. The penetrative nature of gamma radiation would work well for this experimentation, though the specialized nebulizer and observation equipment made it impractical for this work. Short-lived reactive oxygen species generated by ionizing radiation are inherently difficult to study, though the H_2DCFDA fluorescence observed here failed to find a difference in ROS concentration in leaf tissue collected directly after treatment.

The cellular and genomic damage induced by gamma radiation did not result in widespread apoptosis seventy-two hours after treatment (Figure 4.1C). Plants utilize programmed cell death (PCD) throughout their lifecycle (senescence) and in pathogen response (hypersensitive response)[43], so it is important to note that radiation treatments at these levels does not lead to any appreciable cell death for the delineation of repair and PCD pathways observed in the transcriptomic dataset. Compared to human cancer cell lines, where half to all cells undergo apoptosis within forty-eight hours after treatment with 6 Gy[44], potato leaves stained with trypan blue showed no appreciable staining at similar treatment levels (Figure 4.1C). It is possible that single cells within the stained leaves undergo apoptosis but were not observed by macroscopic analysis, as gamma radiation induces random mutagenesis and some cell types could be more prone to undergo apoptosis than others. In Arabidopsis roots, cell death around the quiescent center is observed in response to treatments of ≥ 20 Gy[45]. Since Arabidopsis is generally more radiotolerant than potato[45,34], it cannot be ruled out that some potato cells underwent apoptosis in response to 5 Gy. However, apoptosis typically occurs in meristematic tissues[45], so this may be limited in the leaf tissues stained. Taken together, the H_2DCFDA and trypan blue staining results suggest that post-treatment transcriptional responses in leaf tissue are carried out in the absence of continued oxidative stress and that those responses do not induce a high level of apoptosis in leaf tissue.

The lack of difference in post-treatment physiology yielded little impact on growth and biomass accumulation in the first five weeks after treatment (Figure 4.2). When comparing all treatments, radiation treatment had a significant effect (ANOVA $p < 0.05$) on plant height, leaf number, or meristem length from treatment to six weeks post-treatment at most timepoints, but none of the treated plants were significantly different from untreated plants (Dunnett's test, $p < 0.05$) (Figure 4.2A-C). When comparing only untreated and 5 Gy treated plants (Figure 4.2D-F), 5 Gy treatments significantly (student's t test, $p < 0.05$) reduced meristem length one week post-treatment with no impact on plant height. Surprisingly, 5 Gy treated plants were significantly taller (student's t test $p < 0.05$) one week later. Starting at two weeks post-treatment, 5 Gy treated plants retained lower leaves that are senesced in 0 Gy plants, leading to a significant increase in leaf number (student's t test, $p < 0.05$). Gamma radiation appeared to increase variation in the length of stem growth three weeks post-treatment (Figure 4.2G). A Levene's test for unequal variance fails to find unequal variance among treatment groups ($p < 0.05$), though standard error of the mean consistently increases from 0 Gy to 4 Gy. The random nature of gamma radiation's impacts on individual cells likely leads to the variation seen in growth data at these timepoints, making it difficult to find a significant effect of treatment within the first five weeks after treatment.

At six weeks post-treatment, plant aboveground structure and meristem phenotypes began to change corresponding to gamma radiation treatment. No significant effect (ANOVA, $p < 0.05$) of gamma radiation was detected for plant height, number of leaves on the main stem, or the number of emerged secondary shoots (> 1 cm in length) (Figure 4.3A-C). However, radiation had a significant effect on the number of leaves on secondary shoots. No treatment groups' mean number of leaves on secondary shoots were significantly different than 0 Gy treated plants (Dunnet's post-hoc, $p < 0.05$), though a significant difference was detected between plants treated with 2 Gy and 4 Gy (Figure 4.3D). The high number of leaves on secondary stems produced a bushy phenotype in plants treated with 5 Gy (Figure 4.3E,F). Structural changes corresponded with noticeable changes in meristem phenotype (Figure 4.4). Altered apical meristem phenotypes were noticed in all plants treated with gamma radiation

(Figure 4.4A). These phenotypes typically emerged as a 'pause' in meristematic extension, where multiple mature leaves emerge from the stem much closer together than previous leaves. Gamma radiation induced altered meristem phenotypes in all individuals treated with ≥ 2 Gy, though 'sunken' meristem phenotypes were only observed in plants treated with 4 and 5 Gy (Figure 4.4B, D). The same altered apical meristem phenotypes were observed in secondary shoots in plants treated with ≥ 1 Gy, though a lower percentage of secondary meristems had an altered phenotype compared to apical meristems at all treatments (Figure 4.4C, E).

Physiological data collected in the six weeks after treatment indicated that 0.5 – 5 Gy treatments of gamma radiation caused significant impacts on aboveground phenotype, although this impact could either stimulate or hinder aboveground growth depending on dose and individual. Plants treated with 5 Gy had significantly more leaves than plants treated with 0 Gy, consistent with reports of delayed senescence in Arabidopsis[46].The 'sunken meristem' phenotypes observed at six weeks represent the first clear effect of gamma radiation treatment observed in this study and some of the lowest effects of gamma radiation on plant phenotype observed generally[34, 47] In summary, acute gamma radiation treatment in the 0.5 – 5 Gy range caused statistically significant but relatively minor phenotypic effects until six weeks after dose, at which point effects of treatment on the meristem became apparent. To the lay person, there would be no noticeable difference in their environment, although a potentially human-lethal amount of gamma radiation could be present. This makes the development of low dose gamma radiation phytosensors imperative for future environmental monitoring. These data also suggest that plant responses to this range of gamma radiation are involved in repair and acclimation in somatic tissues, rather than cell death. To facilitate the generation of a low dose phytosensor and uncover the mechanisms potato uses to endure gamma radiation treatment, transcriptomic and gene ontology analysis were pursued.

Gamma radiation response expands with total dose and dose rate.

Transcriptomic analysis of leaf tissue 1.5 hours after treatment was conducted to investigate gamma radiation responses. An excellent read depth of at least 60 million reads was achieved for all but one sample (0 Gy, replicate 1, 42 million reads), representing one of the deepest RNAseq datasets for ionizing radiation studies in plants. After quality control, reads were mapped to the double monoploid potato DM 1-3 516 R44 (v6.1) high confidence CDS gene model set[48] This reference genome was selected for its prevalence of use in the literature and its annotation resources made available through the SpudDB website hosted by the University of Georgia, allowing for streamlined analysis. A key resource for this analysis from SpudDB is the database of *S. tuberosum* loci with assigned gene ontology (GO) terms based on best hit to the Arabidopsis proteome (TAIR10). This allowed for high confidence in conclusions taken from GO term analysis, though it does exclude loci that do not align well with *Arabidopsis* loci.

Differential gene expression analysis and subsequent GO term enrichment analysis indicated that the response to ionizing radiation changes over the range of treatments tested (Table 4.1, Figures 4.5-19). The number of DEGs generally increased as ionizing radiation treatment increases, though plants treated with 1 Gy had the lowest number of DEGs of all treatments (Table 4.1). There is a clear delineation in number of DEGs between 0.5 - 2 Gy treatments and 4 - 5 Gy treatments, with more than two thousand additional DEGs detected in the higher treatments. The delineation between 2 and 4 Gy remained when comparing only highly (>4×) upregulated and downregulated genes, though the number of highly upregulated genes increased 4.22× from 0.5 to 5 Gy while the number of highly downregulated genes only

increased 1.89×. The number of highly up- and downregulated genes in plants treated with 0.5-2 Gy mirrored those reported for a 1 Gy acute dose[29] while 4 and 5 Gy treatment numbers appeared similar to high dose (70-120 Gy) effects[27, 30, 31] indicating that there may be a threshold for response at 4 Gy. The highest response of differentially expressed genes (5889 loci in response to 5 Gy) represents approximately ten percent of the working gene models identified in the DM 1-3 516 R44 (v6.1) reference genome, similar to the ~7% observed in Arabidopsis irradiated with 100 Gy[32]. This further suggested that most of the radiation-responsive genes are activated in the higher end of this treatment range.

Significant GO term enrichment (FDR < 0.05) revealed interesting trends in highly upregulated genes' cellular compartment (Figures 4.5-9), biological processes (Figures 4.10-14), and molecular function (Figures 3.15-19). Enriched cellular compartment GO terms in plants treated with 0.5 Gy dealt exclusively with the chloroplast and the apoplast (Figure 4.5). Chloroplast terms remained enriched until 4 Gy (Figure 4.8) and nuclear chromosome terms are significantly enriched in the response to 2-5 Gy. Cell membrane, wall, and apoplast GO terms were present at 0.5 Gy treatments, absent at 1-2 Gy, and began to dominate at 4-5 Gy treatments. In this range, it appeared that the cell perimeter is reactive at all doses (assuming the absence in response to 1-2 Gy is an artifact), while chloroplast-related genes dominated the response to < 5 Gy treatments and nucleus-related genes become increasingly important starting in treatments of 2 Gy and above.

Biological process GO terms for highly upregulated genes also indicated differences in response across the 0.5 – 5 Gy treatment range. It was clear that potato plants experienced oxidative stress in response to 0.5 Gy due to enrichment of terms such as "response to light stress" (GO:0009416, FDR = 0.001), "response to oxygen-containing compound" (GO:1901700, FDR = 0.0007) and other oxidation/reduction-related GO terms (Figure 4.10). In addition, terms related to cell wall biogenesis (especially xylan biosynthesis) were present in the response to 0.5 Gy. Unlike the enriched cell compartment terms, the biological process terms present in 0.5 Gy remained in all treatments, with the number of processes having a strong positive correlation with dose. Terms related to the nucleus and DNA repair began in response to 1 Gy, a lower dosage than the nuclear chromosome GO term appeared in the cellular compartment analysis. A clear jump was made from 2 Gy to 4 Gy, with a wider variety of "response to" (e.g. organonitrogen species, ozone, bacterium) terms significantly enriched in addition to more specific DNA repair, cell wall biosynthesis, and transmembrane kinase terms in response to the higher treatment (Figures 4.12,13). The response to 5 Gy included even more "response to" GO terms that are farther from ionizing radiation (ex. salt, jasmonic acid, chitin, ABA, ethylene, wounding), as well as hypersensitive response and cell death GO terms (Figure 4.14).

Enriched molecular function GO terms mirrored the results of the biological process GO terms. The response to 0.5 Gy involved typical ROS quenching terms such as oxygen binding, oxireductase/monooxygenase activity, heme/iron binding, carboxy-lyase, methyltransferase, and UDP-glucosyltransferase activity (Figure 4.15). These terms remained in response to 2 Gy, while DNA specific ATPase and helicase activities are significantly enriched for the first time. In addition, cofactor-binding and protein binding activities appeared at this treatment (Figure 4.17). Coenzyme binding, peptidase terms, and serine/threonine kinase activity terms became significant in response to 4 Gy, in addition to all previous terms listed (Figure 4.18). In response to 5 Gy, all terms significant at 4 Gy remained, with the addition of transmembrane signaling/kinase activity (Figure 4.19).

The number and variety of highly upregulated genes that respond to 4 and 5 Gy treatments compared to 0.5-2 Gy treatments indicated that some threshold is crossed between 2 Gy and 4 Gy at the dose rates tested. In response to 2 Gy and below, cells appeared to only upregulate core oxidative stress and DNA damage response genes. In response to 4 Gy treatment and above, activation of more general stress responses was apparent, with upregulation of many kinases, some of which are membrane specific. This culminated in the 5 Gy treatment group with the expression of genes related to programmed cell death (Figure 4.14), though expression of these genes does not result in widespread cell death based on trypan blue staining (Figure 4.1C).

Transcriptomic analysis suggests that oxidative stress is minor and single-cell apoptosis is a possibility.

H_2DCFDA fluorescence and trypan blue staining suggested that oxidative stress does not continue post-treatment and that the oxidative stress induced by these gamma radiation treatments did not lead to widespread apoptosis (Figure 4.1). To investigate whether the transcriptomic data supports these conclusions, expression data for specific loci associated with membrane antioxidant and programmed cell death pathways were extracted. Membrane antioxidant systems in plants utilize the ascorbate-glutathione cycle to quench ROS generated by a variety of stressors[49]. The ascorbate-glutathione cycle utilizes ascorbate peroxidase and glutathione reductase to quench hydrogen peroxide, and genes encoding these enzymes are differentially expressed in response to a variety of abiotic and biotic stressors across plant species[50-53]. No significant differential expression of loci annotated as ascorbate peroxidases or glutathione reductase was detected (Table 4.2). Two loci annotated as superoxide dismutases showed significant, but slight downregulation in response to 5 Gy treatment (Table 4.2). Typically, superoxide dismutase genes are upregulated in response to higher Gy treatments than those tested here[54, 55]. Significant up- and down-regulation with a > 4-fold change in transcript count was observed in loci annotated as catalases and NADPH:quinone oxireductases, indicating that ROS scavenging enzymes operating outside of the ascorbate-glutathione cycle are differentially expressed in response (Table 4.2). Expression levels and enzymatic activity of these classes of enzymes often do not correspond in response to stress, indicating that significant downregulation could represent in an increase in ROS scavenging activity[49].

In contrast, a greater number of loci annotated as protein repair enzymes such as thioredoxins, glutaredoxins, and peroxiredoxins, were differentially expressed compared to the loci associated with ROS scavenging pathways (Table 4.2). These enzymes fix oxidative damage to amino acid chains induced by ROS and are a key to the repair of oxidative stress[39]. The differential expression of NADPH:quinone oxireductases and catalases in response to 5 Gy indicated that ROS quenching makes up part of the transcriptomic response 1.5 hours post-treatment. However, a lack of change in the membrane antioxidant enzymes related to the ascorbate-glutathione cycle or superoxide dismutase, in contrast to the enrichment of cellular membrane GO terms, suggest that the membrane-associated response is focused on repair and cell-cell signaling rather than quenching ROS. Comparison of ROS scavenging and protein repair pathways suggests that a larger transcriptional response is elicited to repair ROS damage rather than scavenge existing ROS 1.5 hours post-treatment. Taken with the H_2DCFDA data that found no significant difference in ROS levels in leaf tissue after treatment with 0.5 – 5 Gy, this suggests that oxidative stress does not continue post-treatment.

The RNAseq dataset also suggested that cells in leaf tissue expressed loci associated with programmed cell death in response to 5 Gy, in contrast with the results of macroscopic trypan

blue staining. A 'hypersensitive response' biological function GO term was significantly enriched in list of four-fold upregulated loci in response to 5 Gy (Figure 4.14). However, most of the potato loci associated with this GO term are annotated as chitinases, NB-ARC domain-containing disease resistance proteins, and other proteins related to cell-cell signaling and pathogen detection (Table 4.3). These proteins act as sensors of pathogens and often require a specific non-host substrate, such as chitin, to activate programmed cell death pathways[56,57]. It is unlikely that these proteins bound their target substrate and activated the hypersensitive response, as no disease pressure was noted in the phenotypic analysis over the lifetime of the plants. Instead, it is likely that expression of these loci was erroneously activated by the ROS produced by ionizing radiation treatment[58]. It cannot be determined whether the transcript observed was produced only during treatment or afterwards, though if these loci were upregulated after the end of treatment it could suggest that oxidative stress continues after treatment[58], contrary to the H_2DCFDA results (Table 4.2, Figure 4.1). The expression dynamics of these pathogen sensor loci would help determine whether oxidative stress continues after treatment, if a RNAseq time course experiment was conducted.

Further exploration of the RNAseq dataset reveals that loci annotated with terms related to various plant cell death mechanisms are differentially expressed in response to a 5 Gy treatment. Loci labelled as metacaspases, aspartyl proteases, BCL-2-associated athanogenes, and papain-like cysteine proteases were all significantly differentially expressed in response to a 5 Gy treatment, with many loci having a greater than four-fold change in transcript count (Table 4.4). Although apoptosis in plants is not as well-understood as in animals[59], metacaspases[60], aspartyl proteases[61], BCL-2-associated athanogenes[62], and papain-like cysteine proteases[63] each play a role in activating apoptosis, so differential expression of similar loci in response to a 5 Gy treatment could indicate that programmed cell death pathways could have been activated. Microscopic examination of the stained leaves would reveal whether cell death occurred in these tissues, though it is clear that if there is cell death it is not widespread as was observed in human cells.

Recommendations for radioprotection strategies based on gene ontology analysis.

Radioprotection is achieved mainly by proteins and metabolites that quench ROS and repair oxidative damage, making it difficult to devise strategies based solely on transcriptomic data[64]. However, it is clear from this dataset that three organelles were the focus of the transcriptomic response: the chloroplast, the cell membrane, and the nucleus. A variety of chloroplast genes were upregulated in response to 0.5 Gy (Table 4.5), with many involved in the electron transport chain that occurs through the thylakoid membrane. Protection of thylakoid membranes could be achieved through increases in intermembrane antioxidants such as carotenoids[65] and tocopherols[66]. This has already been done in rice for UV protection[67] and many of these molecules' biosynthesis pathways are being optimized[68-70]. Ascorbate is an obvious choice for protection of plant cell membranes, although maximization of ascorbate is not advised as this can inhibit stress responses[71]. It should be noted that if carotenoids, tocopherols, and ascorbate concentrations were increased in plant tissue, this would also create a highly nutritious food source for astronauts[72]. The most difficult challenge will be providing adequate protection to the plant genome (see CHAPTER III). Polyploidy's effect on radioprotection is currently debated[73, 74], though without any genome protection mechanisms and in light of plants' preference for destructive non-homologous end joining[75], polyploid plants are likely a good choice for radiation applications.

Top candidate loci for low dose phytosensor development.

To facilitate the creation of low-dose gamma radiation phytosensors, a curated list of twenty upregulated and downregulated loci was compiled (Table 4.6). Of these, those with the most favorable gene expression profiles for a single gene off-to-on phytosensor were "Soltu.DM.02G034230.1 - Ferritin/ribonucleotide reductase-like family protein", "Soltu.DM.08G019390.1 - poly(ADP-ribose) polymerase", "Soltu.DM.05G011490.1 - P-loop containing nucleoside triphosphate hydrolases superfamily protein", and "Soltu.DM.01G031990.1 – Ku80 family protein". Each of these loci had very low (0 – 250) mean adjusted transcript count detected in untreated plants but over four-fold increases at 0.5 Gy, with mean adjusted transcript counts in the tens of thousands in response to 5 Gy. In addition, each of these loci are likely related to DNA repair but are different from those tested in the latest phytosensor publication[34]. Ferritin/ribonucleotide reductase proteins catalyze the synthesis of deoxyribonucleotides for DNA repair[76], Ku80 and poly(ADP-ribose) polymerase (PARP) are well known DNA repair proteins[77, 78], and P-loop containing nucleoside triphosphate hydrolases are required for the addition of DNA polymerase clamps so that repair can be carried out[79].

There were fewer options for efficient downregulation in a radiation sensor genetic circuit. A similar range of basal expression is represented in untreated samples, though loci generally had a smaller dynamic range and none turn completely "off" at any of the treatments tested. This makes the promoters of these loci difficult to use in genetic switches if paired with highly efficient activators or repressors. The best locus on the list with a high basal transcript count is "Soltu.DM.03G015520.1 - Plant invertase/pectin methyltransferase inhibitor superfamily protein" and the best with low transcript count is "Soltu.DM.07G017280.1 – Terpenoid cyclases/Protein prenyltransferases superfamily protein". Additionally, post-transcriptional repression could be exerted using the ribonucleases upregulated associated with stress response[80]. An example is "Soltu.DM.01G002470.1 - Polynucleotidyl transferase, ribonuclease H-like superfamily protein", with greater than eleven-fold upregulation in response to 5 Gy.

Based on this transcriptomic dataset, it is clear that a low dose gamma radiation phytosensor is feasible with native promoters. Performance in this range could be improved with the creation of synthetic promoters[81] and multi-switch genetic systems to minimize basal output and maximize activated output[82].

Conclusion

Small phenotypic changes induced by low dose gamma radiation belie the large transcriptional change required for plants to quench reactive oxygen species and repair cell parts. Cellular responses centered around chloroplast and apoplast at very low doses, indicating that oxidative stress in cell membranes was the main concern for a plant cell responding to 0.5 – 2 Gy treatments. Treatments of 4-5 Gy induced a much larger response that also involved a large proportion of genome repair loci, indicating that a coordinated stress response was taking place throughout the cell. Transcript data suggested that this response can be harnessed to make a radiation phytosensor sensitive to as low as 0.5 Gy if native promoters can be effectively harnessed. Responses also suggested that increased membrane antioxidants would increase cellular resistance to radiation, which would be beneficial for human nutrition as well. The information uncovered here creates a clear path to future low dose radiation phytosensors and radiation tolerant crop plants, indicating humanity will remain safe and well fed as we proceed in our relationship with ionizing radiation.

Materials and methods

Plant material and growth conditions

Wild type *Solanum tuberosum* cv. 'Desiree' was procured from the Wisconsin Seed Potato Certification Program at the University of Wisconsin - Madison and kept in sterile culture on modified Murashige and Skoog media[83].

For experimentation, plants were removed from tissue culture and placed into a 10 cm plastic pot filled with a soilless media and allowed to adjust to ambient humidity for one week under a closed lid inside of a growth chamber. After this the lid was removed, plants were grown within the growth chamber an additional three weeks until the beginning of the experiment. Growth chambers were set to a 16-hour light / 8-hour dark daylight regime, with daytime temperature set to 20 ºC and nighttime temperature set to 18 ºC. Plants were fertilized with Peter's 20-20-20 fertilizer after hardening and after 3 weeks in soil. For subsequent growth analysis, plants were fertilized equally with Peter's 20-20-20 every two weeks.

Gamma radiation treatment

Gamma radiation treatment was done by adjusting plants' distance and dosage time from a Cobalt-60 source to reach a total dose (reported in this paper in Gray). Treatment times and rates (rad / sec) were kept consistent across two irradiation events by adjusting distance for natural degradation of the sensor. Treatment times, rates, and distances can be found for each of the experiments in Table 4.7.

H_2DCFDA fluorescence assays

Analysis of reactive oxygen species through 2',7'-dichlorodihydrofluorescein diacetate (H_2DCFDA) fluorescence was conducted according to previous protocols[84]. Briefly, three leaf discs were collected from the topmost three leaves (one per leaf) of three biological replicates per radiation treatment and stored in 1.5 ml tubes on dry ice. Tissue was quickly weighed and homogenized using a metal bead and shaker (30 seconds, 30 shakes / second), then 1 ml of 10 mM Tris-HCl buffer (pH 7.3) was added. Tubes were centrifuged for five minutes at 15,000 g, supernatant was moved to a new tube, and tubes were centrifuged again for five minutes at 15,000 xG, and then 198 µl of supernatant was added to four wells of an optical 96-well plate and the plate was read for fluorescence in the fluorescein range (ex. 485 nm, em. 528 nm) using a BioTek Synergy H1 plate reader. After background fluorescence was quantified, 1 mM H_2DCFDA was added to each well for a final concentration of 10 µM. Fluorescein and the plate was placed in darkness for five minutes. Fluorescein fluorescence was then measured once per minute for twenty minutes with a H_2O_2 standard curve used as a positive control. Pre- H_2DCFDA fluorescence values were subtracted from the twentieth read fluorescence data, then fluorescence was normalized to the weight of tissue collected for each sample.

Trypan blue staining

Trypan blue staining was conducted according to previously described protocols[85]. Briefly, leaves were collected 72-h post-treatment and quickly visualized using an Epson Perfection V300 Photo scanner. After visualization, leaf tissues were submerged in a 1:1:1:1 solution of lactic acid (85% w:w) (Thermo), phenol (TE buffer equilibrated pH 6.6) (Thermo), 99% glycerol (Thermo), and distilled water with trypan blue powder (Sigma) added at a concentration of 10 mg / ml. Leaves were completely submerged in the staining solution for one hour with brief

agitation every ten minutes. After one hour, leaves were removed from the staining solution and bleached with washes of 95% ethanol until no chlorophyll remained. Leaves were then visualized using the same Epson scanner.

Phenotypic analysis

Phenotypic measures were taken four days before treatment to ensure randomized and consistent phenotype in the selected plants for treatment. Phenotypic data was then collected at one week intervals beginning at seventy two hours post-treatment (0 weeks post-treatment in Figure 3.2). Leaf number, plant height from the soil line, and "meristem length" were measured at each timepoint. Meristem length measures were calculated as the length in millimeters from the first secondary node to the top of the apical meristem (height of young leaves around the meristem were not included). This phenotype was done to observe any 'sunken meristem' phenotypes that are common at higher radiation doses in potato[34]. "Height increase" data in Figure 3.2G was calculated as the height at three weeks post-treatment minus plant height pre-treatment. Data for all phenotypic measures was analyzed per timepoint using ANOVA ($p < 0.05$) and a post-hoc Dunnett's test ($p < 0.05$) for mean comparison with 0 Gy used as the control group. For 0 vs 5 Gy comparisons, a student's t test ($p < 0.05$) was used.

RNAseq data collection

Three leaf discs were collected from the topmost three leaves (one disc per leaf) of three biological replicates per radiation treatment and stored in RNAlater solution (Sigma-Aldrich) after dosing. RNA was extracted and cleaned using the Quick RNA miniprep kit (Zymo Research) and One step PCR inhibitor removal kit (Zymo Research). RNA integrity was checked using an Agilent 4200 Tapestation (Agilent) and its quantitation was measured by Qubit4 fluorometer before the generation of cDNA libraries.

RNAseq data analysis

The cDNA libraries for reading paired-end 150 bases were generated using the TruSeq Stranded mRNA Library Kit (Illumina, San Diego, CA, USA). Raw sequencing reads were sequenced by NovaSeq6000 S4 (Illumina). Initial quality control was performed using FastQC[86]. Read trimming was done using Sickle[87]. Reads were aligned to the genome assembly for doubled monoploid potato DM 1-3 516 R44 (v6.1) with high confidence CDS gene models gff3 format annotation[48] using STAR[88]. Aligned reads were mapped to features of the model set HTSeq 2.0[89] and differential expression analysis was calculated using DESeq2[90]. Normalization factors can be found in Table 4.8.

Gene ontology analysis

Gene ontology analysis was conducted by assigning highly (4×) upregulated and downregulated potato loci to the GO terms for their best hit to the Arabidopsis proteome (TAIR10)[48]. Once converted, enriched GO terms of highly upregulated genes from each gamma radiation treatment were identified using AgriGO[91].

Statistical analysis

All phenotypic statistics were calculated using JMP Pro 15 software (SAS, Cary, NC). ANOVA function ($p < 0.05$) and mean separation with either a post-hoc Dunnett's test ($p < 0.05$) or a Tukey's HSD ($p < 0.05$)

References

1. Russell, E. The effect of radium on the growth of plants. *Nature* **96**, 147-148 (1915).
2. Gudkov, S. et al. Effect of ionizing radiation on physiological and molecular processes in plants. *Journal of Environmental Radioactivity* **202**, 8-24 (2019).
3. Kuzin, A. et al. Molecular mechanisms stimulating the action of ionizing radiation on seeds. 3. Role of radiotoxins in stimulating the development of irradiated seeds. *Radiobiologiia* **16**, 261-264 (1976).
4. Breslavets, L. Plants and X-rays. *Soil Science* **92**, 147 (1961).
5. Donini, B. et al. Effects of chronic gamma irradiation in Durum and bread wheats. *Radiation Botany* **4**, 387-393 (1964).
6. Gregory, W. A radiation breeding experiment with peanuts. *Radiation Botany* **8**, 81-147 (1968).
7. Real, A. et al. Effects of ionising radiation exposure on plants, fish and mammals: relevant data for environmental radiation protection. *Journal of Radiological Protection* **24**, A123-A137 (2004).
8. Mousseau, T. & Møller, A. Plants in the light of ionizing radiation: What have we learned from Chernobyl, Fukushima, and other “hot” places? *Frontiers in Plant Science* **11,** 552 (2020).
9. Medvedev, Z.A. The legacy of Chernobyl / Zhores A. Medvedev. (W.W. Norton, New York; 1990).
10. Yoschenko, V. et al. Radioactive contaminated forests in Fukushima and Chernobyl. *Journal of Forest Research* **23**, 3-14 (2018).
11. Allisy, A. Henri Becquerel: The discovery of radioactivity. *Radiation Protection Dosimetry* **68**, 3-10 (1996).
12. Fan, J. et al. Regulation of photosynthetic performance and antioxidant capacity by 60Co γ-irradiation in *Zizania latifolia* plants. *Journal of Environmental Radioactivity* **129**, 33-42 (2014).
13. Shelp, B. et al. Radiation-induced changes in the export and distribution of photoassimilated carbon in soybean plants. *Environmental and Experimental Botany* **19**, 245-252 (1979).
14. Kebeish, R. et al. Effect of gamma radiation on growth, oxidative stress, antioxidant system, and alliin producing gene transcripts in *Allium sativum. International Journal of Research Studies in Biosciences* **3**, 161-174 (2015).
15. Qi, W. et al. ROS and ABA signaling are involved in the growth stimulation induced by low-dose gamma irradiation in Arabidopsis seedling. *Applied Biochemistry and Biotechnology* **175**, 1490-1506 (2015).
16. Wang, J. et al. Ionizing radiation: Effective physical agents for economic crop seed priming and the underlying physiological mechanisms. *International Journal of Molecular Sciences* **23**, 15212 (2022).
17. Vanhoudt, N. et al. The combined effect of uranium and gamma radiation on biological responses and oxidative stress induced in *Arabidopsis thaliana. Journal of Environmental Radioactivity* **101**, 923-930 (2010).
18. Boratyński, Z. et al. Ionizing radiation from Chernobyl affects development of wild carrot plants. *Scientific Reports* **6**, 39282 (2016).
19. Sahr, T. et al. Low-level radiocaesium exposure alters gene expression in roots of Arabidopsis. *New Phytologist* **168**, 141-148 (2005).

20. Zaka, R. et al. Effects of low chronic doses of ionizing radiation on antioxidant enzymes and G6PDH activities in *Stipa capillata* (Poaceae). *Journal of Experimental Botany* **53**, 1979-1987 (2002).
21. Waselenko, J. et al. Medical management of the acute radiation syndrome: recommendations of the Strategic National Stockpile Radiation Working Group. *Annals of Internal Medicine* **140**, 1037-1051 (2004).
22. Gapeyev, A. et al. Hydrogen peroxide induced by modulated electromagnetic radiation protects the cells from DNA damage. *Open Life Sciences* **9**, 915-921 (2014).
23. Ye, L. et al. Radiation-induced lipid peroxidation triggers ferroptosis and synergizes with ferroptosis inducers. *ACS Chemical Biology* **15**, 469-484 (2020).
24. Afify, A. et al. Antioxidant enzyme activities and lipid peroxidation as biomarker compounds for potato tuber stored by gamma radiation. *Asian Pacific Journal of Tropical Biomedicine* **2**, S1548-S1555 (2012).
25. Borzouei, A. et al. Biochemical response of two wheat cultivars (*Triticum aestivum* L.) to gamma radiation. *Pakistan Journal of Botany* **45**, 473-477 (2013).
26. Barshishat-Kupper, M. et al. Effect of ionizing radiation on liver protein oxidation and metabolic function in C57BL/6J mice. *International Journal of Radiation Biology* **90**, 1169-1178 (2014).
27. Kim, J. et al. Ionizing radiation manifesting DNA damage response in plants: An overview of DNA damage signaling and repair mechanisms in plants. *Plant Science* **278**, 44-53 (2019).
28. Borrego-Soto, G. et al. Ionizing radiation-induced DNA injury and damage detection in patients with breast cancer. *Genetics and Molecular Biology* **38**, 420-432 (2015).
29. Kovalchuk, I. et al. Transcriptome analysis reveals fundamental differences in plant response to acute and chronic exposure to ionizing radiation. *Mutation Research/Fundamental and Molecular Mechanisms of Mutagenesis* **624**, 101-113 (2007).
30. Van Hoeck, A. et al. *Lemna minor* plants chronically exposed to ionising radiation: RNA-seq analysis indicates a dose rate dependent shift from acclimation to survival strategies. *Plant Science* **257**, 84-95 (2017).
31. Hwang, S. et al. Identification of altered metabolic pathways of γ-irradiated rice mutant via network-based transcriptome analysis. *Genetica* **143**, 635-644 (2015).
32. Culligan, K. et al. ATR and ATM play both distinct and additive roles in response to ionizing radiation. *The Plant Journal* **48**, 947-961 (2006).
33. Peng, Y. et al. 'Fukusensor:' a genetically engineered plant for reporting DNA damage in response to gamma radiation. *Plant Biotechnol Journal* **12**, 1329-1332 (2014).
34. Sears, R. et al. Engineered gamma radiation phytosensors for environmental monitoring. *Plant Biotechnology Journal* **21**, 1745-1756 (2023).
35. Volkova, P. et al. Radiation hormesis in plants. *Current Opinion in Toxicology* **30**, 100334 (2022).
36. Kim, J. et al. Application of ionizing radiation as an elicitor to enhance the growth and metabolic activities in *Chlamydomonas reinhardtii. Frontiers in Plant Science* **14**, 1087070 (2023).
37. Sakata, K. et al. Roles of ROS and PKC-βII in ionizing radiation-induced eNOS activation in human vascular endothelial cells. *Vascular Pharmacology* **70**, 55-65 (2015).

38. Ren, J. et al. Physiological and morphological responses induced by α-particle radiation on *Arabidopsis thaliana* embryos. *Genetics and Molecular Research* **13**, 9569-9577 (2014).
39. Mittler, R. et al. Reactive oxygen species signalling in plant stress responses. *Nature Reviews Molecular Cell Biology* **23**, 663-679 (2022).
40. Murphy, M. et al. Guidelines for measuring reactive oxygen species and oxidative damage in cells and in vivo. *Nature Metabolism* **4**, 651–662 (2022).
41. Kristiansen, K. et al. Monitoring reactive oxygen species formation and localisation in living cells by use of the fluorescent probe CM-H_2DCFDA and confocal laser microscopy. *Physiologia Plantarum* **136**, 369-383 (2009).
42. Fichman, Y. et al. Whole-plant live imaging of reactive oxygen species. *Molecular Plant* **12**, 1203-1210 (2019).
43. Jones, A. Programmed cell death in development and defense. *Plant Physiology* **125**, 94-97 (2001).
44. Siles, E. et al. Apoptosis after gamma irradiation. Is it an important cell death modality? *British Journal of Cancer* **78**, 1594–1599 (1998).
45. Furukawa, T. et al. A shared DNA-damage-response pathway for induction of stem-cell death by UVB and by gamma radiation. *DNA Repair* **9**, 940-948 (2010).
46. Kim, J.. et al. Characterization of metabolic disturbances closely linked to the delayed senescence of Arabidopsis leaves after γ irradiation. *Environmental and Experimental Botany* **67**, 363-371 (2009).
47. Sekiguchi, F. et al. Radiation damage in shoot apical meristems of *Antirrhinum majus* and somatic mutations in regenerated buds. *Radiation Botany* **11**, 157-169 (1971).
48. Pham, G. et al. Construction of a chromosome-scale long-read reference genome assembly for potato. *GigaScience* **9**, giaa100 (2020).
49. Pandey, P. et al. Redox homeostasis via gene families of ascorbate-glutathione pathway. *Frontiers in Environmental Science* **3**, 25 (2015).
50. Yamane, K. et al. Transcription profiles of genes encoding catalase and ascorbate peroxidase in the ride leaf tissues under salinity. *Plant Production Science* **13**, 164-168 (2010).
51. Teixeira, F. et al. Analysis of the molecular evolutionary history of the ascorbate peroxidase gene family: Inferences from the rice genome. *Journal of Molecular Evolution* **59**, 761-770 (2004).
52. Ma, Y. et al. Effects of high temperature on activities and gene expression of enzymes involved in ascorbate-glutathione cycle in apple leaves. *Plant Science* **175**, 761-766 (2008).
53. Tao, D. et al. Active oxygen scavengers during cold acclimation of Scots Pine seedlings in relation to freezing tolerance. *Cryobiology* **37**, 38-45 (1998).
54. Kim, S. et al. Genome-wide transcriptome profiling of ROS scavenging and signal transduction pathways in rice (*Oryza sativa* L.) in response to different types of ionizing radiation. *Molecular Biology Reports* **39**, 11231-11248 (2012).
55. Cho, H. et al. Expression patterns of diverse genes in response to gamma irradiation in *Nicotiana tabacum*. *Journal of Plant Biology* **43**, 82-87 (2000).
56. van Ooijen, G. et al. Structure-function analysis of the NB-ARC domain of plant disease resistance proteins. *Journal of Experimental Botany* **59**, 1383-1397 (2008).

57. Vaghela, B. et al. Plant chitinases and their role in plant defense: A comprehensive review. *Enzyme and Microbial Technology* **159**, 110055 (2022).
58. Torres, M. et al, Reactive oxygen species signaling in response to pathogens. *Plant Physiology* **141**, 373-378 (2006).
59. Dickman, M. et al. Reassessing apoptosis in plants. *Nature Plants* **3**, 773-779 (2017).
60. Basak, S. & Kundu, P. Plant metacaspases: Decoding their dynamics in development and disease. *Plant Physiology and Biochemistry* **180**, 50-63 (2022).
61. Li, Y. et al. Aspartyl protease-mediated cleavage of BAG6 is necessary for autophagy and fungal resistance in plants. *The Plant Cell* **28**, 233-247 (2016).
62. Gu, L. et al. The Bcl-2-associated athanogene gene family in tobacco (*Nicotiana tabacum*) and the function of *NtBAG5* in leaf senescence. *Frontiers in Plant Science* **14**, 1108588 (2023).
63. Han, J. et al. The papain-like cysteine protease CEP1 is involved in programmed cell death and secondary wall thickening during xylem development in Arabidopsis. *Journal of Experimental Botany* **70**, 205-215 (2019).
64. Conesa, A. et al. A survey of best practices for RNA-seq data analysis. *Genome Biology* **17**, 13 (2016).
65. Ramel, F. et al. Carotenoid oxidation products are stress signals that mediate gene responses to singlet oxygen in plants. *Proceedings of the National Academy of Sciences* **109**, 5535-5540 (2012).
66. Eugeni Piller, L. et al. Role of plastoglobules in metabolite repair in the tocopherol redox cycle. *Frontiers in Plant Science* **5**, 298 (2014).
67. Jan, R. et al. Drought and UV radiation stress tolerance in rice is improved by overaccumulation of non-enzymatic antioxidant flavonoids. *Antioxidants (Basel)* **11**, 917 (2022).
68. Duan, L. et al. Biosynthesis and engineering of kaempferol in *Saccharomyces cerevisiae. Microbial Cell Factories* **16**, 165 (2017).
69. Li, Y. et al. Engineering tocopherol biosynthetic pathway in Arabidopsis leaves and its effect on antioxidant metabolism. *Plant Science* **178**, 312-320 (2010).
70. Yang, J. & Guo, L. Biosynthesis of β-carotene in engineered *E. coli* using the MEP and MVA pathways. *Microbial Cell Factories* **13**, 160 (2014).
71. Xiao, M. et al. The multiple roles of ascorbate in the abiotic stress response of plants: antioxidant, cofactor, and regulator. *Frontiers in Plant Science* **12**, 598173 (2021).
72. Tang, H. et al. Long-term space nutrition: A scoping review. *Nutrients* **14**, 194 (2021).
73. Møller, A. & Mousseau, T. Radiation levels affect pollen viability and germination among sites and species at Chernobyl. *International Journal of Plant Sciences* **178**, 537-545 (2017).
74. Arena, C. et al. Space radiation effects on plant and mammalian cells. *Acta Astronautica* **104**, 419-431 (2014).
75. Gehrke, F. et al. Nonhomologous end joining as key to CRISPR/Cas-mediated plant chromosome engineering. *Plant Physiology* **188**, 1769-1779 (2022).
76. Elledge, S. et al. DNA damage and cell cycle regulation of ribonucleotide reductase. *BioEssays* **15**, 333-339 (1993).
77. Song, J. et al. PARP2 is the predominant Poly(ADP-Ribose) Polymerase in Arabidopsis DNA damage and immune responses. *PLOS Genetics* **11**, e1005200 (2015).

78. Walker, J. et al. Structure of the Ku heterodimer bound to DNA and its implications for double-strand break repair. *Nature* **412**, 607-614 (2001).
79. Qian, J. et al. Interactional similarities and differences in the protein complex of PCNA and DNA replication factor C between rice and Arabidopsis. *BMC Plant Biology* **19**, 257 (2019).
80. Walley, J. et al. Arabidopsis deadenylases AtCAF1a and AtCAF1b play overlapping and distinct roles in mediating environmental stress responses. *Plant Physiology* **152**, 866-875 (2010).
81. Ogita, N. et al. Identifying the target genes of SUPPRESSOR OF GAMMA RESPONSE 1, a master transcription factor controlling DNA damage response in Arabidopsis. *The Plant Journal* **94**, 439-453 (2018).
82. McCarthy, D. & Medford, J. Quantitative and predictive genetic parts for plant synthetic biology. *Frontiers in Plant Science* **11**, 512526 (2020).
83. Chronis, D. et al. Potato transformation. *Bio-Protocol* **4**, e1017-e1017 (2014).
84. Joo, J. et al. Different signaling and cell death roles of Heterotrimeric G Protein α and β subunits in the Arabidopsis oxidative stress response to ozone. *The Plant Cell* **17**, 957-970 (2005).
85. Berrocal-Lobo, M. et al. Constitutive expression of ETHYLENE-RESPONSE-FACTOR1 in Arabidopsis confers resistance to several necrotrophic fungi. *The Plant Journal* **29**, 23-32 (2002).
86. Andrews, S. A quality control tool for high throughput sequence data. Open source. (Babraham Bioinformatics, Babraham Institute, Cambridge, United Kingdom, 2010).
87. Joshi, N. & Fass, J. sickle - A windowed adaptive trimming tool for FASTQ files using quality. Open source (2011).
88. Dobin, A. et al. STAR: ultrafast universal RNA-seq aligner. *Bioinformatics* **29**, 15-21 (2013).
89. Putri, G. et al. Analysing high-throughput sequencing data in Python with HTSeq 2.0. *Bioinformatics* **38**, 2943-2945 (2022).
90. Love, M. et al. Moderated estimation of fold change and dispersion for RNA-seq data with DESeq2. *Genome Biology* **15**, 550 (2014).
91. Tian, T. et al. agriGO v2.0: a GO analysis toolkit for the agricultural community, 2017 update. *Nucleic Acids Research* **45**, W122-W129 (2017).

Appendix

Table 4.1: Differentially expressed genes (DEGs) in response to low dose gamma radiation treatments.

Listed are the total number of significantly ($p_{adj} \leq 0.05$) differentially expressed potato loci in response to 0.5 – 5 Gray of gamma radiation compared to plants treated with 0 Gray. Total differentially expressed genes, as well as 'significantly' (> 4× fold change) upregulated and downregulated loci are shown.

	0.5 Gy	**1 Gy**	**2 Gy**	**4 Gy**	**5 Gy**
Total DEGs ($p_{adj} \leq 0.05$)	2949	1662	2558	5109	5889
Upregulated > 4×	290	135	207	765	1224
Downregulated > 4×	389	246	342	621	736

Table 4.2: Differential expression of loci annotated with terms related to key antioxidant proteins.

Listed are the number of loci annotated with a term relating to eight key antioxidant proteins in the monoploid potato DM 1-3 516 R44 (v6.1) reference genome. Additionally, the number of those differentially expressed in response to 5 Gray and the number of those that showed a greater than four-fold increase or decrease in transcript when compared to untreated plants are listed.

Annotation	# loci with annotation	# loci differentially expressed	# loci with > 4-fold increase, 5 Gy	# loci with > 4-fold decrease, 5 Gy
Ascorbate peroxidase	15	0	0	0
Glutathione reductase	1	0	0	0
Superoxide dismutase	25	2	0	0
Catalase	4	1	0	1
NADPH:quinone oxireductase	2	2	1	0
Thioredoxin	158	20	3	4
Glutaredoxin	27	2	0	0
Peroxiredoxin	6	2	0	1

Table 4.3: Differentially expressed genes in response to 5 Gray that are tagged with the plant-type hypersensitive response gene ontology term.
Listed are the potato loci that are significantly (padj < 0.05, > 4× fold change) upregulated or downregulated in response to 5 Gy that are associated with the plant-type hypersensitive response gene ontology term (GO:0009626). For each locus, the SpudDB and associated TAIR locus are shown, as well as mean adjusted transcript count at each treatment, the standard error of the mean (SE), and the padj for the 5 Gy treatment means comparison to the 0 Gy mean. The protein annotation from SpudDB is also listed.

SpudDB locus	Corresponding TAIR	0 Gy			5 Gy			Protein annotation
		mean	SE	p_{adj}	mean	SE	p_{adj}	
Soltu.DM.06G026420.1	AT3G48090	798.6	362.3	-	3666.4	433.7	0.001	alpha/beta-Hydrolases superfamily protein
Soltu.DM.06G026400.1	AT3G48090	1685.7	592.8	-	3337.7	563.5	0.020	alpha/beta-Hydrolases superfamily protein
Soltu.DM.10G017990.1	AT3G12500	170.1	67.8	-	864.3	93.8	0.000	basic chitinase
Soltu.DM.10G017970.1	AT3G12500	40.7	20.4	-	210.3	38.2	0.003	basic chitinase
Soltu.DM.02G005390.1	AT3G12500	87.9	44.4	-	384.6	56.3	0.002	basic chitinase
Soltu.DM.12G012040.1	AT1G73805	36.9	19.2	-	1161.6	640.5	0.000	Calmodulin binding protein-like
Soltu.DM.03G033680.1	AT1G73805	2046.9	898.1	-	10462.3	478.0	0.000	Calmodulin binding protein-like
Soltu.DM.02G022920.1	AT3G12500	334.4	172.4	-	1286.2	204.2	0.041	Chitinase family protein
Soltu.DM.03G004080.1	AT3G50930	34.8	18.7	-	834.7	106.6	0.000	cytochrome BC1 synthesis
Soltu.DM.03G003920.1	AT3G50930	40.1	24.2	-	275.1	46.8	0.000	cytochrome BC1 synthesis
Soltu.DM.10G002810.1	AT3G50930	580.8	266.0	-	2816.1	1014.7	0.003	cytochrome BC1 synthesis
Soltu.DM.04G009020.1	AT5G20480	6.1	3.8	-	63.4	11.0	0.000	EF-TU receptor
Soltu.DM.04G009650.1	AT5G20480	7.4	4.6	-	73.2	8.3	0.000	EF-TU receptor
Soltu.DM.04G008470.1	AT5G20480	2.4	1.6	-	14.9	1.8	0.021	EF-TU receptor
Soltu.DM.04G008370.1	AT5G20480	8.0	5.5	-	31.3	2.7	0.041	EF-TU receptor
Soltu.DM.04G027770.1	AT3G54420	63.0	36.3	-	496.1	12.1	0.000	homolog of carrot EP3-3 chitinase
Soltu.DM.02G016340.1	AT3G50460	21.8	15.6	-	150.8	37.5	0.003	homolog of RPW8
Soltu.DM.04G009510.1	AT5G20480	0.0	0.0	-	6.6	3.0	0.032	Leucine-rich repeat protein kinase family protein
Soltu.DM.04G009770.1	AT5G20480	3.3	1.7	-	50.4	8.1	0.000	Leucine-rich repeat protein kinase family protein
Soltu.DM.04G009570.1	AT5G20480	10.0	3.1	-	99.9	9.4	0.000	Leucine-rich repeat protein kinase family protein
Soltu.DM.07G005060.1	AT3G46530	0.0	0.0	-	9.3	1.6	0.014	NB-ARC domain-containing disease resistance protein
Soltu.DM.04G032470.1	AT3G46530	0.6	0.3	-	10.8	4.9	0.034	NB-ARC domain-containing disease resistance protein
Soltu.DM.04G005330.1	AT3G46530	34.8	18.0	-	306.5	16.1	0.000	NB-ARC domain-containing disease resistance protein
Soltu.DM.11G003490.1	AT3G07040	8.6	4.8	-	76.5	4.6	0.000	NB-ARC domain-containing disease resistance protein
Soltu.DM.07G017010.1	AT3G46530	50.8	25.4	-	228.6	46.7	0.000	NB-ARC domain-containing disease resistance protein
Soltu.DM.01G000440.1	AT3G46530	575.6	272.2	-	1901.1	61.5	0.020	NB-ARC domain-containing disease resistance protein
Soltu.DM.04G006280.1	AT3G46530	469.1	48.1	-	1351.0	188.2	0.000	NB-ARC domain-containing disease resistance protein
Soltu.DM.04G005400.1	AT3G46530	45.8	20.7	-	134.1	21.8	0.009	NB-ARC domain-containing disease resistance protein
Soltu.DM.04G005520.1	AT3G46530	48.2	24.4	-	134.7	22.0	0.009	NB-ARC domain-containing disease resistance protein
Soltu.DM.01G000450.1	AT3G46530	270.4	41.2	-	679.2	79.0	0.000	NB-ARC domain-containing disease resistance protein
Soltu.DM.10G004030.1	AT3G46530	816.6	255.6	-	1937.6	111.2	0.001	NB-ARC domain-containing disease resistance protein
Soltu.DM.11G007350.1	AT3G46530	60.7	30.4	-	153.9	27.9	0.047	NB-ARC domain-containing disease resistance protein
Soltu.DM.04G005340.1	AT3G46530	45.2	20.5	-	121.0	2.2	0.003	NB-ARC domain-containing disease resistance protein
Soltu.DM.04G005740.1	AT3G46530	47.3	24.3	-	122.5	16.5	0.023	NB-ARC domain-containing disease resistance protein
Soltu.DM.04G006490.1	AT3G46530	47.9	24.1	-	120.5	21.9	0.049	NB-ARC domain-containing disease resistance protein
Soltu.DM.04G004920.1	AT3G46530	24.5	12.8	-	63.2	6.4	0.036	NB-ARC domain-containing disease resistance protein
Soltu.DM.09G029500.1	AT3G46530	443.2	72.3	-	948.0	51.5	0.000	NB-ARC domain-containing disease resistance protein
Soltu.DM.04G006380.1	AT3G46530	144.8	57.1	-	314.6	5.2	0.020	NB-ARC domain-containing disease resistance protein
Soltu.DM.09G029550.1	AT3G46530	215.5	31.7	-	382.8	21.8	0.000	NB-ARC domain-containing disease resistance protein
Soltu.DM.09G010500.1	AT3G46530	178.4	15.0	-	293.9	12.8	0.014	NB-ARC domain-containing disease resistance protein
Soltu.DM.04G006310.1	AT3G46530	175.9	33.6	-	294.2	32.5	0.011	NB-ARC domain-containing disease resistance protein
Soltu.DM.02G013420.1	AT3G07040	365.4	21.5	-	568.1	27.8	0.000	NB-ARC domain-containing disease resistance protein
Soltu.DM.02G029230.1	AT2G26560	1048.8	147.2	-	2330.9	114.2	0.003	PATATIN-like protein
Soltu.DM.04G034160.1	AT2G26560	0.9	0.9	-	17.3	6.6	0.007	phospholipase A 2A
Soltu.DM.01G002670.1	AT3G11820	776.6	145.6	-	4090.7	238.1	0.000	syntaxin of plants

Table 4.4: Differential expression of loci annotated with terms related to key programmed cell death proteins.

Listed are the number of loci annotated with a term relating to four key antioxidant proteins in the monoploid potato DM 1-3 516 R44 (v6.1) reference genome. Additionally, the number of those differentially expressed in response to 5 Gray and the number of those that showed a greater than four-fold increase or decrease in transcript when compared to untreated plants are listed.

Annotation	# loci with annotation	# loci differentially expressed	# loci with > 4-fold increase, 5 Gy	# loci with > 4-fold decrease, 5 Gy
Metacaspase	10	1	1	0
Aspartyl protease	120	19	7	2
BCL-2-associated athanogene	13	4	0	1
Papain-like cysteine proteases	6	1	0	1

Table 4.5: Differentially expressed genes in response to 0.5 Gray that are tagged with the thylakoid membrane gene ontology term.

Listed are the potato loci that are significantly (p_{adj} < 0.05, > 4× fold change) upregulated or downregulated in response to 0.5 Gy that are associated with the thylakoid membrane gene ontology term (GO:0042651)**.** For each locus, the SpudDB and associated TAIR locus are shown, as well as mean adjusted transcript count at each treatment, the standard error of the mean (SE), and the p_{adj} for the 0.5 Gy treatment means comparison to the 0 Gy mean. The protein annotation from SpudDB is also listed.

SpudDB locus	Corresponding TAIR	0 Gy			0.5 Gy			Protein annotation
		$mean_{adj}$	SE	p_{adj}	$mean_{adj}$	SE	p_{adj}	
Soltu.DM.03G000850.1	AT1G29930	186.9	49.4	-	908.6	37.4	1.05E-06	chlorophyll A/B binding protein
Soltu.DM.03G029150.1	AT2G01918	5.5	3.2	-	57.0	14.8	4.16E-04	PsbQ-like
Soltu.DM.12G026740.1	AT2G10940	1835.0	912.9	-	15975.4	8355.8	1.31E-02	Bifunctional inhibitor/lipid-transfer protein/seed storage 2S albumin superfamily protein
Soltu.DM.01G023770.1	AT5G35630	3699.0	863.6	-	20713.4	1410.9	4.30E-08	glutamine synthetase
Soltu.DM.07G013280.1	AT3G26060	428.3	111.8	-	2577.1	376.2	3.35E-06	Thioredoxin superfamily protein
Soltu.DM.08G012190.1	AT2G26340	13.4	13.0	-	0.9	0.5	1.03E-01	conserved hypothetical protein
Soltu.DM.09G025620.1	AT5G43750	669.8	274.3	-	3315.0	279.3	1.93E-04	NAD(P)H dehydrogenase
Soltu.DM.11G007970.1	AT1G74880	0.0	0.0	-	7.1	2.2	8.17E-03	NAD(P)H:plastoquinone dehydrogenase complex subunit O
Soltu.DM.02G023800.1	AT1G20020	10134.4	4003.8	-	40616.3	1143.7	8.22E-04	ferredoxin-NADP(+)-oxidoreductase
Soltu.DM.05G016330.1	ATCG00270	933.5	826.7	-	137.6	13.6	NA	photosystem II reaction center protein D
Soltu.DM.01G009170.5	AT1G14345	766.7	580.2	-	151.0	50.1	1.54E-02	NAD(P)-linked oxidoreductase superfamily protein
Soltu.DM.03G028740.1	AT1G73990	171.9	141.3	-	30.5	6.5	1.88E-02	signal peptide peptidase
Soltu.DM.11G020460.4	AT2G28800	1805.3	1035.6	-	432.4	75.7	1.81E-03	63 kDa inner membrane family protein
Soltu.DM.06G033400.3	AT4G27990	152.6	118.2	-	36.5	12.1	3.84E-02	YGGT family protein
Soltu.DM.04G022190.1	AT4G39710	136.0	91.4	-	1019.9	91.8	4.74E-03	FK506-binding protein 16-2
Soltu.DM.02G025940.2	AT1G67080	0.0	0.0	-	11.8	3.6	6.61E-03	abscisic acid (aba)-deficient
Soltu.DM.12G004790.1	AT1G42970	2675.1	245.8	-	14195.6	915.1	1.54E-09	glyceraldehyde-3-phosphate dehydrogenase B subunit
Soltu.DM.03G012630.1	AT4G39730	1899.2	1499.6	-	174.1	13.0	5.95E-04	Lipase/lipooxygenase, PLAT/LH2 family protein
Soltu.DM.01G002140.1	AT3G45140	1647.3	262.0	-	9981.8	1452.1	1.85E-06	lipoxygenase
Soltu.DM.01G010270.1	ATCG01110	291.2	254.2	-	58.5	1.0	4.00E-02	NAD(P)H dehydrogenase subunit H
Soltu.DM.07G002690.1	AT2G47910	90.9	48.7	-	485.1	45.0	4.29E-03	chlororespiratory reduction
Soltu.DM.12G026250.1	AT1G19150	0.3	0.3	-	9.2	2.3	2.06E-02	photosystem I light harvesting complex gene
Soltu.DM.06G017440.1	AT1G44575	1883.1	292.4	-	8486.4	1352.9	7.56E-06	Chlorophyll A-B binding family protein
Soltu.DM.01G004980.1	AT1G51400	0.3	0.3	-	8.0	2.5	2.09E-02	Photosystem II 5 kD protein
Soltu.DM.10G000060.1	AT2G46820	12.1	6.7	-	86.8	25.5	7.45E-04	photosystem I P subunit

Table 4.6: The top twenty upregulated and downregulated potato loci for future low dose gamma radiation phytosensors.
The top twenty **(A)** upregulated and **(B)** downregulated potato loci for the development of low dose gamma radiation phytosensors. Loci were selected based on having high inducibility and a range of basal and induced transcript counts to accommodate many future designs.

A

		0 Gy			0.5 Gy			1 Gy			2 Gy			4 Gy			5 Gy		
Sequence ID	**SpudDB annotation**	**$mean_{adj}$**	**SE**	**p_{adj}**	**$mean_{adj}$**	**SE**	**p_{adj}**	**$mean_{adj}$**	**SE**	**p_{adj}**	**$mean_{adj}$**	**SE**	**p_{adj}**	**$mean_{adj}$**	**SE**	**p_{adj}**	**$mean_{adj}$**	**SE**	**p_{adj}**
Soltu.DM.07G013480.1	cytochrome P450, family 716, subfamily A, polypeptide	0.0	0.0	-	0.0	0.0	1.000	0.6	0.6	0.751	0.6	0.6	0.727	37.8	24.0	0.000	74.0	13.8	0.000
Soltu.DM.03G021200.1	response to low sulfur	0.0	0.0	-	16.3	9.5	0.002	3.9	2.0	0.078	10.0	1.4	0.006	40.1	17.2	0.000	87.4	23.5	0.000
Soltu.DM.08G019390.2	poly(ADP-ribose) polymerase	0.0	0.0	-	0.0	0.0	1.000	4.9	1.6	0.027	14.6	1.3	0.000	71.0	8.1	0.000	108.2	22.7	0.000
Soltu.DM.08G019980.1	basic helix-loop-helix (bHLH) DNA-binding superfamily protein	0.0	0.0	-	1.4	1.0	0.252	1.2	0.3	0.369	8.6	2.2	0.003	61.2	7.2	0.000	113.7	16.2	0.000
Soltu.DM.03G016280.1	Protein phosphatase 2C family protein	0.3	0.3	-	1.3	0.6	0.659	5.2	1.8	0.140	6.8	2.3	0.074	45.4	23.8	0.000	205.0	44.2	0.000
Soltu.DM.09G001000.1	arogenate dehydrogenase	0.6	0.6	-	8.9	3.3	0.068	0.6	0.6	0.859	1.5	1.5	0.748	49.4	22.2	0.000	276.8	62.9	0.000
Soltu.DM.09G003140.1	Nucleic acid-binding, OB-fold-like protein	0.6	0.6	-	16.7	2.9	0.001	40.5	5.4	0.000	147.5	36.7	0.000	548.4	55.2	0.000	892.2	6.2	0.000
Soltu.DM.03G022860.1	WRKY family transcription factor	0.9	0.9	-	23.9	21.1	0.019	2.5	1.7	0.684	2.8	0.5	0.613	89.2	38.9	0.000	370.4	9.5	0.000
Soltu.DM.04G022220.1	Heavy metal transport/detoxification superfamily protein	1.5	1.5	-	10.1	2.5	0.080	4.7	0.7	0.468	9.1	2.7	0.115	94.5	48.2	0.000	362.2	87.7	0.000
Soltu.DM.11G007980.2	DNA repair metallo-beta-lactamase family protein	1.8	1.0	-	35.4	4.5	0.000	99.0	19.3	0.000	238.8	14.7	0.000	655.6	27.0	0.000	625.5	93.0	0.000
Soltu.DM.01G000070.1	Endomembrane protein 70 protein family	13.6	8.3	-	63.5	22.0	0.005	296.0	31.7	0.000	1372.7	274.0	0.000	3596.7	594.7	0.000	5937.1	452.9	0.000
Soltu.DM.05G011490.1	P-loop containing nucleoside triphosphate hydrolases superfamily protein	13.6	7.1	-	86.6	12.9	0.000	857.4	112.2	0.000	6630.5	588.7	0.000	40591.8	7233.6	0.000	70720.4	6055.8	0.000
Soltu.DM.07G006410.1	RAS associated with diabetes protein	24.2	12.3	-	128.8	2.2	0.000	354.8	56.9	0.000	1333.1	128.8	0.000	3589.3	350.9	0.000	5544.1	316.2	0.000
Soltu.DM.08G019390.1	poly(ADP-ribose) polymerase	25.0	3.8	-	231.3	41.5	0.000	674.6	28.1	0.000	3190.0	286.6	0.000	12054.4	992.0	0.000	20110.8	2362.1	0.000
Soltu.DM.04G021100.1	homolog of RAD54	38.3	19.2	-	211.9	18.7	0.000	282.4	21.7	0.000	652.2	16.1	0.000	1460.4	93.8	0.000	1777.1	99.1	0.000
Soltu.DM.02G034230.1	Ferritin/ribonucleotide reductase-like family protein	47.1	25.7	-	510.7	55.0	0.000	1146.8	177.9	0.000	6385.2	738.8	0.000	39209.6	2855.5	0.000	57765.9	3963.0	0.000
Soltu.DM.05G002860.1	Arabidopsis Hop2 homolog	88.4	15.8	-	213.3	2.5	0.000	357.9	12.8	0.000	821.1	13.8	0.000	2648.7	162.5	0.000	3940.8	200.5	0.000
Soltu.DM.01G031990.1	Ku80 family protein	254.8	27.0	-	1017.3	61.6	0.000	1912.9	118.1	0.000	5074.5	311.0	0.000	10572.2	274.8	0.000	12909.9	255.4	0.000
Soltu.DM.02G026430.1	DNA LIGASE	1245.1	38.9	-	1638.7	53.0	0.001	1945.4	59.4	0.000	2461.5	83.3	0.000	3209.5	32.8	0.000	3517.9	96.5	0.000

B

		0 Gy			0.5 Gy			1 Gy			2 Gy			4 Gy			5 Gy		
Sequence ID	**SpudDB annotation**	**$mean_{adj}$**	**SE**	**p_{adj}**	**$mean_{adj}$**	**SE**	**p_{adj}**	**$mean_{adj}$**	**SE**	**p_{adj}**	**$mean_{adj}$**	**SE**	**p_{adj}**	**$mean_{adj}$**	**SE**	**p_{adj}**	**$mean_{adj}$**	**SE**	**p_{adj}**
Soltu.DM.06G025070.1	conserved hypothetical protein	68224.7	34352.8	-	23426.1	354.0	0.006	28192.6	624.9	0.035	19662.1	840.6	0.001	12741.2	1156.7	0.000	11534.7	1407.6	0.000
Soltu.DM.03G025030.1	MA3 domain-containing protein	25783.7	7345.3	-	11510.6	2370.4	0.014	19488.0	3859.4	0.507	11631.6	802.3	0.016	5944.2	634.2	0.000	4689.9	206.0	0.000
Soltu.DM.07G027590.1	Cwf15 / Cwc15 cell cycle control family protein	24924.7	7271.2	-	9813.0	1988.8	0.003	15245.3	2410.6	0.181	10387.5	490.7	0.005	4980.0	599.0	0.000	4286.4	289.1	0.000
Soltu.DM.03G015520.1	Plant invertase/pectin methylesterase inhibitor superfamily protein	15031.5	5626.7	-	6025.6	1376.2	0.030	10747.3	2164.0	0.532	9467.7	770.6	0.344	4036.9	950.3	0.000	2242.0	88.0	0.000
Soltu.DM.04G022420.1	conserved hypothetical protein	12741.9	6637.0	-	3375.1	802.3	0.010	7840.1	1709.8	0.465	4406.7	410.9	0.050	1157.1	402.7	0.000	776.3	105.3	0.000
Soltu.DM.05G019450.1	myb domain protein	4098.9	508.5	-	2465.9	212.0	0.022	2215.1	145.5	0.007	1603.4	160.2	0.000	722.5	71.6	0.000	561.2	75.8	0.000
Soltu.DM.03G012690.1	Lipase/lipooxygenase, PLAT/LH2 family protein	2148.1	1910.6	-	40.1	13.2	0.007	139.0	64.1	0.101	68.3	58.5	0.024	15.0	10.0	0.000	1.2	0.9	0.000
Soltu.DM.07G013810.1	cell wall-plasma membrane linker protein	2068.8	136.1	-	862.1	102.5	0.039	1513.2	342.7	0.562	1183.7	427.5	0.237	434.9	48.8	0.000	369.6	114.3	0.000
Soltu.DM.03G006490.1	TRICHOME BIREFRINGENCE-LIKE	1921.8	897.0	-	665.3	75.5	0.013	1279.3	303.2	0.456	784.9	48.9	0.043	440.7	59.3	0.000	294.4	45.9	0.000
Soltu.DM.03G012580.1	RNI-like superfamily protein	609.0	266.1	-	585.4	160.0	0.949	894.3	245.1	0.570	414.2	96.5	0.535	139.3	36.8	0.001	88.6	11.2	0.000
Soltu.DM.06G022900.1	myo-inositol oxygenase	505.0	119.2	-	500.0	277.1	0.993	1070.9	222.4	0.374	445.8	98.1	0.895	99.3	42.6	0.010	35.2	14.2	0.000
Soltu.DM.03G034470.1	gibberellin 3-oxidase	281.6	67.4	-	369.3	100.9	0.664	212.7	68.3	0.688	181.4	33.0	0.491	56.3	22.3	0.001	12.2	3.5	0.000
Soltu.DM.10G027420.1	Protein of unknown function DUF92, transmembrane	225.1	68.8	-	75.1	7.9	0.016	95.7	16.7	0.090	99.5	10.4	0.094	41.2	9.5	0.000	33.7	14.2	0.000
Soltu.DM.02G022960.1	basic chitinase	165.7	30.9	-	179.1	90.3	0.945	67.6	36.6	0.411	91.4	72.8	0.578	50.4	18.6	0.175	32.2	6.8	0.046
Soltu.DM.07G017280.1	Terpenoid cyclases/Protein prenyltransferases superfamily protein	93.4	47.4	-	95.7	27.5	0.995	51.2	36.1	0.781	22.4	11.1	0.471	5.5	2.9	0.081	2.9	2.4	0.025
Soltu.DM.04G019370.1	LOB domain-containing protein	83.5	21.5	-	38.2	9.4	0.353	39.2	12.8	0.406	16.5	9.0	0.031	4.4	2.2	0.000	1.8	1.0	0.000
Soltu.DM.05G002140.1	RING/U-box superfamily protein	81.2	12.6	-	85.9	29.3	0.944	46.7	15.2	0.452	15.4	5.2	0.005	14.3	5.7	0.001	3.6	1.0	0.000
Soltu.DM.12G022190.1	Auxin-responsive GH3 family protein	74.2	46.6	-	87.8	33.6	0.912	81.1	21.9	0.958	15.9	9.3	0.170	13.9	5.1	0.095	4.5	3.6	0.003
Soltu.DM.02G008230.1	PATATIN-like protein	72.4	14.3	-	16.4	9.8	0.215	184.5	129.4	0.490	34.3	25.6	0.576	0.8	0.5	0.000	9.5	3.9	0.050
Soltu.DM.04G036930.1	Subtilisin-like serine endopeptidase family protein	34.7	17.4	-	56.9	15.4	0.561	31.6	7.2	0.817	7.3	1.0	0.008	6.7	1.8	0.002	2.7	0.1	0.000

Table 4.7: Gamma radiation treatments used in the study.
Relationship of various radiation metrics and distance from source follows. The intended absorbed dose in Gray, the required dose rate to meet the total dose in a given amount of time (rad / sec), and the calculated distance from the source to receive the desired rate are listed.

Treatment (Gray)	Total Rad	Treatment rate (rad / second)	Distance from source (meters)
0	0	-	-
0.5	50	0.0023	5.581
1	100	0.0046	4.143
2	200	0.0093	3.075
4	400	0.0185	2.283
5	500	0.0231	2.074

Table 4.8: Normalization factors for transcript count calculated based on the relative number of transcripts successfully mapped for each RNAseq sample

Sample	Normalization factor
0 Gy replicate 1	0.228854045
0 Gy replicate 2	1.074587469
0 Gy replicate 3	1.120211908
0.5 Gy replicate 1	1.090631599
0.5 Gy replicate 2	1.02513711
0.5 Gy replicate 3	1.194398812
1 Gy replicate 1	1.025528238
1 Gy replicate 2	1.129778825
1 Gy replicate 3	1.063545982
2 Gy replicate 1	1.10938248
2 Gy replicate 2	1.006789171
2 Gy replicate 3	1.050801927
4 Gy replicate 1	1.118942091
4 Gy replicate 2	1.216257409
4 Gy replicate 3	1.195472476
5 Gy replicate 1	1.116321877
5 Gy replicate 2	1.037741725
5 Gy replicate 3	1.180743394

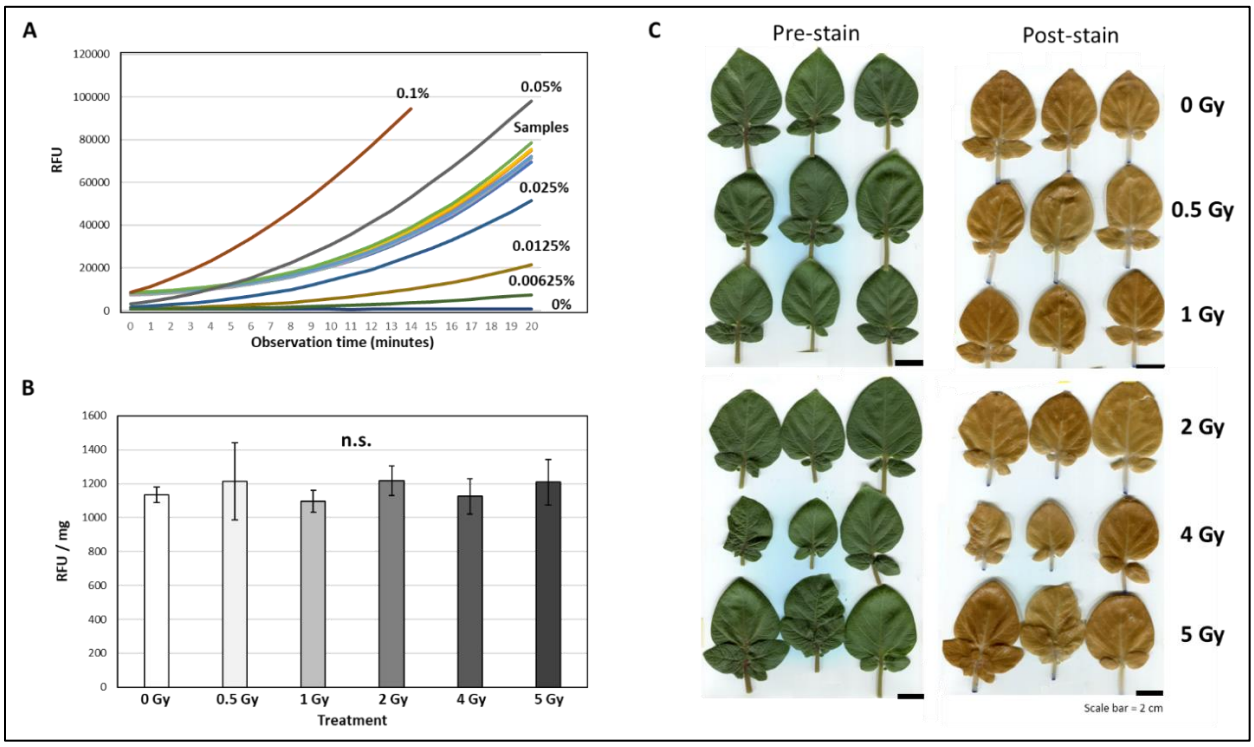

Figure 4.1: H_2DCFDA fluorescence and trypan blue staining of potato leaves after low dose gamma radiation treatment.

(A) Fluorescence curves of potato leaf extracts and a hydrogen peroxide standard treated with through 2',7'-dichlorodihydrofluorescein diacetate (H_2DCFDA**)** over a twenty-minute observation time course. Mean relative fluorescence units (RFU) of three biological replicates and four technical replicates are plotted (excitation: 485 nm, emission 528 nm). **(B)** Mean relative fluorescence units of the leaf tissue treated with 0 – 5 Gy of radiation at the twentieth observation in the time course with pre- H_2DCFDA fluorescence in this range subtracted from each well and normalized to the weight of each tissue sample (RFU / mg). Data represents mean ± standard error of three biological and four technical replicates. Data were analyzed using ANOVA ($p < 0.05$), no significant effect of gamma radiation treatment on RFU / mg was detected (denoted with "n.s." **(C)** Trypan blue staining of mature potato leaves seventy-two hours post-treatment. Leaves are shown pre-stain to show any pre-stain wounding. Post-stain images show negligible trypan blue staining so stained leaf area measurements were not pursued.

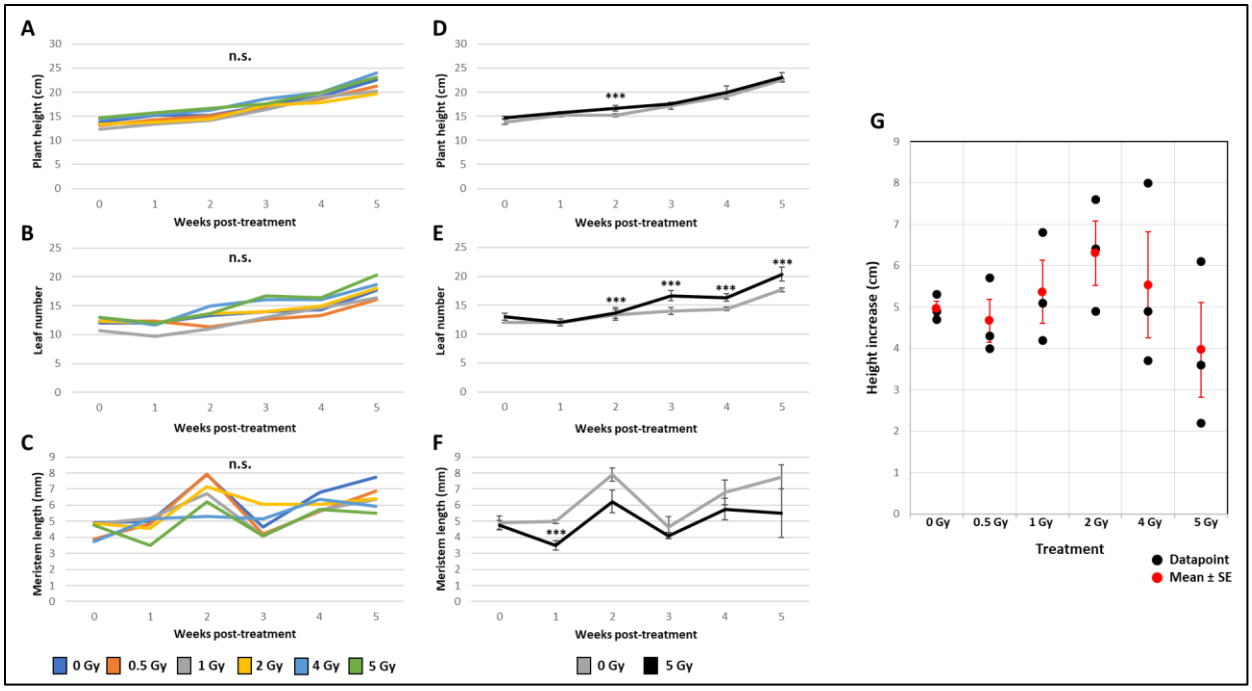

Figure 4.2: Plant aboveground phenotype five weeks after low dose gamma radiation treatment.

(A-C) Mean aboveground phenotypic data taken each week, starting with the week of treatment (week 0). Plant height **(A)**, leaf number **(B)**, and meristem length (**C)** data are displayed as the mean of three biological replicates over six weeks. Significant effect of treatment and mean comparison was conducted with ANOVA ($p < 0.05$) with a post-hoc Dunnett's test ($p < 0.05$) using 0 Gy as the control group. Significant difference from 0 Gy was not detected at any timepoint, denoted by "n.s." **(D-F)** Mean aboveground phenotypic data from only 0 Gy and 5 Gy treated plants. Plant height **(D)**, leaf number **(E)**, and meristem length (**F)** data are displayed as the mean ± standard error of the mean of three biological replicates over six weeks. Significant effect of treatment and mean comparison was conducted with a student's t test ($p < 0.05$), with significant difference from 0 Gy indicated with "***". **(G)** Height increase of all plants at three weeks post-treatment compared to plant height measured before treatment. Individual plant height increases denoted with black dots, while the mean and standard error for each treatment are shown in red.

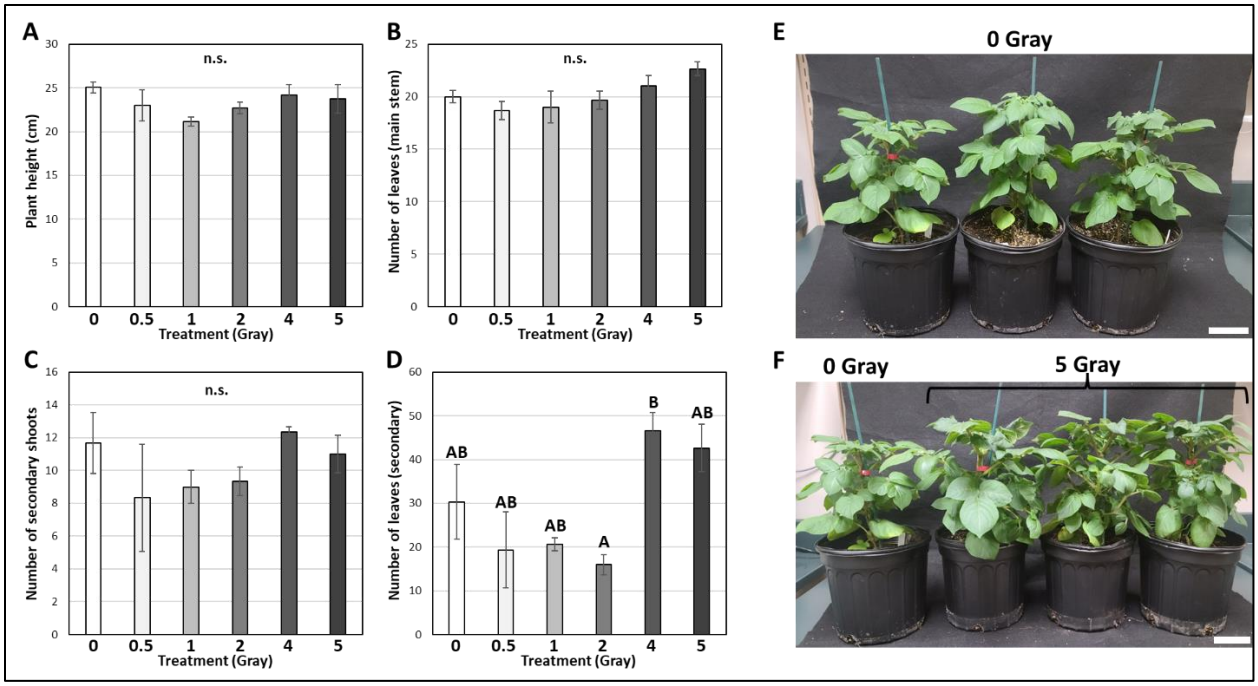

Figure 4.3: Plant aboveground structure six weeks after low dose gamma radiation treatment.

(A-D) Aboveground structure measurements of wild type potato plants irradiated with 0 – 5 Gy six weeks after treatment. Measurements include plant height **(A)**, number of leaves attached to the main stem of the plant **(B)**, number of emerged secondary shoots **(C)**, and number of leaves attached to the emerged secondary shoots **(D)**. Values represent the mean ± standard error of the mean of three biological replicates per treatment. **(E,F)** Images of plants treated with 0 Gray **(E)** and 5 Gray **(F)** six weeks after treatment. Scale bars = 10 cm.

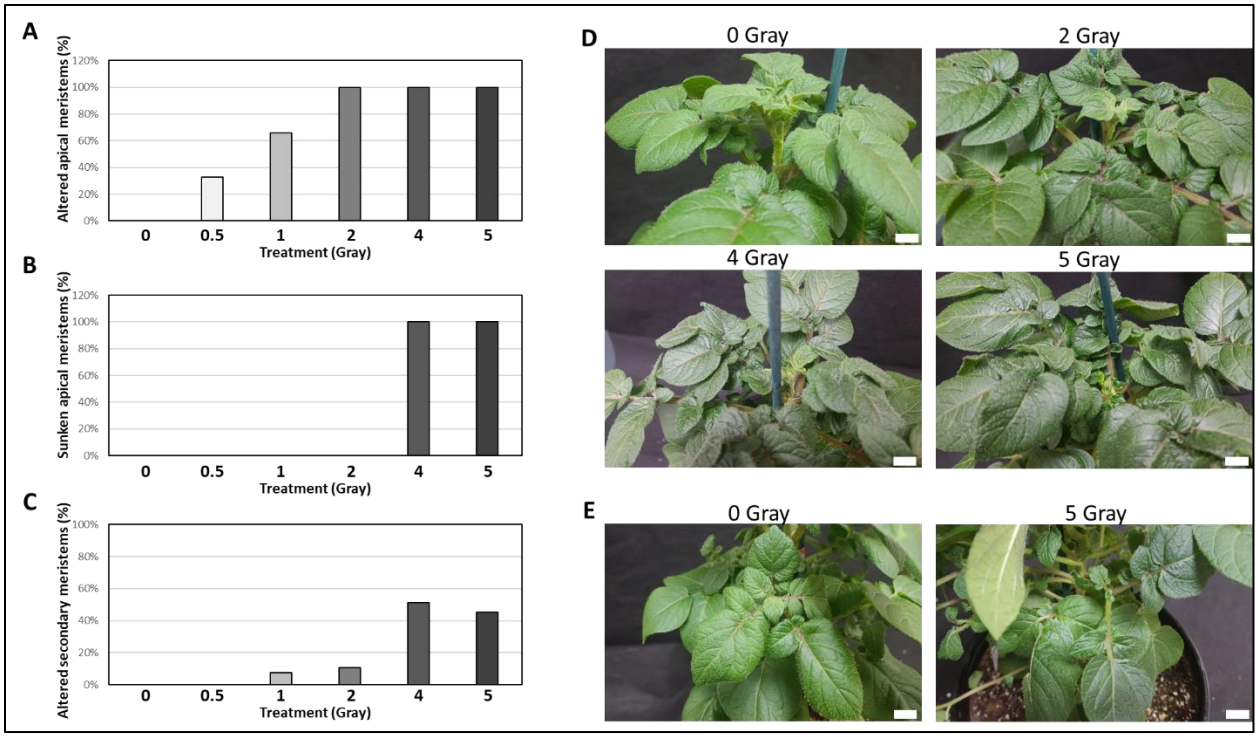

Figure 4.4: Apical and secondary meristem phenotypes six weeks after low dose gamma radiation treatment.

(A-E) Altered meristem phenotypes in three potato plants treated with 0 – 5 Gray of ionizing radiation. **(A)** Percentage of apical meristems an altered phenotype associated with a temporary pause or loss of apical dominance. **(B)** Percentage of apical meristems exhibit a 'sunken' phenotype, where dominance of the apical meristem has been completely lost. **(C)** Percentage of secondary meristems that exhibit the same altered phenotypes as seen in apical meristems. **(D)** Images of meristem structure in plants treated with 0, 2, 4, or 5 Gray. The 0 Gray plant represents a normal meristem structure, while the 2 Gray represents an altered phenotype. Images of the 4 Gray and 5 Gray plants show a 'sunken' meristem phenotype. **(E)** Images of secondary meristems, with the 0 Gray image representing a normal secondary meristem and the 5 Gray image representing an altered meristem phenotype. Scale bars = 1 cm.

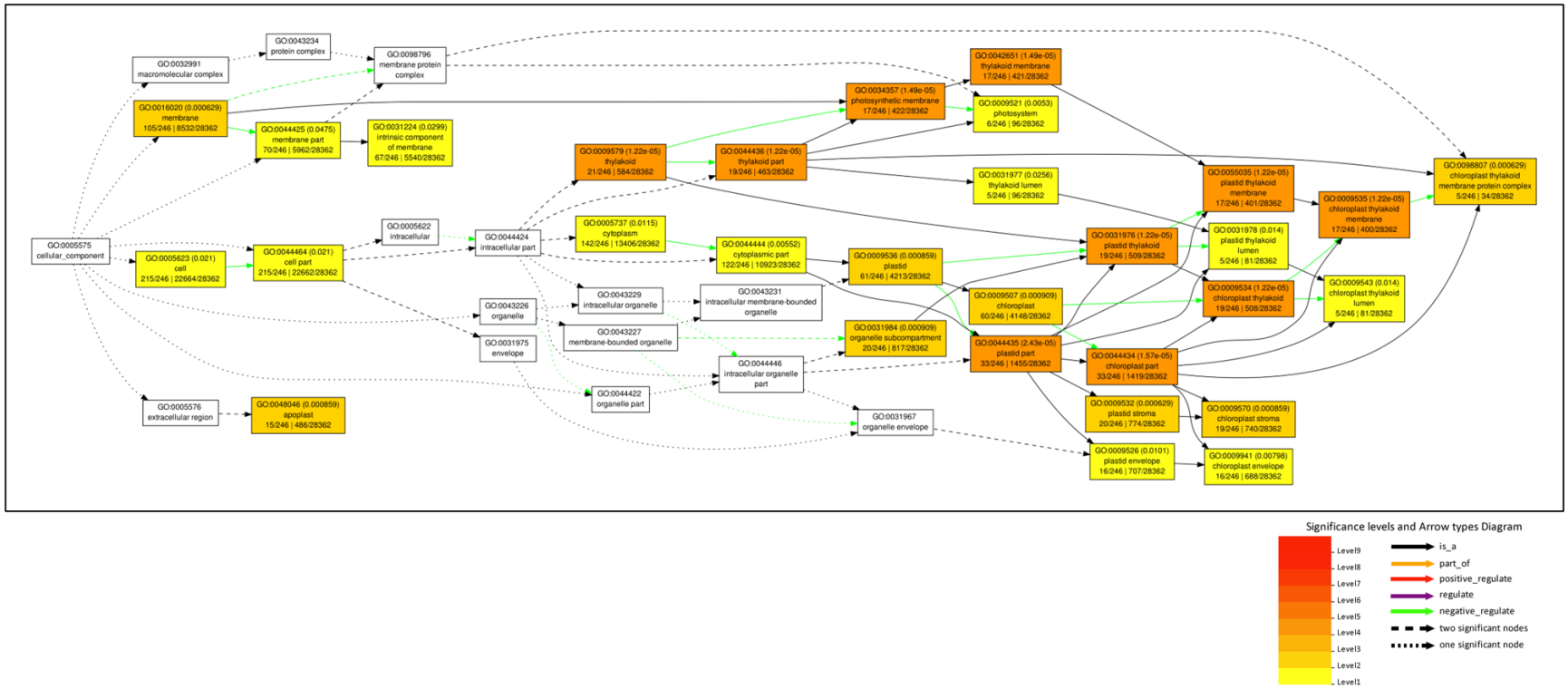

Figure 4.5: Significantly enriched cellular compartment gene ontology terms in potato loci that are upregulated > 4× in response to 0.5 Gy treatment.

Data shown include the gene ontology code, its associated false discovery rate for this analysis in parentheses, the name of the gene ontology code, the number of loci with the GO term / total number of loci in the dataset (bottom left), and the number of loci with this GO term in the *Arabidopsis thaliana* genome / total number of loci in the *A. thaliana* genome. Note that potato loci were converted to *A. thaliana* loci using the resources associated with the doubled monoploid potato DM 1-3 516 R44 (v6.1) reference genome (see methods).

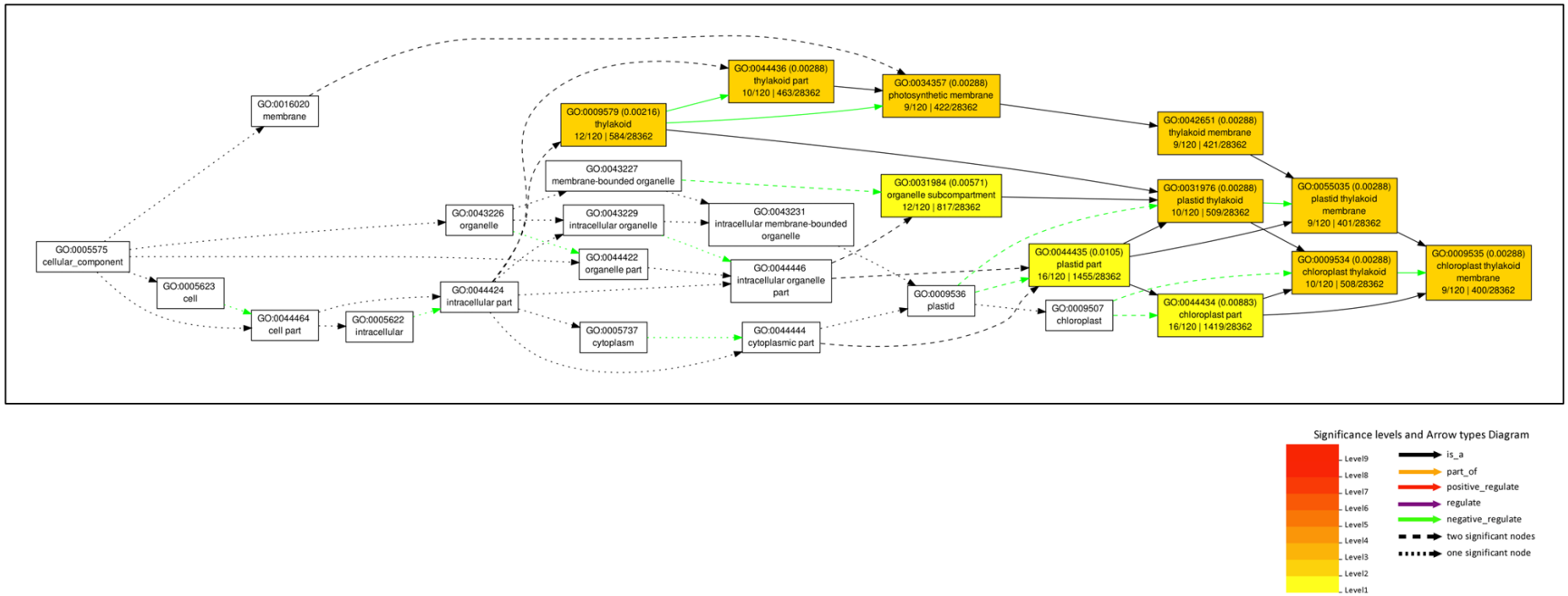

Figure 4.6: Significantly enriched cellular compartment gene ontology terms in potato loci that are upregulated > 4× in response to 1 Gy treatment.

Data shown include the gene ontology code, its associated false discovery rate for this analysis in parentheses, the name of the gene ontology code, the number of loci with the GO term / total number of loci in the dataset (bottom left), and the number of loci with this GO term in the *Arabidopsis thaliana* genome / total number of loci in the *A. thaliana* genome. Note that potato loci were converted to *A. thaliana* loci using the resources associated with the doubled monoploid potato DM 1-3 516 R44 (v6.1) reference genome (see methods).

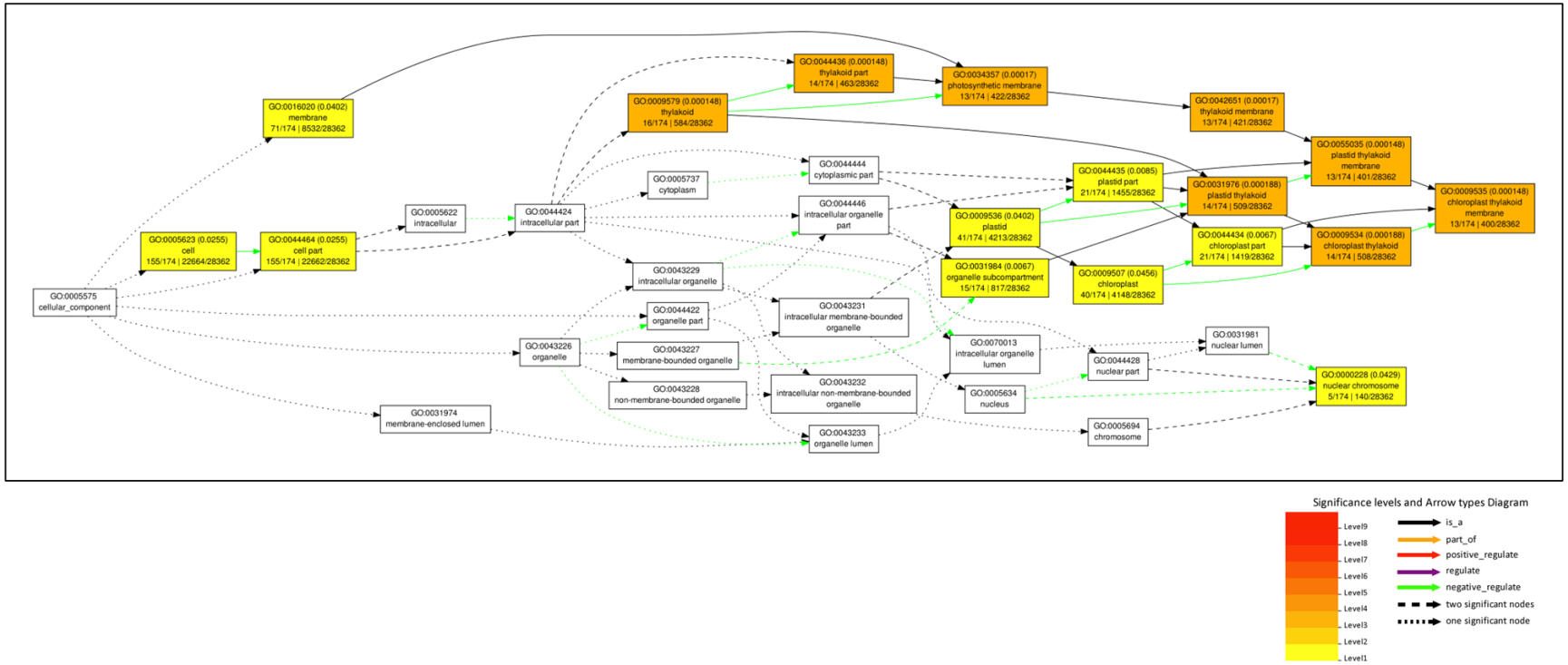

Figure 4.7: Significantly enriched cellular compartment gene ontology terms in potato loci that are upregulated > 4× in response to 2 Gy treatment.

Data shown include the gene ontology code, its associated false discovery rate for this analysis in parentheses, the name of the gene ontology code, the number of loci with the GO term / total number of loci in the dataset (bottom left), and the number of loci with this GO term in the *Arabidopsis thaliana* genome / total number of loci in the *A. thaliana* genome. Note that potato loci were converted to *A. thaliana* loci using the resources associated with the doubled monoploid potato DM 1-3 516 R44 (v6.1) reference genome (see methods).

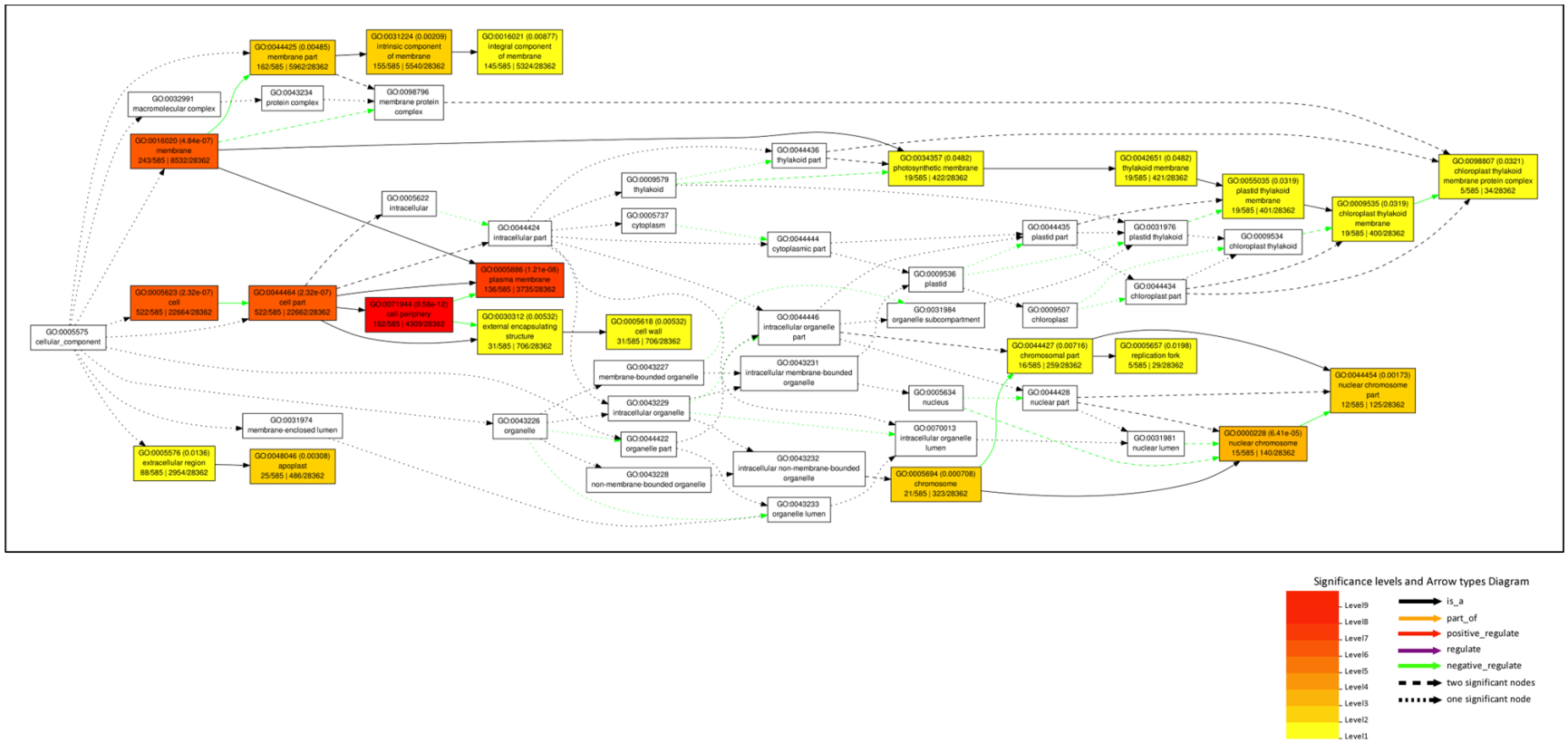

Figure 4.8: Significantly enriched cellular compartment gene ontology terms in potato loci that are upregulated > 4× in response to 4 Gy treatment.

Data shown include the gene ontology code, its associated false discovery rate for this analysis in parentheses, the name of the gene ontology code, the number of loci with the GO term / total number of loci in the dataset (bottom left), and the number of loci with this GO term in the *Arabidopsis thaliana* genome / total number of loci in the *A. thaliana* genome. Note that potato loci were converted to *A. thaliana* loci using the resources associated with the doubled monoploid potato DM 1-3 516 R44 (v6.1) reference genome (see methods).

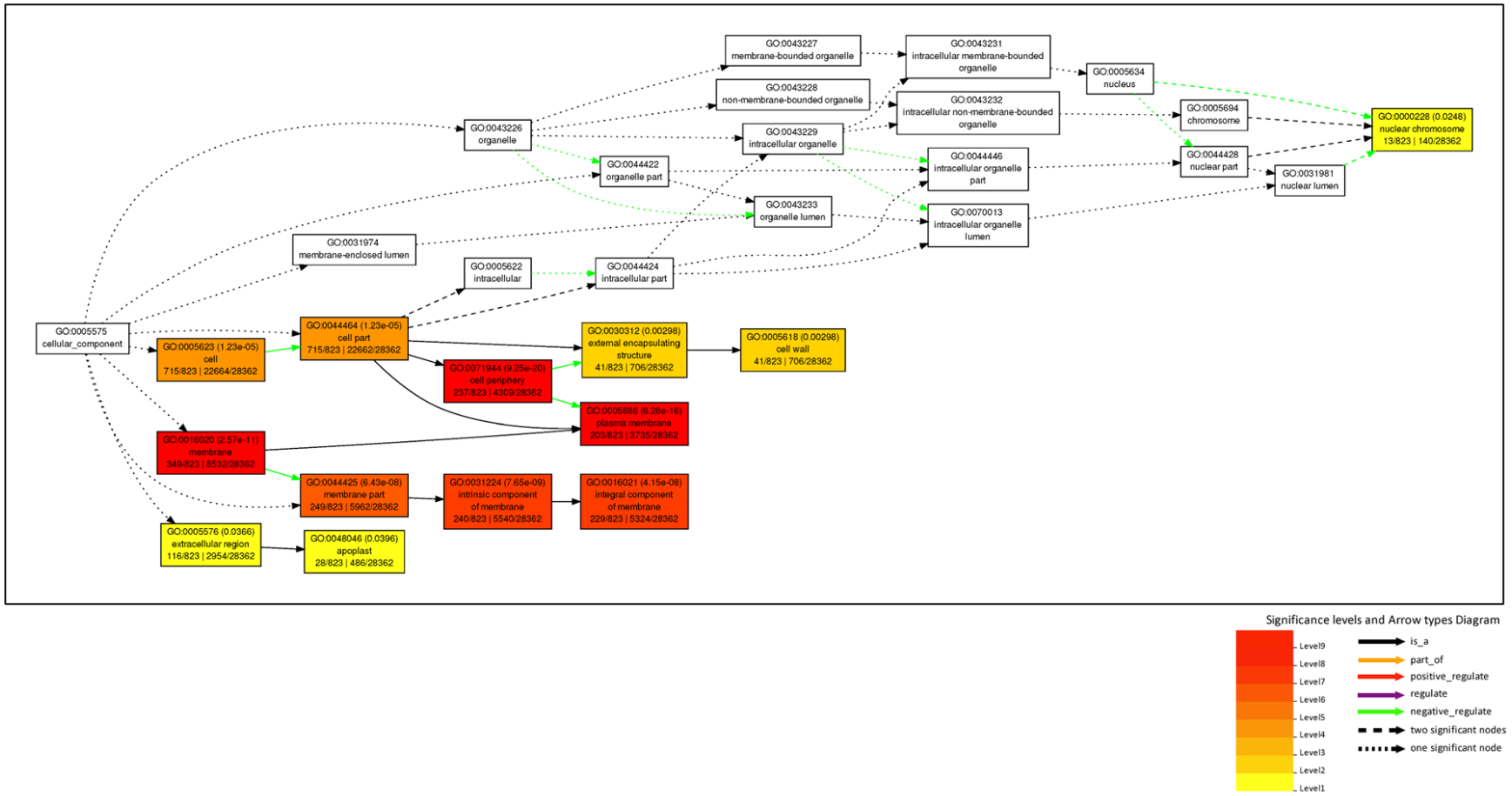

Figure 4.9: Significantly enriched cellular compartment gene ontology terms in potato loci that are upregulated > 4× in response to 5 Gy treatment.
Data shown include the gene ontology code, its associated false discovery rate for this analysis in parentheses, the name of the gene ontology code, the number of loci with the GO term / total number of loci in the dataset (bottom left), and the number of loci with this GO term in the *Arabidopsis thaliana* genome / total number of loci in the *A. thaliana* genome. Note that potato loci were converted to *A. thaliana* loci using the resources associated with the doubled monoploid potato DM 1-3 516 R44 (v6.1) reference genome (see methods).

Figure 4.10: Significantly enriched biological process gene ontology terms in potato loci that are upregulated > 4× in response to 0.5 Gy treatment.
Data shown include the gene ontology code, its associated false discovery rate for this analysis in parentheses, the name of the gene ontology code, the number of loci with the GO term / total number of loci in the dataset (bottom left), and the number of loci with this GO term in the *Arabidopsis thaliana* genome / total number of loci in the *A. thaliana* genome. Note that potato loci were converted to *A. thaliana* loci using the resources associated with the doubled monoploid potato DM 1-3 516 R44 (v6.1) reference genome (see methods).

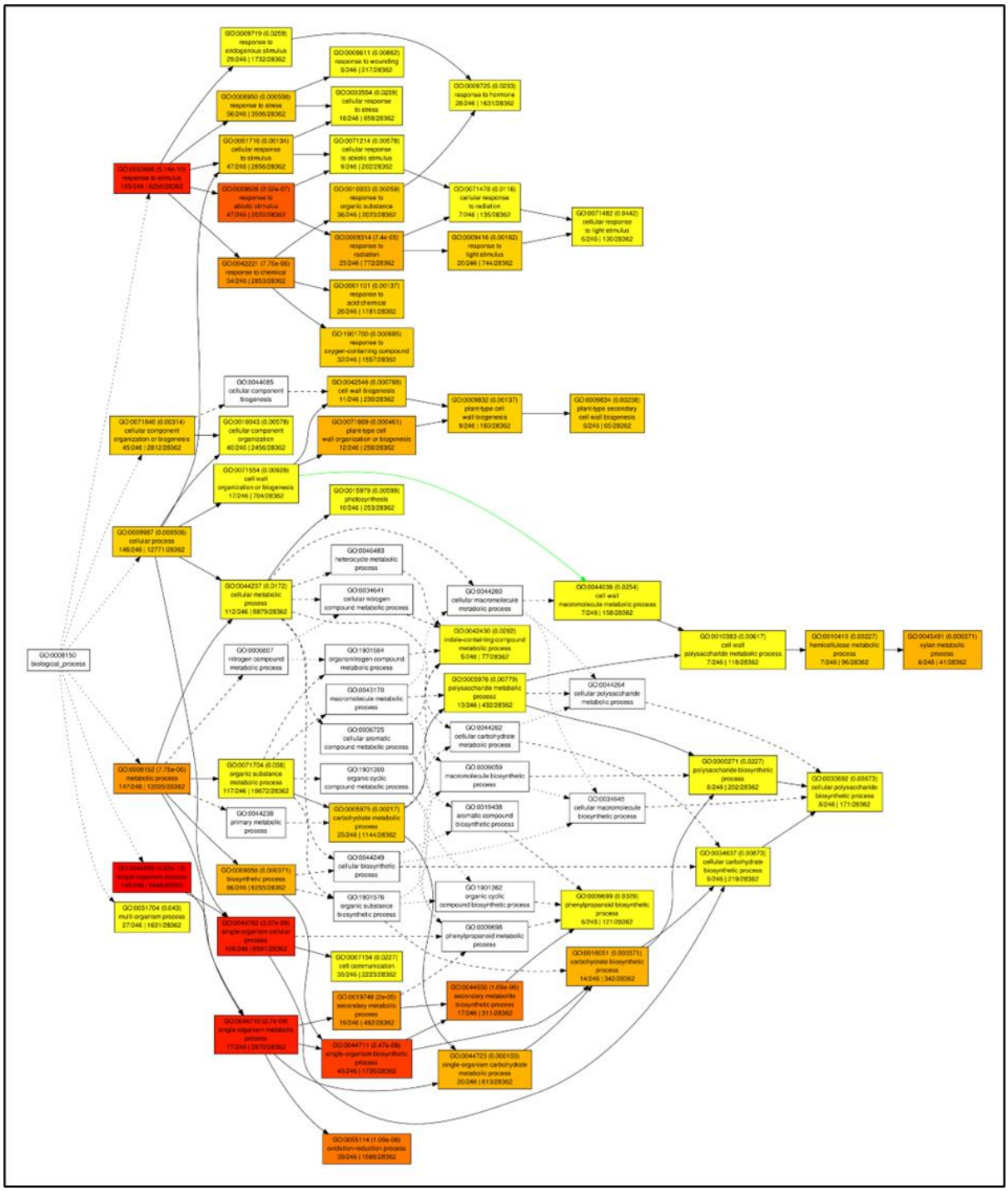
GO:0009719 (0.0259)
response to endogenous stimulus
29/246 | 732/28362
GO:0009611 (0.00862)
response to wounding
9/246 | 217/28362
GO:0009725 (0.0233)
response to hormone
28/246 | 1431/28362
GO:0006950 (0.000598)
response to stress
56/246 | 3506/28362
GO:0033554 (0.0259)
cellular response to stress
18/246 | 858/28362
GO:0051716 (0.00134)
cellular response to stimulus
47/246 | 2856/28362
GO:0071214 (0.00578)
cellular response to abiotic stimulus
9/246 | 202/28362
GO:0009628 (2.52e-07)
response to abiotic stimulus
47/246 | 2023/28362
GO:0010033 (0.00259)
response to organic substance
36/246 | 2023/28362
GO:0071478 (0.0116)
cellular response to radiation
7/246 | 135/28362
GO:0071482 (0.0442)
cellular response to light stimulus
5/246 | 130/28362
GO:0009314 (7.4e-05)
response to radiation
25/246 | 772/28362
GO:0009416 (0.00182)
response to light stimulus
20/246 | 744/28362
GO:0042221 (7.75e-06)
response to chemical
54/246 | 2853/28362
GO:0001101 (0.00137)
response to acid chemical
26/246 | 1181/28362
GO:1901700 (0.000685)
response to oxygen-containing compound
32/246 | 1557/28362
GO:0044085
cellular component biogenesis
GO:0042546 (0.000788)
cell wall biogenesis
11/246 | 239/28362
GO:0009832 (0.00137)
plant-type cell wall biogenesis
9/246 | 163/28362
GO:0009834 (0.00238)
plant-type secondary cell wall biogenesis
6/246 | 65/28362
GO:0071840 (0.00314)
cellular component organization or biogenesis
45/246 | 2812/28362
GO:0016043 (0.00578)
cellular component organization
40/246 | 2456/28362
GO:0071669 (0.000461)
plant-type cell wall organization or biogenesis
12/246 | 256/28362
GO:0071554 (0.00928)
cell wall organization or biogenesis
17/246 | 764/28362
GO:0015979 (0.00599)
photosynthesis
10/246 | 253/28362
GO:0009987 (0.000506)
cellular process
146/246 | 12771/28362
GO:0046483
heterocycle metabolic process
GO:0044237 (0.0172)
cellular metabolic process
112/246 | 9879/28362
GO:0034641
cellular nitrogen compound metabolic process
GO:0044260
cellular macromolecule metabolic process
GO:0044036 (0.0254)
cell wall macromolecule metabolic process
7/246 | 158/28362
GO:0042430 (0.0292)
indole-containing compound metabolic process
5/246 | 77/28362
GO:0010383 (0.00617)
cell wall polysaccharide metabolic process
7/246 | 118/28362
GO:0010410 (0.00227)
hemicellulose metabolic process
7/246 | 96/28362
GO:0045491 (0.000371)
xylan metabolic process
6/246 | 41/28362
GO:0006807
nitrogen compound metabolic process
GO:1901564
organonitrogen compound metabolic process
GO:0005976 (0.00779)
polysaccharide metabolic process
13/246 | 432/28362
GO:0044264
cellular polysaccharide metabolic process
GO:0043170
macromolecule metabolic process
GO:0006725
cellular aromatic compound metabolic process
GO:0044262
cellular carbohydrate metabolic process
GO:0008150
biological_process
GO:0008152 (7.75e-06)
metabolic process
147/246 | 12005/28362
GO:0071704 (0.038)
organic substance metabolic process
117/246 | 10672/28362
GO:1901360
organic cyclic compound metabolic process
GO:0009059
macromolecule biosynthetic process
GO:0000271 (0.0227)
polysaccharide biosynthetic process
6/246 | 202/28362
GO:0033692 (0.00673)
cellular polysaccharide biosynthetic process
6/246 | 171/28362
GO:0044238
primary metabolic process
GO:0005975 (0.00217)
carbohydrate metabolic process
25/246 | 1144/28362
GO:0019438
aromatic compound biosynthetic process
GO:0034645
cellular macromolecule biosynthetic process
GO:0044249
cellular biosynthetic process
GO:0034637 (0.00873)
cellular carbohydrate biosynthetic process
9/246 | 219/28362
GO:0009058 (0.000371)
biosynthetic process
96/246 | 6255/28362
GO:1901362
organic cyclic compound biosynthetic process
GO:1901576
organic substance biosynthetic process
GO:0009699 (0.0329)
phenylpropanoid biosynthetic process
6/246 | 121/28362
GO:0009698
phenylpropanoid metabolic process
GO:0051704 (0.043)
multi-organism process
27/246 | 1631/28362
GO:0044763 (3.07e-09)
single-organism cellular process
105/246 | 8501/28362
GO:0007154 (0.0227)
cell communication
35/246 | 2223/28362
GO:0016051 (0.003371)
carbohydrate biosynthetic process
14/246 | 342/28362
GO:0019748 (2e-05)
secondary metabolic process
19/246 | 492/28362
GO:0044550 (1.09e-06)
secondary metabolite biosynthetic process
17/246 | 311/28362
GO:0044710 (2.7e-08)
single-organism metabolic process
77/246 | 3970/28362
GO:0044711 (2.47e-08)
single-organism biosynthetic process
43/246 | 1735/28362
GO:0044723 (0.000103)
single-organism carbohydrate metabolic process
20/246 | 613/28362
GO:0055114 (1.09e-06)
oxidation-reduction process
39/246 | 1585/28362
Significance levels and Arrow types Diagram
Level9
Level8
Level7
Level6
Level5
Level4
Level3
Level2
Level1
is_a
part_of
positive_regulate
regulate
negative_regulate
two significant nodes
one significant node

Figure 4.11: Significantly enriched biological process gene ontology terms in potato loci that are upregulated > 4× in response to 1 Gy treatment.
Data shown include the gene ontology code, its associated false discovery rate for this analysis in parentheses, the name of the gene ontology code, the number of loci with the GO term / total number of loci in the dataset (bottom left), and the number of loci with this GO term in the *Arabidopsis thaliana* genome / total number of loci in the *A. thaliana* genome. Note that potato loci were converted to *A. thaliana* loci using the resources associated with the doubled monoploid potato DM 1-3 516 R44 (v6.1) reference genome (see methods).

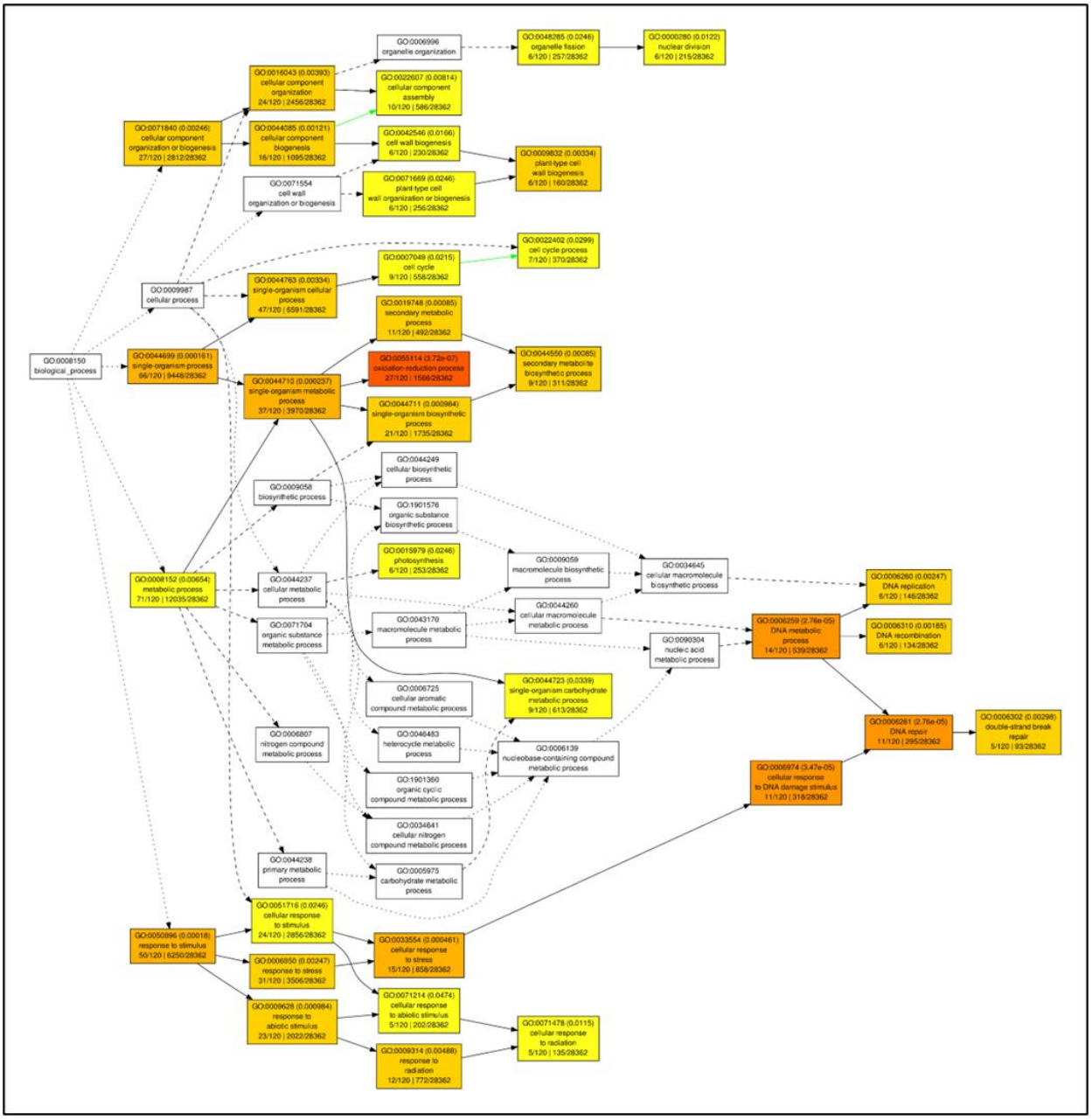
GO:0008150
biological_process
GO:0044699 (0.000161)
single-organism process
66/120 | 9448/28362
GO:0009987
cellular process
GO:0071840 (0.00246)
cellular component
organization or biogenesis
27/120 | 2812/28362
GO:0008152 (0.00654)
metabolic process
71/120 | 12035/28362
GO:0050896 (0.00018)
response to stimulus
50/120 | 6250/28362
GO:0006996
organelle organization
GO:0016043 (0.00393)
cellular component
organization
24/120 | 2456/28362
GO:0044085 (0.00121)
cellular component
biogenesis
16/120 | 1095/28362
GO:0071554
cell wall
organization or biogenesis
GO:0044763 (0.00334)
single-organism cellular
process
47/120 | 6591/28362
GO:0044710 (0.000237)
single-organism metabolic
process
37/120 | 3970/28362
GO:0009058
biosynthetic process
GO:0044237
cellular metabolic
process
GO:0071704
organic substance
metabolic process
GO:0006807
nitrogen compound
metabolic process
GO:0044238
primary metabolic
process
GO:0051716 (0.0246)
cellular response
to stimulus
24/120 | 2856/28362
GO:0006950 (0.00247)
response to stress
31/120 | 3506/28362
GO:0009628 (0.000984)
response to
abiotic stimulus
23/120 | 2022/28362
GO:0022607 (0.00814)
cellular component
assembly
10/120 | 586/28362
GO:0042546 (0.0166)
cell wall biogenesis
6/120 | 230/28362
GO:0071669 (0.0246)
plant-type cell
wall organization or biogenesis
6/120 | 256/28362
GO:0007049 (0.0215)
cell cycle
9/120 | 558/28362
GO:0019748 (0.00085)
secondary metabolic
process
11/120 | 492/28362
GO:0055114 (3.72e-07)
oxidation-reduction process
27/120 | 1566/28362
GO:0044711 (0.000984)
single-organism biosynthetic
process
21/120 | 1735/28362
GO:0044249
cellular biosynthetic
process
GO:1901576
organic substance
biosynthetic process
GO:0015979 (0.0246)
photosynthesis
6/120 | 253/28362
GO:0043170
macromolecule metabolic
process
GO:0006725
cellular aromatic
compound metabolic process
GO:0046483
heterocycle metabolic
process
GO:1901360
organic cyclic
compound metabolic process
GO:0034641
cellular nitrogen
compound metabolic process
GO:0005975
carbohydrate metabolic
process
GO:0033554 (0.000461)
cellular response
to stress
15/120 | 858/28362
GO:0071214 (0.0474)
cellular response
to abiotic stimulus
5/120 | 202/28362
GO:0009314 (0.00488)
response to
radiation
12/120 | 772/28362
GO:0048285 (0.0246)
organelle fission
6/120 | 257/28362
GO:0000280 (0.0122)
nuclear division
6/120 | 215/28362
GO:0009832 (0.00334)
plant-type cell
wall biogenesis
6/120 | 160/28362
GO:0022402 (0.0299)
cell cycle process
7/120 | 370/28362
GO:0044550 (0.00085)
secondary metabolite
biosynthetic process
9/120 | 311/28362
GO:0009059
macromolecule biosynthetic
process
GO:0044260
cellular macromolecule
metabolic process
GO:0090304
nucleic acid
metabolic process
GO:0044723 (0.0339)
single-organism carbohydrate
metabolic process
9/120 | 613/28362
GO:0006139
nucleobase-containing compound
metabolic process
GO:0034645
cellular macromolecule
biosynthetic process
GO:0006259 (2.76e-05)
DNA metabolic
process
14/120 | 539/28362
GO:0006974 (3.47e-05)
cellular response
to DNA damage stimulus
11/120 | 318/28362
GO:0006260 (0.00247)
DNA replication
6/120 | 146/28362
GO:0006310 (0.00185)
DNA recombination
6/120 | 134/28362
GO:0006281 (2.76e-05)
DNA repair
11/120 | 295/28362
GO:0006302 (0.00298)
double-strand break
repair
5/120 | 93/28362
GO:0071478 (0.0115)
cellular response
to radiation
5/120 | 135/28362

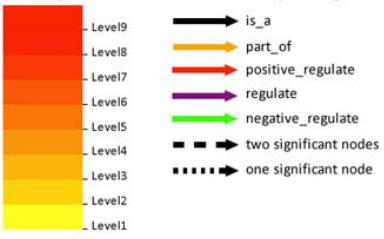
Significance levels and Arrow types Diagram
Level9
Level8
Level7
Level6
Level5
Level4
Level3
Level2
Level1
is_a
part_of
positive_regulate
regulate
negative_regulate
two significant nodes
one significant node

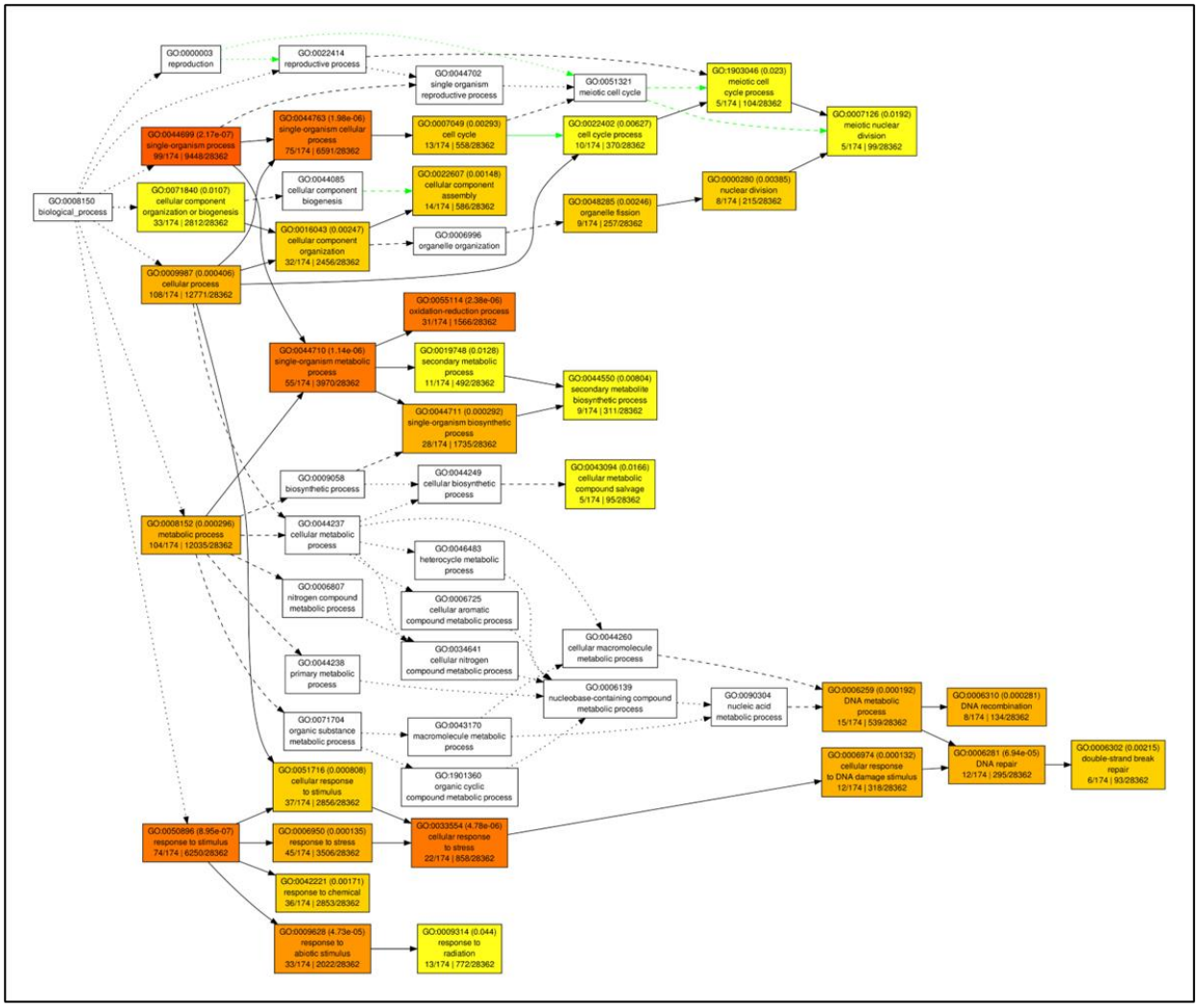

Figure 4.12: Significantly enriched biological process gene ontology terms in potato loci that are upregulated > 4× in response to 2 Gy treatment.
Data shown include the gene ontology code, its associated false discovery rate for this analysis in parentheses, the name of the gene ontology code, the number of loci with the GO term / total number of loci in the dataset (bottom left), and the number of loci with this GO term in the *Arabidopsis thaliana* genome / total number of loci in the *A. thaliana* genome. Note that potato loci were converted to *A. thaliana* loci using the resources associated with the doubled monoploid potato DM 1-3 516 R44 (v6.1) reference genome (see methods).

Figure 4.13: Significantly enriched biological process gene ontology terms in potato loci that are upregulated > 4× in response to 4 Gy treatment.

Data shown include the gene ontology code, its associated false discovery rate for this analysis in parentheses, the name of the gene ontology code, the number of loci with the GO term / total number of loci in the dataset (bottom left), and the number of loci with this GO term in the *Arabidopsis thaliana* genome / total number of loci in the *A. thaliana* genome. Note that potato loci were converted to *A. thaliana* loci using the resources associated with the doubled monoploid potato DM 1-3 516 R44 (v6.1) reference genome (see methods).

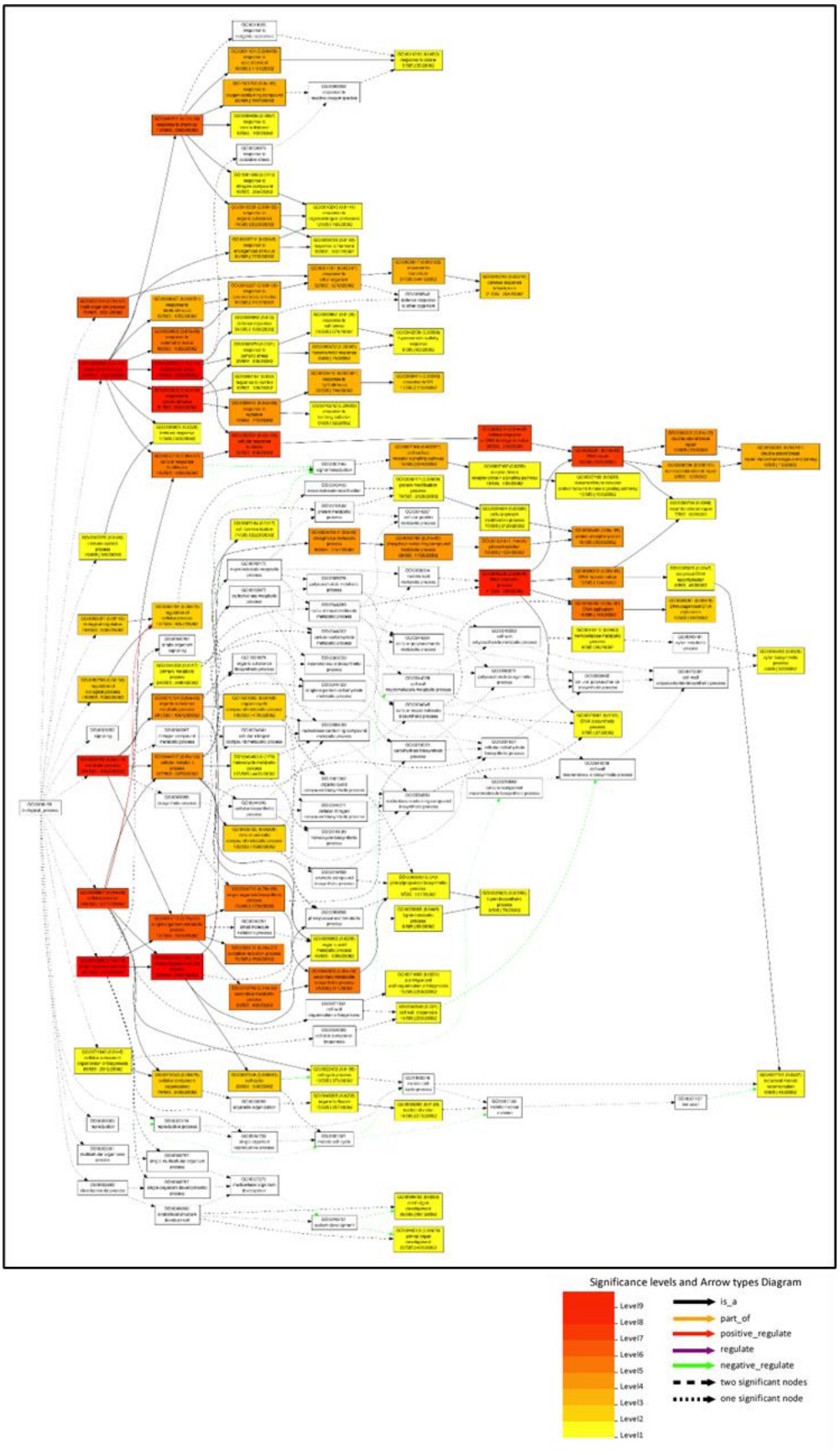
Significance levels and Arrow types Diagram
Level9
Level8
Level7
Level6
Level5
Level4
Level3
Level2
Level1
is_a
part_of
positive_regulate
regulate
negative_regulate
two significant nodes
one significant node

Figure 4.14: Significantly enriched biological process gene ontology terms in potato loci that are upregulated > 4× in response to 5 Gy treatment.
Data shown include the gene ontology code, its associated false discovery rate for this analysis in parentheses, the name of the gene ontology code, the number of loci with the GO term / total number of loci in the dataset (bottom left), and the number of loci with this GO term in the *Arabidopsis thaliana* genome / total number of loci in the *A. thaliana* genome. Note that potato loci were converted to *A. thaliana* loci using the resources associated with the doubled monoploid potato DM 1-3 516 R44 (v6.1) reference genome (see methods).

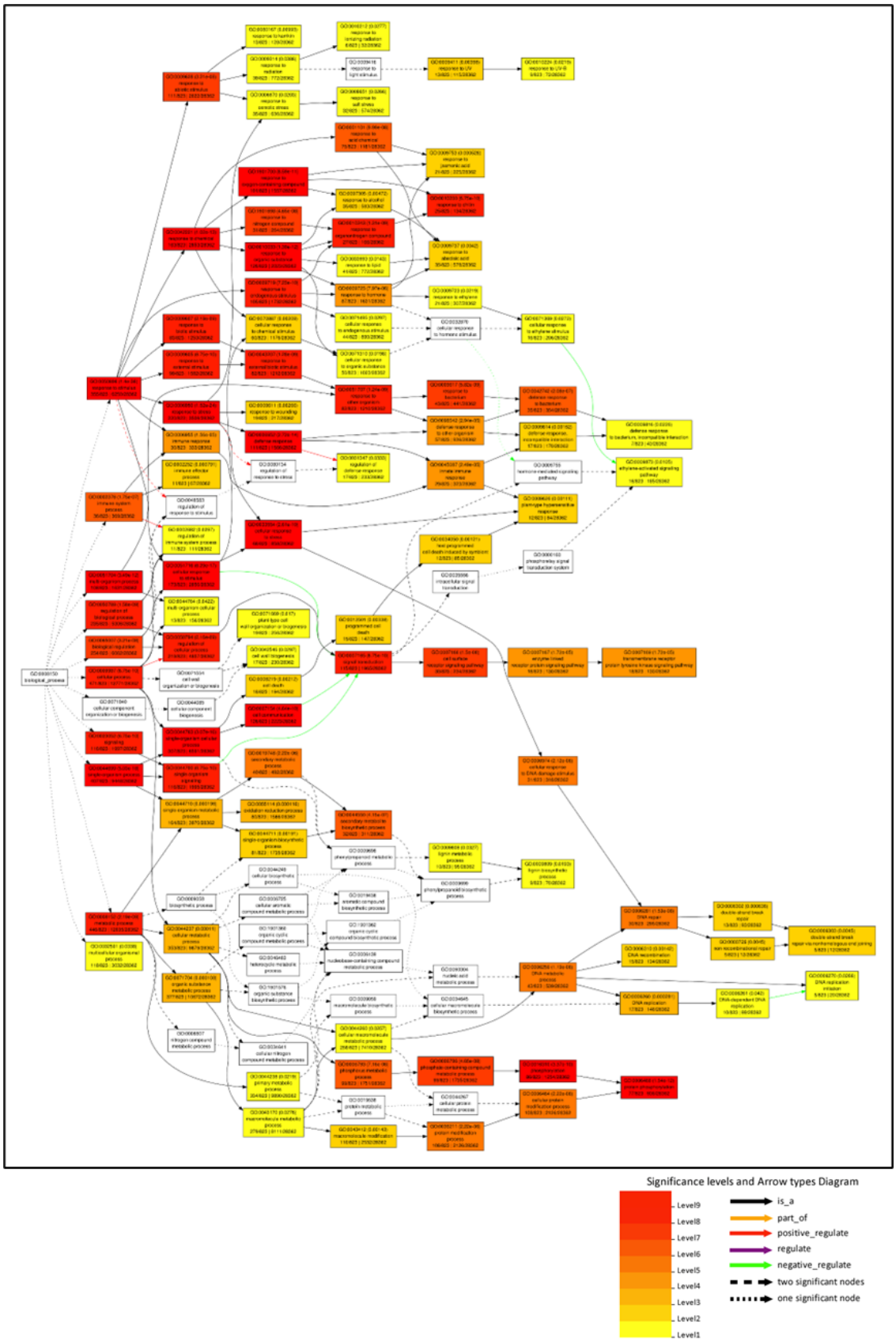
Significance levels and Arrow types Diagram
Level9
Level8
Level7
Level6
Level5
Level4
Level3
Level2
Level1
is_a
part_of
positive_regulate
regulate
negative_regulate
two significant nodes
one significant node

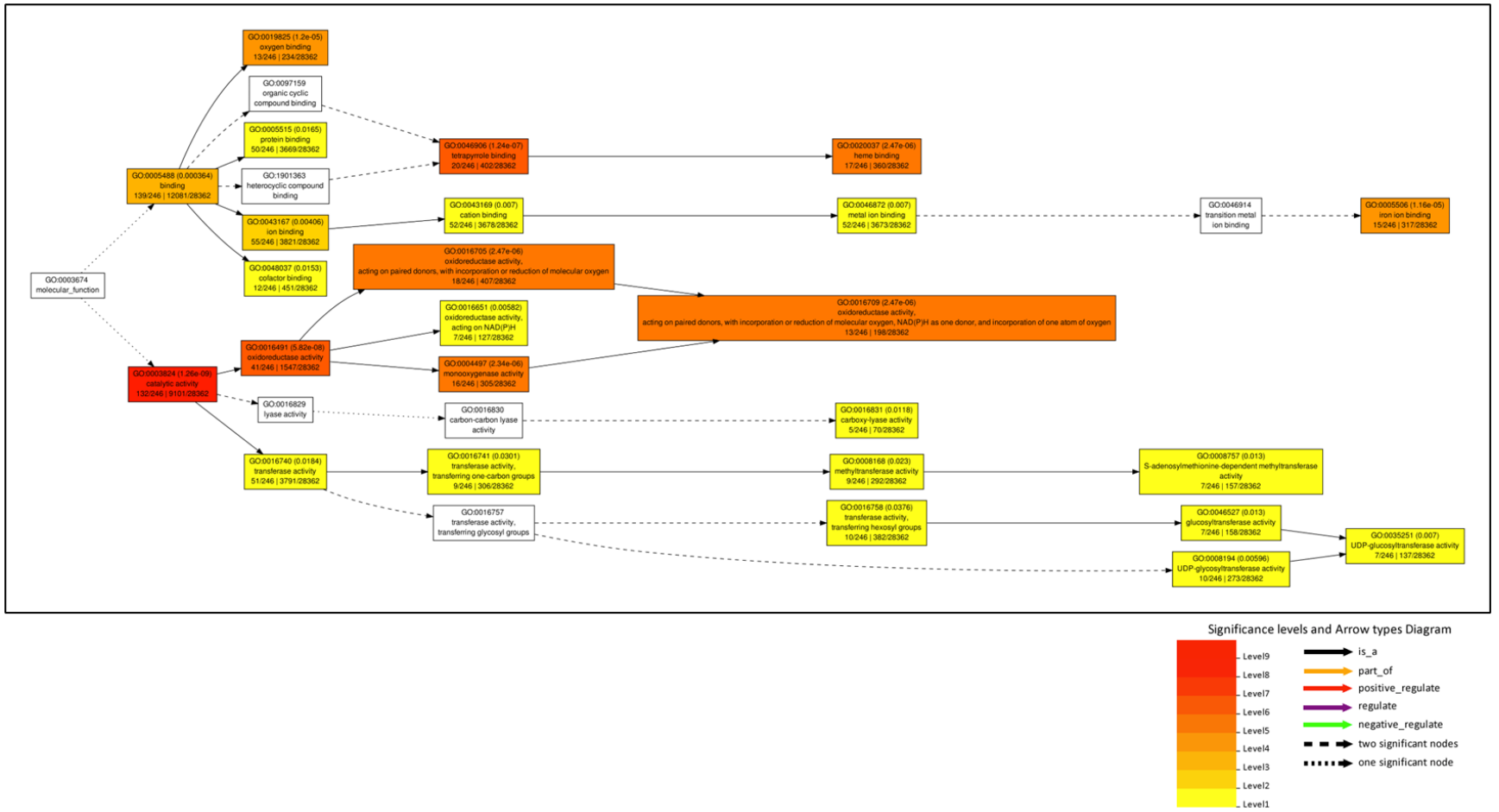

Figure 4.15: Significantly enriched molecular function gene ontology terms in potato loci that are upregulated > 4× in response to 0.5 Gy treatment.

Data shown include the gene ontology code, its associated false discovery rate for this analysis in parentheses, the name of the gene ontology code, the number of loci with the GO term / total number of loci in the dataset (bottom left), and the number of loci with this GO term in the *Arabidopsis thaliana* genome / total number of loci in the *A. thaliana* genome. Note that potato loci were converted to *A. thaliana* loci using the resources associated with the doubled monoploid potato DM 1-3 516 R44 (v6.1) reference genome (see methods).

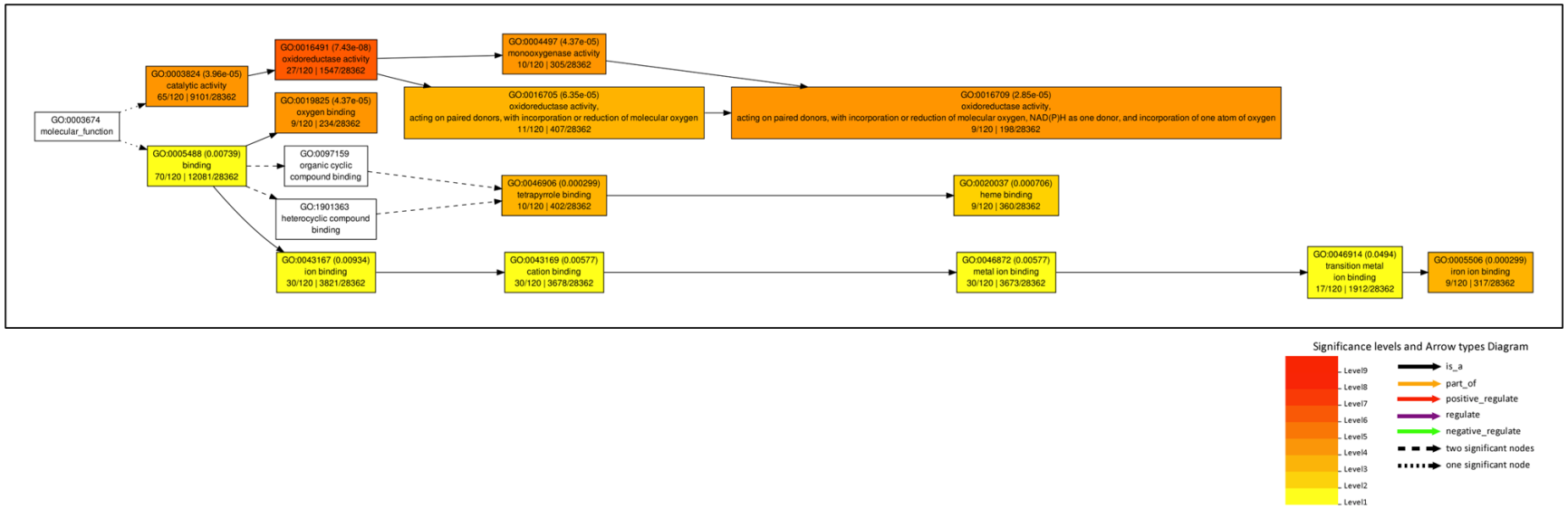

Figure 4.16: Significantly enriched molecular function gene ontology terms in potato loci that are upregulated > 4× in response to 1 Gy treatment.
Data shown include the gene ontology code, its associated false discovery rate for this analysis in parentheses, the name of the gene ontology code, the number of loci with the GO term / total number of loci in the dataset (bottom left), and the number of loci with this GO term in the *Arabidopsis thaliana* genome / total number of loci in the *A. thaliana* genome. Note that potato loci were converted to *A. thaliana* loci using the resources associated with the doubled monoploid potato DM 1-3 516 R44 (v6.1) reference genome (see methods).

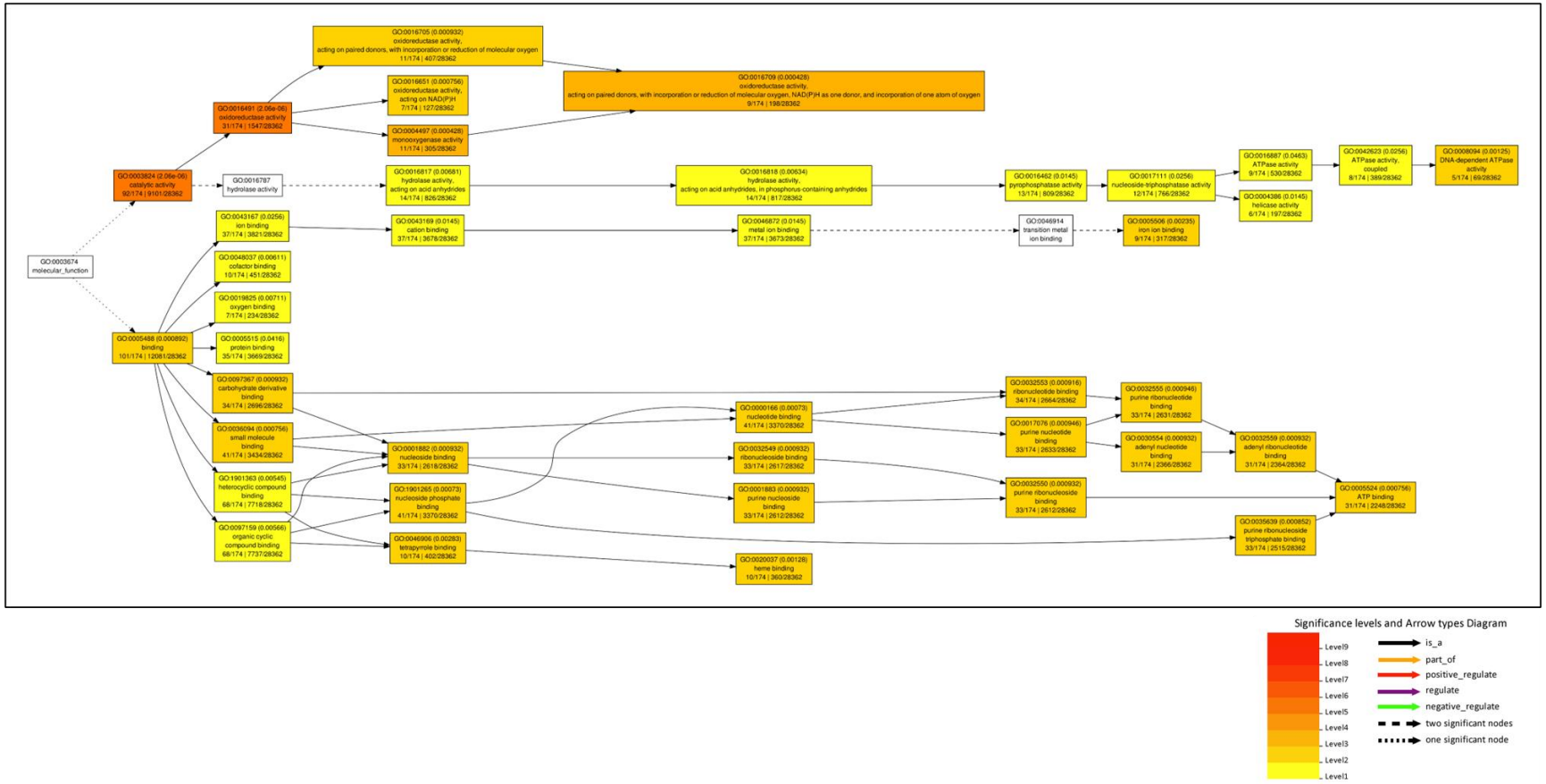

Figure 4.17: Significantly enriched molecular function gene ontology terms in potato loci that are upregulated > 4× in response to 2 Gy treatment.

Data shown include the gene ontology code, its associated false discovery rate for this analysis in parentheses, the name of the gene ontology code, the number of loci with the GO term / total number of loci in the dataset (bottom left), and the number of loci with this GO term in the *Arabidopsis thaliana* genome / total number of loci in the *A. thaliana* genome. Note that potato loci were converted to *A. thaliana* loci using the resources associated with the doubled monoploid potato DM 1-3 516 R44 (v6.1) reference genome (see methods).

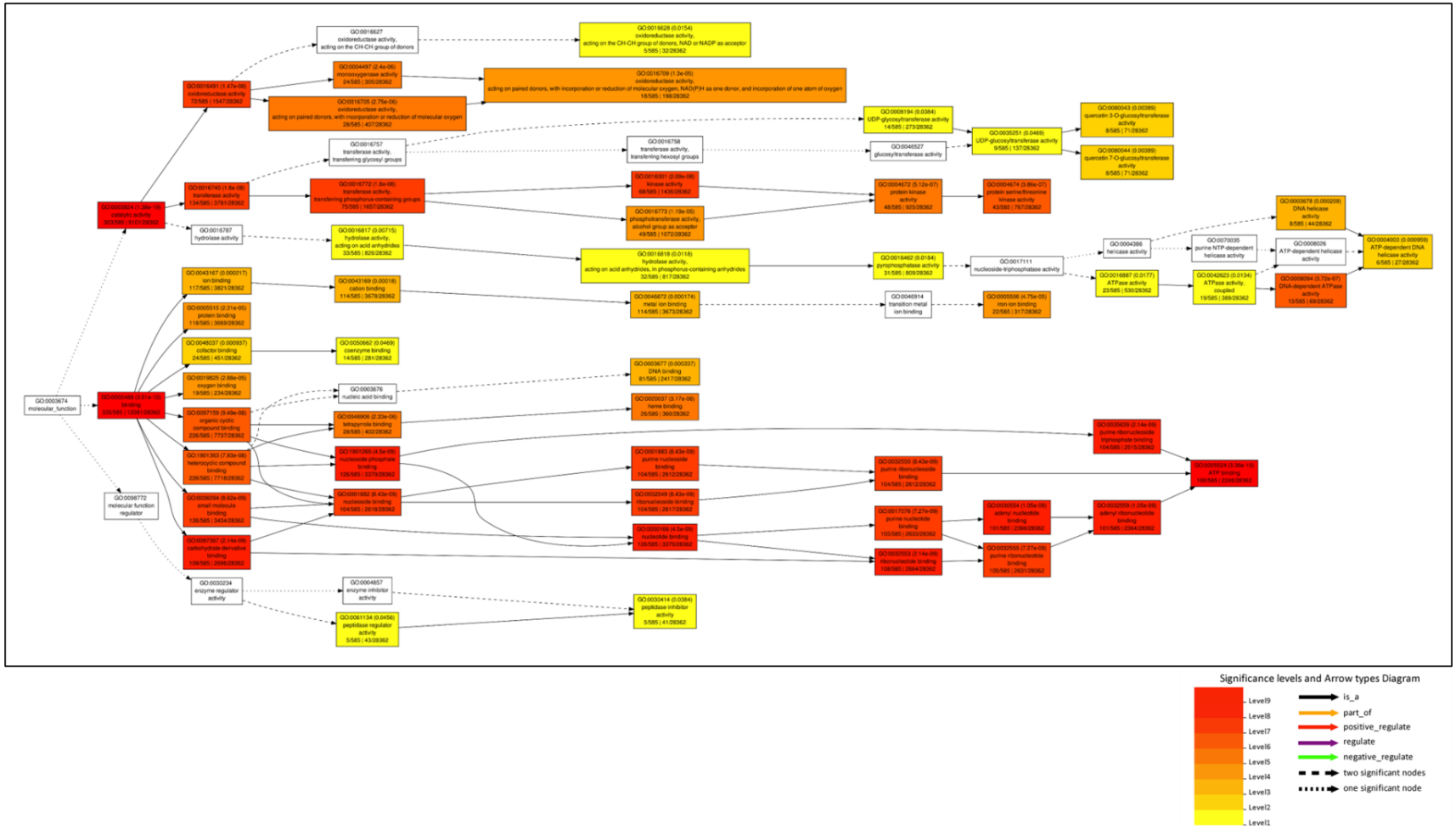

Figure 4.18: Significantly enriched molecular function gene ontology terms in potato loci that are upregulated > 4× in response to 4 Gy treatment.

Data shown include the gene ontology code, its associated false discovery rate for this analysis in parentheses, the name of the gene ontology code, the number of loci with the GO term / total number of loci in the dataset (bottom left), and the number of loci with this GO term in the *Arabidopsis thaliana* genome / total number of loci in the *A. thaliana* genome. Note that potato loci were converted to *A. thaliana* loci using the resources associated with the doubled monoploid potato DM 1-3 516 R44 (v6.1) reference genome (see methods).

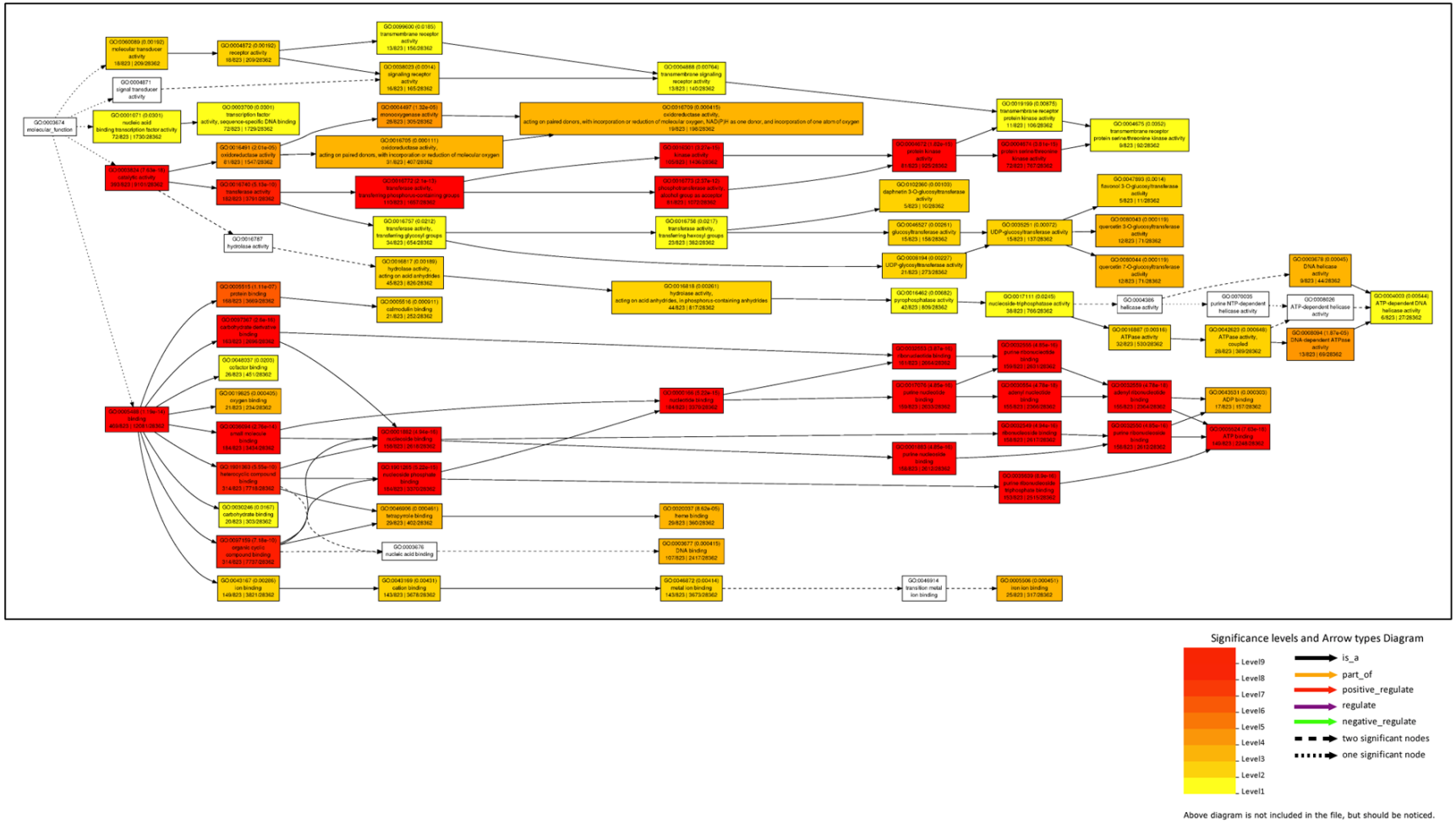

Figure 4.19: Significantly enriched molecular function gene ontology terms in potato loci that are upregulated > 4× in response to 5 Gy treatment.

Data shown include the gene ontology code, its associated false discovery rate for this analysis in parentheses, the name of the gene ontology code, the number of loci with the GO term / total number of loci in the dataset (bottom left), and the number of loci with this GO term in the *Arabidopsis thaliana* genome / total number of loci in the *A. thaliana* genome. Note that potato loci were converted to *A. thaliana* loci using the resources associated with the doubled monoploid potato DM 1-3 516 R44 (v6.1) reference genome (see methods).

CHAPTER V: AI TO ENABLE PLANT CELL METABOLIC ENGINEERING

This chapter has been published in the journal Trends in Plant Science:
Sears, R. G., Lenaghan, S. C., & Stewart, C. N., Jr. AI to enable plant cell metabolic engineering. Trends in plant science, S1360-1385(23)00299-6 (2023). Advance online publication. https://doi.org/10.1016/j.tplants.2023.09.006

The idea and writing were generated by R.G. Sears, S.C. Lenaghan, and C. N. Stewart.

Abstract

Plant metabolic engineering must take into consideration the heterogeneous cell types that play a role in metabolite production; cells do not participate equally. We posit that artificial intelligence developed for biomedical purposes can be applied to plant cell characterization to accelerate the development of metabolic engineering strategies in plants.

Results and Discussion

Plant metabolic engineering is limited by biomass quantification and cell typing.

Metabolic engineering seeks to maximize the flux (see Glossary) of a certain metabolite's biosynthesis in a population of cells (reported as $\frac{\text{“mass of metabolite”}}{\text{”biomass” x “time”}}$). Maximizing flux requires identification of all relevant reactions in a biosynthetic pathway. This is no small task in a single cell organism, as flux has to be inferred from metabolite timepoint measurements using a mass spectrometer, *in vitro* enzyme activity assays, and cell physiology data. In multicellular organisms such as plants, heterogeneous populations of cell types coordinate metabolite biosynthesis and complicate the path from fundamental analysis of metabolic flux to metabolic engineering. These complications have slowed plant metabolic engineering progress; thus, few engineered plants have successfully been commercialized.

Modelling metabolic engineering strategies typically utilize metabolic flux analysis (MFA), in which all reactions relevant to production of a metabolite are reduced to a simple mathematical model. An essential component to MFA is the biomass equation, which is based upon the macromolecular composition of a cell, its growth rate, and the established pathways of the central metabolism. The biomass equation is relatively easy to generate when the cell population of interest is homogenous and specific growth rate is consistent. However, neither of these assumptions are true in plant tissues, necessitating cell-type specific MFA[1] to understand an organ's overall metabolic map. The tools to generate single cell omics datasets and infer a metabolic map already exist. The missing technologies are those that can use these single-cell datasets to accurately characterize all of the plant cell types and the relationships between types in an organ to facilitate the development of cellular engineering strategies that produce the highest flux.

A recent study[2] exemplifies the current limitations of plant metabolic engineering (Figure 5.1). All figures and tables are located in an appendix at the end of the chapter. With a one-enzyme system, it should be easy to predict, measure, and improve the flux of

L-DOPA in tomato fruits using existing metabolic maps of tomato fruits and adding the single chemical equation to the list of equations for MFA[3]. However, the unknown cell-type population dynamics of a tomato fruit resulted in the study basing their engineering strategy on organ-level data rather than cell-level (Figure 5.1). The complications of different cell morphologies and spatiotemporal expression of the transgene leave many questions unanswered. Plant metabolic engineers need a high-throughput method that characterizes cells, develops cell-specific metabolic maps, and links the maps of cell populations so that engineering strategies can be devised. The amount of data analysis needed to characterize plant cells makes the task ripe for application of AI, though most plant-centric AI development is directed towards crop phenomic analysis. We posit that existing AI developed for biomedical applications already have these capabilities and they could now be adapted for plant metabolic engineering.

AI developed for biomedical applications should be applied to plant metabolic engineering.

Enhanced characterization of cells and cell communities is needed to overcome the challenges of metabolic engineering in multicellular organisms. The technologies needed to answer the questions posed in Figure 5.1 should characterize and group plant cells based on their physical morphology and context, as well as through molecular markers found within cell-specific omics datasets. If a program could read a cross section of a plant organ, identify the cells contributing to metabolite production, and characterize those cells' metabolic map, cell-type specific MFA could be conducted and regulatory elements common to the most desirable cell types could be uncovered. AI technologies for biomedical applications have already been developed with similar capabilities and they can be adapted to plant datasets, ideally in tandem to leverage each AI's specific capabilities (Figure 5.2).

Many different AI programs have been developed to characterize cell types based on their morphology, context, and omics datasets[4]. Most of these technologies are based upon a machine learning approach. Powerful cell characterization AI such as BIAS[5] could serve as a platform for plant cell metabolic modelling. BIAS uses a deep neural network to extract physiological cell data from slide images of fixed tissue. The slide is then fed to a laser dissection microscope for single-cell proteomic data collection. A machine learning algorithm then characterizes cells based on cell physiology and proteomic data. BIAS identified novel cell types and provided physiological and proteomic markers in four human cancer types, though accuracy of slide feature recognition ranged depending on cell type and feature of interest (F1 score from 0.3 – 0.8). An algorithm such as DIABLO can be used to facilitate more accurate characterization and integration of multiple omic layers[6] . DIABLO incorporates multiple levels of omics data to predict cell type and make associations between omics datasets. A key feature of DIABLO is the ability to infer active metabolic pathways in a cell type based on transcript data, which is directly applicable to selecting ideal cell types for engineering. In a case study using DIABLO, the authors input transcriptomic, metabolomic, and cell type datasets to identify allergen response in human cells. The AI then differentiated between cells responding to the allergen with 98% accuracy and

provided which cell types, genes, and metabolic pathways were involved in the response. Together, BIAS and DIABLO could identify cell types, gather biomass and population data for each cell type, report differentially active metabolic pathways, and provide marker genes that are specific to cell types of interest. The authors of BIAS and DIABLO demonstrate their algorithms performance on a variety of mammalian cell types, indicating that the machine learning and deep learning algorithms they developed can be easily adapted to new contexts.

Once cell populations are characterized, an AI such as MESSI can uncover the relationships between the identified cell types[7]. This algorithm uses a mixture of experts machine learning strategy to predict cell interactions based on the expression of known effectors and ligands in single-cell transcriptomics datasets paired with cells' proximity. Using effector/ligand, transcriptomic, and spatial location data, MESSI is able to predict a cell's gene expression patterns based on neighboring cell's expression of effectors with a mean absolute error of ~0.27-0.38 across four mouse cell types. Though designed for understanding neurons, MESSI is directly applicable to the effector/ligand interactions that occur between plant cells. In addition, we propose that a similar AI approach could be used instead with known reactants and products within a metabolic pathway. Using the same methodology as MESSI, an AI could uncover metabolic relationships in communities of plant cells to define a metabolic pathway that spans multiple cell types.

Though powerful, the neural network strategies proposed here require large training datasets to become accurate. Annotated omics and effector/ligand datasets for cell characterization are readily available in databases such as the Plant Cell Marker Database[8] and PlantPhoneDB[9], though training datasets will have to be generated *de novo* for specific tissues and species not found in the database. Additionally, most available single-cell datasets are transcriptomic, meaning proteomic and metabolomic datasets will need to be generated in order to effectively use the described AI. Generation of annotated slide images for characterization is another labor-intensive requirement for AI cell physiology characterization. Although a considerable workload will be required of plant cell biologists, tools such as nucleAIzer[10] can be used to expand a small, annotated image set[5]. The work of creating training datasets will be essential to adapting biomedical AI to plant systems and will require the expertise of many plant scientists whose research goals do not involve metabolic engineering. Conveniently, the tools generated will be useful for explorative characterization of plant cells and contribute to the proposed plant cell atlas[11] in addition to directed characterization to generate engineering strategies.

Adopting existing biomedical AI to plant systems and/or creating new plant-specific software will be a collaborative effort needing metabolic engineers, AI scientists, and most especially plant cell biologists whose skillsets will be essential to training accurate AI. Similar multidisciplinary work is being pursued in the burgeoning fields of spatial metabolomics[12] and plant anatomics[13], making scientists in these fields especially valuable to developing plant metabolic engineering AI. We would like to use this article to issue a call for collaboration amongst these disparate groups of scholars. By creating high-throughput plant cell characterization platform, plant metabolic engineering can begin delivering crop plants that produce cheaper medicines, offer rural economies higher value crops, and production systems that release less CO_2 into the atmosphere.

References

1. Rossi, M. et al. Cell-type specific metabolic flux analysis: A challenge for metabolic phenotyping and a potential solution in plants. *Metabolites* **7**, 59 (2017).
2. Breitel, D. et al. Metabolic engineering of tomato fruit enriched in L-DOPA. *Metabolic Engineering* **65**, 185-196 (2021).
3. Ara, T. et al. TOMATOMET: A metabolome database consists of 7118 accurate mass values detected in mature fruits of 25 tomato cultivars. *Plant Direct* **5**, e00318 (2021).
4. Cooper, L. et al. Novel genotype-phenotype associations in human cancers enabled by advanced molecular platforms and computational analysis of whole slide images. *Laboratory Investigation* **95**, 266-376 (2015).
5. Mund, A. et al. Deep visual proteomics defines single-cell identity and heterogeneity. *Nature Biotechnology* **40**, 1231–1240 (2022).
6. Singh, A. et al. DIABLO: an integrative approach for identifying key molecular drivers from multi-omics assays. *Bioinformatics* **35**, 3055–3062 (2019).
7. Li D. et al. Identifying signaling genes in spatial single-cell expression data. *Bioinformatics* **37**, 968-975 (2021).
8. Jin, J. et al. PCMDB: a curated and comprehensive resource of plant cell markers. *Nucleic Acids Research* **50**, D1448-D1455 (2022).
9. Xu, C. et al. PlantPhoneDB: A manually curated pan-plant database of ligand-receptor pairs infers cell–cell communication. *Plant Biotechnology Journal* **20,** 2123-2134 (2022).
10. Hollandi, R. et al. nucleAIzer: A parameter-free deep learning framework for nucleus segmentation using image style transfer. *Cell Systems* **10**, 453-458 (2020).
11. Rhee, S. et al. Towards building a plant cell atlas. *Trends in Plant Science* **24**, 303-310 (2019).
12. Alexandrov, T. Spatial metabolomics and imaging mass spectrometry in the age of artificial intelligence. *Annual Review of Biomedical Data Science* **3,** 61-87 (2020).
13. Strock, C. et al. Anatomics: High-throughput phenotyping of plant anatomy. *Trends in Plant Science* **27**, 520-523 (2022).
14. Kneissl, M. & Deikman, J. The tomato E8 gene influences ethylene biosynthesis in fruit but not in flowers. *Plant Physiology* **112**, 537–547 (1996).
15. Matas A. et al. Tissue- and cell-type specific transcriptome profiling of expanding tomato fruit provides insights into metabolic and regulatory specialization and cuticle formation. *Plant Cell* **23**, 3893-3910 (2011).

Appendix

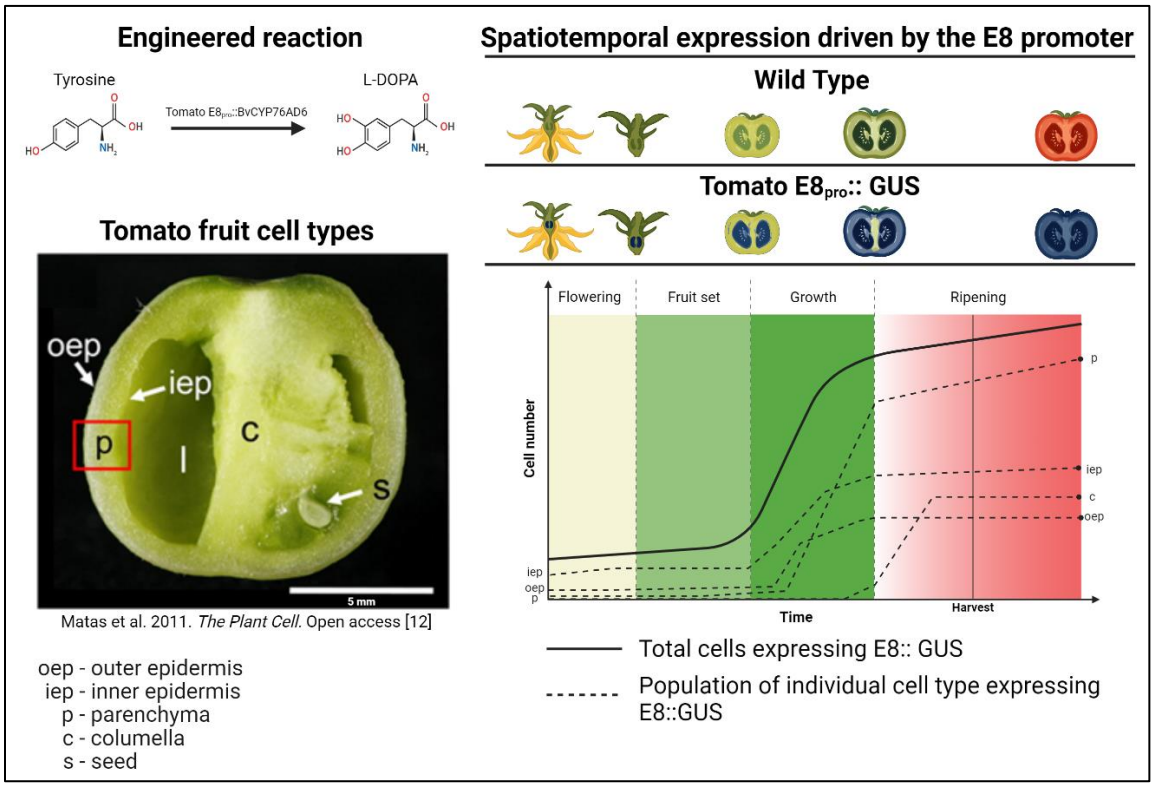

Figure 5.1: Calculating L-DOPA flux is complicated by heterogeneous expression in tomato fruit.

Breitel et al.[2] sought to engineer tomato fruit to synthesize L-DOPA, a standard therapy for humans suffering from Parkinson's disease. The tomato fruit was selected based on high accumulation of the substrate tyrosine, which is converted to L-DOPA by the beet enzyme BvCYP76AD6. Expression of this beet enzyme gene is driven by the fruit specific tomato E8 promoter, which has uneven expression patterns in the five major tomato cell types[14]. Each of these cell types have unique metabolic maps[15]. In order to maximize the flux and yield of L-DOPA synthesis in tomato fruit, the following questions need to be answered:

1. What are the cell types present in the tomato fruit over time?
2. What are the growth rates of the populations of each cell type?
3. Which of those cell types have the greatest opportunity for L-DOPA production over the life of the organ?
4. What regulatory elements drive expression of a transgene within the ideal cell types?
5. Which cell types are not ideal for L-DOPA biosynthesis but contribute to tyrosine accumulation in the cells that are ideal for L-DOPA biosynthesis?

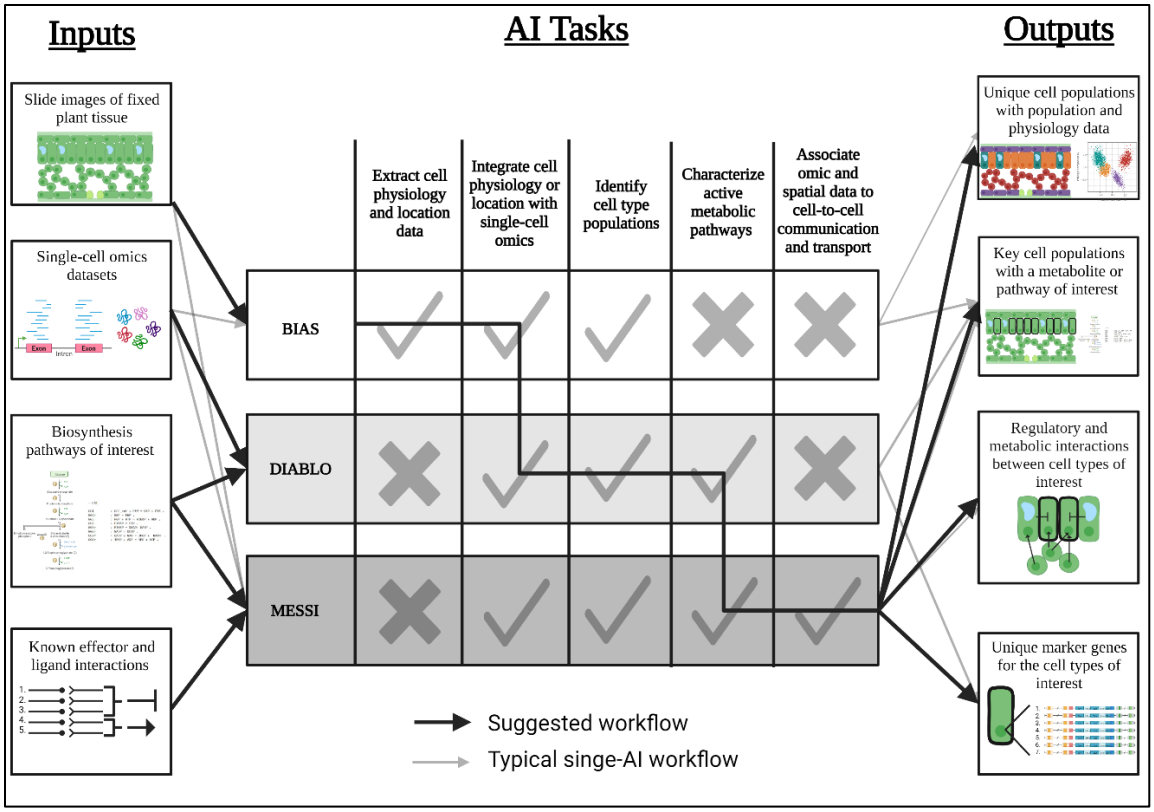

Figure 5.2: Proposed integration of multiple AI for plant cell characterization. A graphical representation of the inputs, tasks, and outputs for the cell characterization AI discussed in this paper. The workflow reported by the authors of these AI (light gray arrows) and the combined workflow suggested here (bold, black arrows) are both shown. Each AI has tasks that it is capable of (marked with a ✓) and those that it is not designed to perform (marked with an ×). The workflow suggested in this figure makes the capabilities of each AI complementary, resulting in the output of all data that is needed for the metabolic engineering of plant cells.

CHAPTER VI: CONCLUSION

The power of radioactive decay and ionizing radiation have inspired human curiosity and fear since their discovery in the 1890s. Humans quickly turned to using plants as test subjects for understanding radiation's impact on biology, continuing the historical tradition of using plant life as a tool for understanding unobservable factors in the environment. Whether for understanding simple resource availability (food, water, shelter) or something as complex as ionizing radiation, humans have been using plants as environmental sensors for as long as we have walked on two feet and likely before. This dissertation aimed to revolutionize how humanity uses plant life to observe ionizing radiation. By using the DNA damage response associated with ionizing radiation, the first dosimetric gamma radiation phytosensor was generated (Chapter II). This sensor produces a fluorescent response observable at a standoff, allowing for clearer and safer observation than what would be required to see the small phenotypic changes in plant architecture induced by ionizing radiation in wild type plants (Chapters II, III, and IV).

This dissertation also aimed to increase plant radiotolerance so that sensor, bioremediation, and food generation capabilities could continue in areas of high ionizing radiation. Unfortunately, expression of the *Ramazzottius varieornatus* 'damage suppressor' protein gene did not improve plant radiotolerance, indicating mechanisms of genome protection from animals do not reliably protect plant cells from the impacts of gamma radiation (Chapter III).

It is clear that the transcriptomic response to ionizing radiation is focused on plastid and cell membranes as much as the genome in acute, low dose treatments. This suggests that future engineered radiotolerance strategies should protect these regions as well as the genome (Chapter IV). Transcriptomic data also reveals that it is possible to develop a low dose radiation phytosensor using native promoters in potato, which would allow for better sensor performance than the phytosensor developed in Chapter II. A key factor in the development of future phytosensor and radiotolerance strategies is the tissue-specific expression patterns of the genetic elements used. Engineering strategies need to account for factors such as the high fluorescent protein expression observed in vascular tissue of the 4×RAD51 phytosensor (Chapter II) and the phenotypic effects of gamma radiation on meristematic tissue but not leaf tissue (Chapter IV). In order to quickly and precisely engineer specific plant tissues, single-cell -omics technologies that are already developed in animal systems need to be adapted and integrated for plant research (Chapter V). These technologies integrate -omics, physiological, and cell-cell interaction datasets using artificial intelligence (AI) algorithms, allowing for exact and efficient cell typing. Implementation of these artificial intelligence technologies could allow for faster development of phytosensor, radiotolerance, or other metabolic engineering strategies.

As humans pursue nuclear energy and long-term spaceflight in the next decades, the sensor capabilities and radiotolerance of plants will need to be improved. This dissertation represents a step forward in both of these areas by testing engineering strategies developed on current literature and paving the way towards future strategy development with analysis of low dose transcriptomic data and the adaptation of existing AI for plant cell typing. Through utilization of the plant-centric tools and strategies developed in this dissertation, humanity can ensure a safer relationship with ionizing radiation.

VITA

Robert Sears was born in Durham, North Carolina. He remained in Durham until beginning his undergraduate degree in Plant Science at the University of Tennessee-Knoxville. During his undergraduate study, he took on a Soil Sciences minor, participated in undergraduate research, and pursued a summer internship at Neogen Corporation in Lansing, MI. After the completion of his undergraduate degree, he then stayed in Knoxville to begin the PhD that culminated in this dissertation.